UNIVERSIDADE FEDERAL DO PARANÁ
CENTRO DE ESTUDOS DO MAR
PROGRAMA DE PÓS-GRADUAÇÃO EM SISTEMAS COSTEIROS E OCEÂNICOS

Marcio Machado Cintra

PROCESSOS TERMODINÂMICOS E HIDRODINÂMICOS NO OCEANO ATLÂNTICO TROPICAL SUDOESTE

Pontal do Paraná-PR

Março de 2015

Marcio Machado Cintra

PROCESSOS TERMODINÂMICOS E HIDRODINÂMICOS NO OCEANO ATLÂNTICO TROPICAL SUDOESTE

Tese apresentada ao programa de Pós-graduação em Sistemas Costeiros e Oceânicos da Universidade Federal do Paraná, como parte dos requisitos para obtenção do grau de Doutor em Sistemas Costeiros e Oceânicos, na linha de pesquisa: Dinâmica Oceânica e Costeira.

Orientador: Carlos Alessandre Domingos Lentini
Co-Orientador: Eduardo Marone

Pontal do Paraná-PR
Março de 2015

CATALOGAÇÃO NA FONTE:
UFPR / SIBI - Biblioteca do Centro de Estudos do Mar

Cintra, Marcio Machado
C575p Processos termodinâmicos e hidrodinâmicos no oceano Atlântico Tropical Sudoeste / Marcio Machado Cintra. - Pontal do Paraná, 2015.
127 f.; 29 cm.

Orientador: Dr. Carlos Alessandre Domingos Lentini
Co-orientador: Dr. Eduardo Marone.

Tese (Doutorado) – Programa de Pós-Graduação em Sistemas Costeiros e Oceânicos, Centro de Estudos do Mar, Setor de Ciências da Terra, Universidade Federal do Paraná.

1. Oceanos. 2. Termodinâmica. 3. Hidrodinâmica. 4.Oceanografia física. 5. Interações oceano-atmosfera. I. Título. II. Lentini, Carlos Alessandre Domingos. III. Marone, Eduardo. IV. Universidade Federal do Paraná.

CDD 551.5246

PGSISCO
CURSO DE PÓS-GRADUAÇÃO EM SISTEMAS COSTEIROS E OCEÂNICOS
Centro de Estudos do Mar - Setor Ciências da Terra - UFPR
Avn. Beira-mar, s/nº - Pontal do Sul – Pontal do Paraná – Paraná - Brasil
Tel. (41) 3511-8644 - Fax (41) 3511-8648 - www.cem.ufpr.br - E-mail: pgsisco@ufpr.br

TERMO DE APROVAÇÃO

Marcio Machado Cintra

PROCESSOS HIDRODINÂMICOS E TERMODINÂMICOS NO ATLÂNTICO TROPICAL

Tese aprovada como requisito parcial para a obtenção do grau de Doutor(a) em Sistemas Costeiros e Oceânicos, da Universidade Federal do Paraná, pela Comissão formada pelos professores:

Dr. Carlos Alessandre Domingos Lentini (UFBA)
Orientador e Presidente

Dr. Marcus André Silva (UFPE)
Membro Examinador

Dr. José Eduardo Gonçalves (SIMEPAR)
Membro Examinador

Dr. Maurício Almeida Noernberg (UFPR)
Membro Examinador

Marcelo Sandin Dourado (UFPR)
Membro Examinador

Pontal do Paraná, 26/03/2015.

DEDICATORIA

Dedico esta tese a minha família. À Scheyla e Rafael, que foram meus fiéis escudeiros durante todo período que dediquei a este estudo. Ambos chegaram a miha vida via meio acadêmico, de surpresa e hoje e para sempre serão meu alento, minha alegria, razão de viver.

AGRADECIMENTOS

Antes de tudo, gostaria de agradecer a família de modo geral. Aos meus pais pela educação e incentivo. Aos tios e primos que estiveram em minha casa dando apoio. Ao meu cunhado, cunhada, sogro e sogra pelas frequentes visitas e várias ajudas.

Agradeço a minha esposa, pelo sacrifício em prol de meus estudos, mas especialmente por ter me dado a melhor surpresa que já tive, de longe minha melhor invenção, nosso filho.

Aos meus orientadores, Carlos Lentini e Eduardo Marone, pela paciência que tiveram e pelo esforço dedicado para que eu tivesse condições de passar tudo que passei e chegar ao final mais maduro, preparado e totalmente focado ao estudo.

A CAPES por prover a bolsa de estudos que me permitiu desenvolver minha vida com dedicação exclusiva à pós-graduação.

A UFPR por proporcionar esta oportunidade de refinamento e desenvolvimento intelectual, que em muito servirá para as futuras experiências, profissionais e de vida.

Aos funcionários do CEM, por sempre estarem aptos a resolver nossas necessidades em pronto atendimento.

A todos os professores que participaram de minha formação.

Agradeço a Marcelo Dourado, por ter me recebido no CEM, pela paciência e amizade no período inicial onde também foi meu orientador.

Aos colegas de Mestrado e Doutorado, pelos momentos de descontração e amizade que proporcionaram ao longo dessa jornada.

Agradeço à Moacyr Araújo e Jacques Servain pela parceiria de publicação, por seus comentários e sugestões em nosso artigo e por estarem sempre prontos a nossas empreitadas científicas.

RESUMO

O Atlântico tropical é uma região de extrema complexidade termodinâmica. Os fluxos de massa e energia que ocorrem na interface ar-mar como também os que ocorrem na camada de mistura, são capazes de influenciar e serem influenciados pela dinâmica oceânica, também bastante complexa. Na região equatorial, um complexo sistema de correntes e contra correntes, somados a ocorrência de processos como a divergência de Ekman e ressurgência equatorial, sob um regime de ventos oscilante e com a presença de ondas de instabilidade faz com que a variabilidade nesse meio seja identificável em uma ampla gama de escalas (espacial e temporal). A medida que nos afastamos do equador essa complexidade diminue, entretanto, muitos desses fenômenos continuam ocorrendo sobre os giros tropicais (norte e sul) e ao longo das regiões costeiras, sobretudo com a atuação das correntes de contorno (leste e oeste). Do ponto de vista termodinâmico o Atlântico tropical (AT) tem sido estudado em seus diversos modos de variabilide com grande preocupação voltada aos fenômenos que tem impacto sobre o clima regional e global. Diversos estudos focaram para o entendimento dos modos de variabilidade da temperatura da superfície do mar (TSM) e suas implicações para o regime de chuvas sobre os continentes Americano e Africano. Hodiernamente, não só as variações de TSM têm sido consideradas, mas muitos pesquisadores também voltam seus esforços para avaliações do conteúdo térmico armazenado na camada superior, como forma de obter uma avaliação mais completa do real estado termodinâmico nessa camada. Levando em consideração que embora a maioria destes estudos se preocupou em mensurar a variabilidade dos fenômenos atuantes no AT e como esta variabilidade tem forçado os oceanos, pouco se fez a respeito de buscar um entendimento profundo das causas de tal variabilidade termodinâmica. A presente tese estudou os processos termodinâmicos sobre o AT, avaliando os termos individuais que resultam na tendência de temperatura dentro da camada de mistura, com foco para anomalias quentes que possam estar ligadas a eventos meteorológicos sobre os continentes adjacentes. Foram abordadas neste estudo as escalas sazonal e interanual. Para avaliação dos processos termodinâmicos no AT, foram utilizadas duas simulações numéricas. As simulações utilizaram o modelo *Regional Ocean Modeling System (ROMS)*, ambas com resolução horizontal de $1/6^{o}$ (~ 18 km) e alta concentração de pontos verticais na camada superior do oceano, focando na melhor reprodução da camada de mistura. A primeira simulação, com forçantes climatológicos foi utilizada para avaliação dos processos sazonais com foco para eventos quentes sobre o Atlântico tropical

sudoeste. A outra simulação, com forçantes interanuais, simulou os anos de 2000 a 2010, onde foram avaliados o desenvolvimento da piscina quente do Atlântico tropical sudoeste (PQATSO), suas distinções em relação à piscina quente equatorial (PQE) e a avaliação das anomalias quentes e frias no AT. A avaliação sazonal do desenvolvimento da PQATSO revelou que o forçante superficial (fluxo de calor líquido) é o principal termo responsável pelo seu aparecimento e extinção no outono austral. Na escala interanual esse padrão foi mantido, considerando que o sinal sazonal é preponderante no AT. Entretanto, a termodinâmica da piscina quente sobre o atlântico tropical sudoeste foi avaliada de 2000 a 2010, e mostrou que durante os meses de Março, Abril e Maio, quando as águas quentes da PQATSO usualmente se encontram fundidas com as águas quentes da PQE, duas áreas distinguíveis, dinâmica e termodinamicamente, foram encontradas. Embora pela simples avaliação da TSM sobre essa região, tendo como limite de identificação da piscina quente a isoterma de 28 ^{o}C, seja difícil apontar qualquer diferenciação entre áreas. Avaliando a profundidade da camada de mistura, profundidade da isoterma da piscina quente e conteúdo térmico dentro da camada de mistura, duas regiões distintas termodinâmicamente foram apontadas. Com essa abordgem, foi possível diferenciar a PQATSO da PQE, mesmo durantes os meses em que essas águas quentes se encontram fundidas na superfície do oceano. A PQATSO possui uma profundidade da camada de mistura maior do que a PQE, conferindo também maior conteúdo térmico dentro dessa camada. Essas diferenças são atribuídas ao regime de ventos diferenciado entre as duas regiões nessa época do ano, que implica em diferentes configurações do fluxo líquido de calor para cada região. Os termos oceânicos de tendência da temperatura também apresentaram diferentes configurações entre essas duas regiões. Enquanto a advecção horizontal é mais importante para a PQATSO a difusão vertical é preponderante no oceano para a PQE. As tendências interanuais da temperatura dentro da camada de mistura foram avaliadas de 2000 a 2010. Nesse perído foi notado que na região equatorial os termos oceânicos são mais importantes do que nas regiões mais afastadas, próximas aos trópicos. Nessa região o termo forçante superficial é dominante como também na região sudoeste próximo à costa Brasileira. Os termos oceânicos verticais (controlados pela difusão vertical) e advectivos horizontais foram preponderantes em proporcionar um balaço ao forçante superficial (atmosférico), entretanto um padrão de distribuição espacial dos termos oceânicos foi mais difícil de ser identificado, sendo que cada região avaliada, apresentou peculiaridades.

ABSTRACT

The tropical Atlantic is a region of a very complex thermodynamics. The mass and energy fluxes which occur over the air-sea interface as well as inside the mixed layer are able to influence and be influenced by the ocean dynamics. At the equatorial region, a complex system of currents and counter currents, added to other processes like the Ekman divergence and equatorial upwelling, under influence of an oscillatory winds system and the presence of instability waves, makes the variability in this region can be identified over a wide range of scales (spatial and temporal). As we move away from the equator, this complexity decreases, however, some of these phenomena keep happening inside the tropical gyres (north and south) and along the coastal regions, mostly over the action of the boundary currents (east and west). From the thermodynamic point of view, the tropical Atlantic (TA) has been studied in its various variability modes, presenting a huge concern to the phenomena whose effects reflect over the regional and global climate. Many studies have focused on understanding the variability modes of the sea surface temperature (SST) and its implications to the rainfall regime over the American and African continents. Nowadays, not only the SST variations has been considered, but many researchers also focused their efforts to evaluations of the heat content stored over the upper layer, as a more complete way to obtain the real thermodynamic state of this layer. Considering that most of these studies were concerned in to measure the variability of the acting phenomena over the TA and how this variability has forced the oceans, little has been done about to pursuit a deep understanding of the causes of such thermodynamic variability. This thesis studied the thermodynamic processes over the TA, evaluating the individuals terms which result in the temperature trend inside the mixed layer, we focused on the warm anomalies that can be linked to the meteorological events over the surrounding continents. The approach used in this study comprehends the seasonal and interannual time scales. To perform the evaluation of the thermodynamics processes over the TA, it was used two numerical simulations. The model used in the simulations was the Regional Ocean Modeling System (ROMS), and both simulations with $1/6^{o}$ (~ 18 km) of horizontal resolution and with a high resolution of vertical points inside the upper ocean, to better reproduce the mixed layer. The first simulation, climatologically forced, it was performed to evaluate the seasonal processes focusing on the warm events over the southwestern tropical Atlantic. The other simulation, interannual forced, simulate the years from 2000 to 2010, to perform evaluations of the southwestern tropical Atlantic warm pool (SWTAWP) evolution, possible distinctions between the SWTAWP and the equatorial warm

pool (EWP), and the evaluation of the warm and cool anomalies over the TA. The seasonal evaluation of the SWTAWP evolution showed that the surface forcing (net heat flux) is the main term responsible to the appearance and extinction of the warm pool during the austral autumn. At the interannual time scale, this pattern it was also verified, especially considering that the seasonal cycle is preponderant over the TA. The SWTAWP thermodynamics was evaluated from 2000 to 2010, results showed that during the months of March to May, when the warm waters of the SWTAWP are usually verified merged at surface with the EWP waters, two distinguished regions, thermodynamically and dynamically, were founded. Although through a simple SST evaluation over this region, considering the 28^{o}C isotherm as a threshold value to the warm pool identification, it is hard to point out any distinction between these areas. Evaluating the mixed layer depth, the depth of the threshold isotherm of warm pool and the heat content inside the mixed layer, two thermodynamic distinguished regions were pointed out. Through this approach, it was possible differentiate the SWTAWP and EWP, even during the months that the warm waters are merged over the ocean surface. The SWTAWP has a larger mixed layer depth when compared with the EWP, resulting in higher heat content inside this layer. These differentiations were attributed to different strength of the winds over these two regions at this time of the year, which implies in different configurations of the net heat flux to each region. The oceanic temperature terms also showed different configurations between these two regions. While the horizontal advection is most important oceanic term to the SWTAWP, the vertical diffusion is the preponderant term to the EWP. The interannual temperature trends inside the mixed layer were evaluated from 2000 to 2010. During this period it was noted that over the equatorial region the oceanic terms are more important than the regions away from equator, near the tropics. Over these last regions, the surface forcing term is preponderant as well over the southwestern tropical Atlantic, near the Brazilian coast. The oceanic vertical terms (controlled by the vertical diffusion) and the horizontal advection terms, were responsible to develop the role to balance the surface forcing term (atmospheric term), however, is difficult to point out a clear pattern of the terms distribution for each region, considering that each region presented peculiarities.

LISTA DE FIGURAS

LIST OF FIGURES (CHAPTER 1)

LIST OF FIGURES (CHAPTER 2)

LIST OF FIGURES (CHAPTER 3)

LISTA DE ABREVIAÇÕES

Correntes superficiais do Oceano Atlântico

CAS – Corrente do Atlântico Sul

CB – Corrente de Benguela

CB – Corrente do Brasil

CNB – Corrente Norte do Brasil

SCNB – Subcorrente Norte do Brasil

CNE – Corrente Norte Equatorial

CSE – Corrente Sul Equatorial

Outras abreviações

CM – Camada de mistura

AT – Atlântico Tropical

ATSO - Atlântico Tropical Sudoeste

OAN - Oscilação do Atlântico Norte

PQ – Piscina quente

PQATSO – Piscina Quente do Atlântico Tropical Sudoeste

PQHO- Piscina Quente do Hemisfério Oeste

TSM – Temperatura da Superfície do Mar

ZCIT – Zona de Convergência Intertropical

LIST OF ABBREVIATIONS

ACT – Atlantic Cold Tongue

BC – Brazilian Current

CESG – Cross Equatorial SST Gradient

COADS – Comprehensive Ocean-Atmosphere Data Set

ITCZ – Intertropical Convergence Zone

ML – Mixed Layer

MLD – Mixed Layer Depth

NBC – North Brazilian Current

NBUC – North Brazilian Under Current

ROMS – Regional Ocean Modeling System

SCUD – Surface Currents from Diagnostic model

SEC – South Equatorial Current

SODA – Simple Ocean Data Assimilation

SST – Sea Surface Temperature

SWTA – Southwestern Tropical Atlantic

SWTAWP – Southwestern Tropical Atlantic Warm Pool

TA – Tropical Atlantic

TAV – Tropical Atlantic Variability

WOA – World Ocean Atlas

WES – Wind Evaporation SST feedback

WP – Warm Pool

SUMÁRIO

INTRODUÇÃO GERAL

A bacia do oceano Atlântico Tropical (AT) destaca-se como uma área que sofre uma influência muito forte das condições impostas pelo sistema acoplado oceano-atmosfera, tanto remota como local, e em diversas escalas de tempo (Carton et al., 1996; Nobre & Shukla, 1996; Servain et al., 2003). Por exemplo, remotamente o AT sofre influência dos eventos associados ao El Niño-Oscilação Sul (ENOS) e ao índice de Oscilação do Atlântico Norte (Enfield & Mayer, 1997; Enfield et al., 1999; Taylor et al., 2002). Localmente, o AT é governado pelas condições impostas pelos balanços de massa e calor oceânico, assim como pelo sistema de monção (Lazar et al., 2001; Schott et al., 1998, 2002, 2003).

A variabilidade no AT é dominada por um forte ciclo anual forçado pela tensão de cisalhamento do vento. Superimposto a este ciclo estão flutuações em outras escalas temporais que, embora mais fracas do que o sinal anual, apresentam variações sistemáticas que são consideradas como um dos fatores mais importantes e responsáveis pelo aparecimento de anomalias climáticas regionais (Moura & Shukla, 1981; Nobre & Shukla, 1996).

Do ponto de vista oceanográfico, o AT é uma região importante para a circulação de larga escala e para o clima global. Isso ocorre devido ao escoamento inter-hemisférico dos fluxos líquidos de massa e calor associados à circulação termohalina (Fratantoni et al., 2000; Lazar et al., 2001; Schott et al., 2003). Do ponto de vista atmosférico, a circulação sobre os trópicos é extremamente sensível às flutuações dos campos de TSM, variável oceânica extremamente importante para o estudo de processos de interação ar-mar, para a previsão do tempo e estudos climáticos (Foltz et al., 2003; Frankignoul et al., 1998; Lindzen & Nigam, 1987).

O comportamento da TSM no AT tem um forte impacto no clima regional sobre o continente americano e africano. Ela modula o comportamento anômalo de precipitação responsável pela ocorrência de eventos extremos (e.g., secas severas e inundações) sobre áreas tropicais do nordeste do Brasil (Moura & Shukla, 1981; Nobre & Shukla, 1996) e do Sahel africano (Palmer, 1986; Lough, 1986; Parker et al., 1988). Por exemplo, anomalias de TSM do oceano Atlântico, podem afetar a posição meridional média da Zona de Convergência Intertropical (ZCIT) causando impacto no transporte de umidade para o continente e, consequentemente, afetando o regime de chuvas sobre a região nordeste do Brasil (Nobre & Shukla, 1996, Rao et al., 2006). Outro exemplo desta relação foi descrito no trabalho pioneiro de

Huang et al. (1995). Pela primeira vez, os autores apresentaram evidências numéricas da existência de uma piscina quente sobre o oceano Atlântico Tropical Sudoeste (ATSO), sendo que uma dessas regiões de acúmulo de água quente localiza-se a leste da região nordeste do Brasil (**Figura 1**). Essa "Piscina Quente do Atlântico Tropical Sudoeste" (PQATSO) contribui para modular a variabilidade da TSM sobre a bacia do AT, e, em conjunção com o sistema da língua fria do Atlântico equatorial ("equatorial Atlantic cold tongue system"), favorece a formação do ramo sul da ZCIT (Grodsky & Carton, 2002). A formação deste ramo, que acontece preferencialmente durante o inverno austral (Jun-Jul-Ago), tem consequências importantes na modulação da variabilidade interanual da estação chuvosa sobre o nordeste brasileiro. A região sudoeste do AT também está associada ao padrão de chuvas sobre o nordeste da Amazônia (Liebmann & Marengo, 2001) uma vez que valores positivos de TSM colaboram para o atraso na estação chuvosa sobre o esta região.

Em decorrência de tantos fenômenos de interação oceano-atmosfera e suas implicações climáticas, esta tese visa avançar no entendimento dos processos oceanográficos responsáveis pela formação das anomalias térmicas verificadas no oceano Atlântico Tropical Sudoeste e implementar o cálculo de variáveis termodinâmicas ainda não realizadas para essa região, como o conteúdo térmico armazenado por tais anomalias e o balanço de calor apresentado termo a termo. Com isso, esper-se aprimorar o conteúdo científico para essa região, proporcionando um estudo focado para a escala regional, que por vezes tem sido negligenciado na maioria das publicações que envolvem essa temática.

FUNDAMENTAÇÃO TEÓRICA E PROBLEMÁTICA DO TEMA

1. A dinâmica das correntes no oceano Atlântico Tropical.

A banda equatorial do oceano Atlântico compreende um complexo sistema de correntes e contracorrentes que fluem principalmente na direção Leste-Oeste (**Figura 1**), promovendo trocas de massa e de energia em diferentes níveis da coluna d´água. Esse sistema é movimentado pela circulação dos Giros Equatorial e Tropical, e por sua interação com os forçantes atmosféricos. As principais correntes zonais fluindo para oeste na camada superficial dessa região são a Corrente

Norte Equatorial (CNE) e a Corrente Sul Equatorial (CSE). Enquanto a CNE se apresenta como um fluxo relativamente largo e contínuo, a CSE é formada por três ramos zonais, separados por contra-correntes de intensidades relativamente fracas (Stramma, 1991). Segundo Molinari (1982) a parcela de fluxo situada mais ao norte é denominada de CSE norte (CSEn); a porção situada entre os ramos extremos é denominada CSE central (CSEc), enquanto que o fluxo situado mais ao sul é conhecido como CSE sul (CSEs).

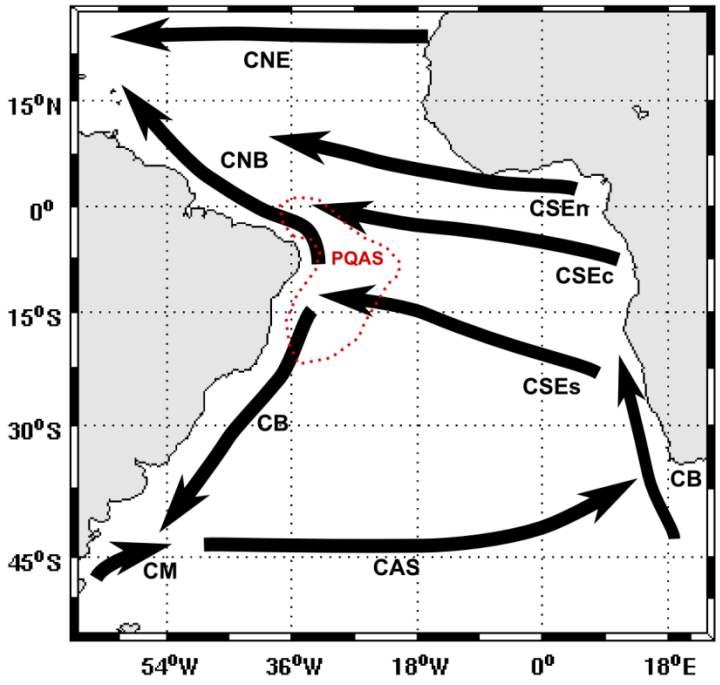

Figura 1 Esquema de correntes no oceano Atlântico Sul. Em pontilhado vermelho, representação da piscina quente do Atlântico Sudoeste.

O ramo sul da CSE se bifurca alimentando duas correntes que margeiam a costa brasileira, a Sub - Corrente Norte do Brasil (SCNB) que flui em direção norte, e a Corrente do Brasil (CB) que flui para o sul (Peterson & Stramma, 1991; Stramma et al., 2005). A SCNB alimenta o fluxo superficial da Corrente Norte do Brasil (CNB) mais ao norte. Então, as águas superficiais que margeiam a costa brasileira, são, de maneira geral, águas quentes e salinas trazidas pela SEC e distribuídas ao largo da plataforma continental pelas SCNB, CNB e CB. Ao percorrerem a região intertropical, as águas superficiais podem encontrar regiões com condições

favoráveis (ventos, radiação) ao acúmulo da energia térmica, estabelecendo então regiões anomalamente quentes.

2. Variabilidade sazonal e interanual no Atlântico Tropical

O ciclo sazonal é o sinal atmosférico e oceânico mais robusto no AT (Merle, 1980; Servain, 1991). Essa sazonalidade é responsável por algumas características espaciais e temporais da TSM e pela evolução meridional sazonal da Zonal de Convergência Intertropical (ZCIT).

Devido a forte presença do sinal sazonal sobre o AT, a sua variabilidade interanual é consideravelmente mais fraca do que a do Pacífico Tropical e, conseqüentemente, tem sido muito menos estudada. De fato, a análise de séries temporais (e.g., Servain, 1991) mostra a dominância da componente anual sobre a variabilidade, talvez como resultado do AT estar tão próximo e cercado pelos continentes Americano e Africano, além do fato de ser impactado pela dinâmica do sistema de monção. Mesmo assim, flutuações interanuais e decadais, por exemplo, não são de maneira alguma negligíveis (Chang et al., 1997; Huang et al., 2004; Servain et al., 2003).

Superimposto ao ciclo sazonal existem dois modos de variabilidade no AT com impactos significantes no clima regional das Américas e da África. Um desses modos, que não tem um análogo no oceano Pacífico, é caracterizado por um gradiente inter-hemisférico norte-sul de TSM, o então chamado "dipolo do Atlântico" (Moura & Shukla, 1981; Servain 1991; Nobre & Shukla, 1996). Esse modo envolve variações espaciais coerentes de TSM em ambos hemisférios entre 50° N – 25° N e 50° S – 20° S, com escalas temporais que vão desde a sazonal, interanual até a decadal. Essas anomalias de TSM afetam significativamente a posição e intensidade da ZCIT e, portanto, exercem uma influência considerável no padrão de chuvas do NE brasileiro e do Sahel (Moura & Shukla, 1981; Servain, 1991; Enfield & Mayer, 1997). Particularmente, anomalias quentes (frias) de TSM ao norte (sul) do equador estão associadas à intensificação e à migração para norte da ZCIT da sua posição média. Quando isso acontece, ocorre um período de seca no NE e chuvas acima do normal no Sahel. Analogamente, anomalias de TSM com sinais opostos ao descrito acima enfraquecem a ZCIT e a deslocam para sul, favorecendo um padrão de

chuvas acima do normal no NE do Brasil e secas no Sahel. Essas anomalias superficiais geralmente aparecem com sinais opostos em cada hemisfério, embora o desenvolvimento desse padrão não seja sempre simultâneo. Além disso, existe a questão se as componentes norte e sul do dipolo estão dinamicamente acopladas ou não (Enfield et al., 1999; Houghton & Tourre, 1992). Estudos que utilizam modelagem numérica do sistema atmosfera-oceano para a avaliação do modo dipolar estão ainda em estágio de desenvolvimento, embora alguns resultados (Chang et al., 1997; Murtugudde et al., 1996) indiquem que os processos físicos responsáveis pelas variações inter-hemisféricas de TSM no AT envolvam trocas ("*feedbacks*") positivas entre TSM, ventos em superfície e fluxos de calor latente.

O segundo modo de variabilidade climática do AT é semelhante ao do ENOS no Pacífico, com manifestações localizadas nas proximidades do equador (Zebiak, 1993; Chang et al, 1997). Esse "modo equatorial", assim como o modo do dipolo do Atlântico, varia tanto na escala sazonal como na interanual. Durante uma fase quente, os Alíseos da porção oeste do AT são fracos e as TSM próximas do equador são excepcionalmente altas (anomalias positivas), especialmente na porção leste da bacia do AT. Durante a fase negativa (anomalias fria), os Alíseos da porção oeste do AT são fortes e as TSM próximas do equador são excepcionalmente baixas. O surgimento de um evento equatorial quente ou frio pode ocorrer rapidamente em escalas temporais de algumas semanas a meses, controlado em parte pela excitação e propagação de ondas de Kelvin e Rossby equatoriais forçadas pelo padrão de ventos.

Existem fortes evidências de que o calor transportado pelas correntes oceânicas desenvolve um papel importantíssimo no balanço climático do planeta (Fratantoni et al., 2000; Schott et al., 1998). Porém, pode-se aprimorar o conhecimento sobre o papel desenvolvido pelas flutuações de curto prazo no clima, especialmente nas baixas latitudes – tropical e equatorial, e quais os processos hidrodinâmicos e termodinâmicos responsáveis pela temperatura observada no oceano.

Com base nos argumentos acima, nota-se que a TSM é sem dúvida a variável física chave do acoplamento atmosfera-oceano. Diversos estudos empíricos apontam para a relação entre a distribuição das anomalias de TSM e o padrão anômalo de chuvas (Moura & Shukla, 1981; Nobre & Shukla, 1996; Taylor et al., 2002; Uvo et al., 1998; Wagner & da Silva, 1994). Entretanto, para compreender a distribuição espaço-temporal da TSM e os seus impactos, torna-

se imprescindível estimar também a quantidade de calor contida na camada superior do oceano, pois estudos apontam para essa variável como sendo um indicador mais robusto do estado termodinâmico do oceano do que a TSM *per se* (e.g., Deser et al., 1996; Kelly, 2004). As anomalias térmicas de superfície e subsuperfície geradas nos giros subtropicais e contidas na camada de mistura podem ser subduzidas devido à divergência de Ekman e, posteriormente, advectadas para dentro do AT oeste pelo escoamento médio via Célula Subtropical Rasa (Kelly, 2004; Lazar et al., 2001). Portanto, para se compreender a distribuição espaço-temporal da TSM, torna-se imprescindível estimar a quantidade de calor contida na camada superior do oceano e analisar a contribuição relativa de cada um dos termos responsáveis pelo balanço de calor resultante (Cronin & McPhaden, 1997; Weingartner & Weisberg, 1991). Arruda & Lentini (2011), estudaram a variabilidade do conteúdo térmico armazenado na camada superior do Atlântico Sul, e apontaram que algumas discordâncias observadas em sua análise podem ser decorrentes de fenômenos que atuam na área como El Niño e OAS. Esses autores ainda recomendaram a utilização do banco de dados WOA (2009) para análises climatológicas, considerando que essa fonte de informação passou a assimilar dados das bóias PIRATA do Atlântico Sul, podendo melhorar a qualidade das avaliações térmicas nessa área.

3. Piscina quente do oceano Atlântico tropical sudoeste e suas implicações regionais.

De acordo com Wang & Enfield (2001), uma região do oceano coberta por águas com temperatura acima de 28,5 °C é chamada de Piscina Quente do Hemisfério Oeste (PQHO), e embora esses autores afirmem que esse processo é restrito aos oceanos do hemisfério norte, outros autores reportaram a presença de uma Piscina Quente do oceano Atlântico Tropical Sudoeste (PQATSO), sendo esta uma região marcada por temperatura da superfície do mar com valores >28°C (Silva et al., 2009; Huang et al., 1995).

Utilizando dados climatológicos em uma análise dos fluxos de calor nas PQHO, Enfield & Lee, (2005) utilizaram diferentes faixas de temperatura limite (T > 27,5 °C , T > 28 °C e T > 28,5 °C) para avaliar o desenvolvimento e as dimensões da piscina quente do Atlântico equatorial, região de águas anomalamente quentes que se encontram desde a costa da África até a Brasileira entre 10° N e 10° S. Revisando as definições a respeito da geografia e ocorrência das

piscinas quentes Enfield et al. (2006) relataram que a piscina quente do Atlântico equatorial não é incluída como PQHO por apresentar características dinâmicas e termodinâmicas distintas das demais e por seus impactos nas Américas Central e Norte não estarem claramente identificados.

Anomalias quentes das TSM, quando apresentam valores elevados, têm impacto significativo na formação da convecção tropical, embora deva ser considerando que tais anomalias normalmente ficam restritas a uma região fechada (Graham & Barnett, 1987). Tal explicação pode embasar uma teoria sobre o porquê de muitos trabalhos estarem concentrando estudos nas grandes piscinas térmicas do hemisfério oeste (Atlântico Norte, Mar do Caribe e Pacífico leste e oeste) já que estas anomalias têm implicações no clima em uma escala maior, enquanto que pouca atenção tem sido dada a anomalia térmica no oceano Atlântico Tropical Sudoeste, possivelmente por acarretar implicações climáticas regionais.

Nobre & Shukla, (1996) utilizando funções ortogonais empíricas enfatizam que as secas no nordeste brasileiro são a manifestação local de um fenômeno de escala maior, o qual engloba o Atlântico equatorial e a região amazônica da América do Sul. Estes autores ainda apresentaram que anomalias negativas nas chuvas durante os meses de março à maio, época chuvosa na região, estão relacionadas com a retirada precoce da ZCIT para as regiões anomalamente quentes da superfície do mar no oceano Atlântico Norte. De acordo com Stramma e Schott (1999), o deslocamento latitudinal da ZCIT é o maior sinal da variabilidade dos mecanismos de interação oceano-atmosfera no Atlântico tropical. As características da evolução sazonal da localização da ZCIT e da temperatura da superfície do mar nesta região dependem da dinâmica das correntes e dos ventos alísios. As variações da circulação superficial respondem, sobretudo, às distribuições sazonais de cisalhamento do vento, afetando assim a migração da ZCIT. Com a migração da ZCIT em direção ao norte no período de inverno austral, observa-se igualmente o deslocamento em direção ao norte das correntes NEC e SEC, alterando em conseqüência o transporte de calor na superfície do Atlântico equatorial.

Wang (2001) reporta que o oceano Atlântico sofre a influência primária das variações sazonais, que são sobrepostas por variações em outras escalas temporais (interanual e interdecadal). Esse autor relata que os principais fenômenos que influenciam na variabilidade climática do Atlântico incluem um modo de variação zonal (semelhante a um pequeno El Niño

no Atlântico), o modo de variação do gradiente meridional de TSM e a chamada Oscilação do Atlântico Norte (OAN).

A interação da PQATSO com as condições meteorológicas, em especial suas consequências sobre os eventos extremos na região nordeste do Brasil (NEB) não são completamente entendidos. Entretanto, há evidências de que a variabilidade interanual de TSM sobre a PQATSO afeta a intensidade desses distúrbios que se propagam para oeste sobre uma faixa latitudinal que se estende do equador até ~ 10° S em direção à costa leste do nordeste. Kouadio et al. (2012) mostraram que existe uma relação entre ondas de leste que se propagam na atmosfera, sistemas convectivos de meso-escala e a ocorrência de eventos extremos de precipitação sobre a região leste do nordeste brasileiro. Esses autores ainda apontaram que há evidências de que processos de interação oceano-atmosfera influenciam nas precipitações anômalas que ocorrem nesta região.

Embora trabalhos científicos apontem para a importância da variabilidade da Zona de Convergência do Atlântico Sul (ZCAS) no padrão de chuvas sobre o NEB (e.g., Barreiro et al., 2002; Chaves & Nobre, 2004), a caracterização e entendimento do comportamento termodinâmico da PQATSO e sua possível relação com o clima do nordeste do Brasil são lacunas científicas que precisam ser investigadas com maior propriedade, dada a sua notória importância para o melhor entendimento dos processos termodinâmicos locais do ATSO.

Referências

Arruda, W. Z.; Lentini, C. A. D. 2011. A remote sensing derived upper ocean heat content dataset for the equatorial Atlantic: A comparison whit PIRATA project data. Brazilian Journal of Geophysics, 29(1), 43-56.

Barreiro, M.; Chang, P.; Saravanan, R. 2002. Variability of the South Atlantic Convergence Zone simulated by an atmospheric general circulation model. Journal of Climate, 15, 745-763.

Carton, J. A.; Cao, X.; Giese, B. S.; da Silva, A. M. 1996. Decadal and interannual SST variability in the Tropical Atlantic Ocean. Journal of Physical Oceanography, 26, 1165-1175.

Chang, P.; Ji, L.; Li, H. 1997. Dynamics and thermodynamics air-sea interactions in the topical Atlantic Ocean. Nature, 385, doi: 10.1038/385516a0

Chaves, R. R.; Nobre, P. 2004. Interactions between sea surface temperature over the South Atlantic Ocean and the South Atlantic Convergence Zone. Geophysical Research Letters, 31, L03204, doi: 10.1029/2003GL018647

Cronin, M. F.; McPhaden, M. J. 1997. The upper ocean heat balance in the western equatorial Pacific warm pool during September-December 1992. Journal Geophysical Research, 102, 8533-8553.

Deser, C.; Alexander, M. A.; Timlin, M. S. 1996. Upper-ocean thermal variations in the North Pacific during 1970-1991. Journal of Climate, 9, 1840-1855.

Enfield, D. B.; Mayer, D. A. 1997. Tropical Atlantic sea surface temperature variability and its relation to El Niño-Southern Oscillation. Journal Geophysical Research, 102(C1), 929-945.

Enfield, D. B.; Mestas-Nunez, A. M.; Mayer, D. A.; Cid-Serrano, L. 1999. How ubiquituous is the dipole relationship in the tropical Atlantic sea surface temperatures? Journal Geophysical Research, 104, 7841-7848.

Enfield, D. B.; Lee, S-K. 2005. The heat balance of the western hemisphere warm pool. Journal of Climate, 18, 2662-2681.

Enfield, D. B.; Lee, S-K.; Wang, C. 2006. How are large western hemisphere warm pools formed? Progress in Oceanography, 70, 346-365.

Foltz, G. R.; Grodsky, S. A.; Carton, J. A.; McPhaden, M. J. 2003. Seasonal mixed layer heat budget of the tropical Atlantic Ocean. Journal Geophysical Research, 108 (C5), 3146, doi:10.1029/2002JC001584

Frankignoul, C.; Czaja, A.; L'Heveder, B. 1998. Air-sea feedback in the North Atlantic and surface boundary conditions for ocean models. Journal of Climate, 11, 2310-2324.

Fratantoni, D. M.; Johns, W. E.; Townsend, T. L.; Hurlburt, H. E. 2000. Low-latitude circulation

and mass transport pathways in a model of the tropical Atlantic Ocean. Journal of Physical Oceanography, 30, 1944-1966.

Graham, N. E.; Barnett, T. P. 1987. Sea surface temperature, surface wind divergence, and convection over tropical oceans. Science, 238, 657–659.

Grodsky, S. A.; Carton, J. A. 2002. The Intertropical Convergence Zone in the South Atlantic and the Equatorial Cold Tongue. Journal of Climate, 16, 723–733.

Houghton, R. W.; Tourre, Y. 1992. Characteristics of low-frequency sea surface temperature fluctuations in the tropical Atlantic. Journal of Climate, 5, 765-771.

Huang, B.; Carton, J. A.; Shukla, J.1995. A numerical simulation of the variability in the tropical Atlantic Ocean, 1980-88. Journal of Physical Oceanography, 25, 835–854.

Huang, B.; Schopf, P. S.; Shukla, J. 2004. Intrinsic ocean-atmosphere variability of the tropical Atlantic Ocean. Journal of Climate, 17, 2058-2077.

Kelly, K. A. 2004. The relationship between oceanic heat transport and surface fluxes in the western North Pacific: 1970-2000. Journal of Climate, 17, 573-588.

Kouadio, Y. K.; Servain, J.; Machado, L. A. T.; Lentini, C. A. D. 2012. Heavy rainfall episodes in the easthern northeast Brazil linked to large-scale ocean-atmosphere conditions in the tropical Atlantic. Advances in Meteorology, 16.

Lazar, A.; Murtugudde, R.; Busalacchi, A. J. 2001. A model study of temperature anomaly propagation from the subtropics to tropics within the South Atlantic thermocline. Geophysical Research Letters, 28, 1271-1274.

Liebmann, B.; Marengo, J. A. 2001. Interannual Variability of the Rainy Season and Rainfall in the Brazilian Amazon Basin. Journal of Climate, 14, 4308-4318.

Lindzen, R. S.; Nigam, S. 1987. On the role of sea surface temperature gradients in forcing low-level winds and convergence in the tropics. Journal of the Atmospheric Sciences, 44, 2418-2436.

Lough, J. M. 1986. Tropical Atlantic sea surface temperatures and rainfall variations in Subsaharan Africa. Monthly Weather Review, 114, 561-570.

Merle, J. 1980. Seasonal heat budget in the equatorial Atlantic Ocean. Journal of Physical Oceanography, 10, 464-469.

Molinari, R. 1982. Observations of eastward currents in the tropical South Atlantic Ocean: 1978-1980. Journal of Geophysical Research, 87, 9707-9714.

Moura, A. D.; Shukla, J. 1981. On the dynamics of droughts in northeast Brazil: observations, theory, and numerical experiments with a general circulation model. Journal of the Atmospheric Sciences, 38, 2653-2675.

Murtugudde, R.; Seager, R.; Busalacchi, A. 1996. Simulation of the tropical oceans with and ocean GCM coupled to an atmospheric mixed-layer model. Journal of Climate, 9, 1795-1815.

Nobre, P.; Shukla, J. 1996. Variations of sea surface temperature, wind stress, and rainfall over the tropical Atlantic and South America. Journal of Climate, 9, 2464–2479.

Palmer, T. N. 1986. Influence of the Atlantic, Pacific and Indian Oceans on Sahel rainfall. Nature, 322, 251-253.

Parker, D. E.; Folland, C. K.; Ward, M. N. 1988. Sea surface temperature anomaly patterns and prediction of seasonal rainfall in the Sahel region of Africa. Nature, 310, 483-485.

Peterson, R. G.; Stramma, L. 1991. Upper-level circulation in the South Atlantic Ocean. Progress in Oceanography, 26, 1-73.

Rao, V. B.; Giarolla, E.; Kayano, M. T.; Franchito, S. 2006. Is the Recent Increasing Trend of Rainfall over Northeast Brazil Related to Sub-Saharan Drought?. Journal of Climate, 4448-4453.

Schott, F. A.; Fischer, J.; Stramma, L. 1998. Transports and pathways of the upper-layer circulation in the western tropical Atlantic. Journal of Physical Oceanography, 28, 1094-1928.

Schott, F. A.; Dengler, M.; Brandt, P.; Affler, K.; Fischer, J.; Bourles, B.; Gouriou, Y.; Molinari, R. L.; Rhein, M. 2003. The zonal currents and transports at 35 W in the tropical Atlantic. Geophysical Research Letters, 30, 1349, doi: 10.1029/2002GL016849

Schott, F. A.; Brandt, P.; Hammann, M.; Fischer, J.; Stramma, L. 2002. On the boundary flow off Brazil at 5-10 S and its connection to the interior tropical Atlantic. Geophysical Research Letters, 29, 1840, doi: 10.1029/2002GL014786

Servain, J.; Clauzet, G.; Wainer, I. 2003. Modes of tropical Atlantic climate variability observed by PIRATA. Geophysical Research Letters, 30, doi: 10.1029/2002GL015147

Servain, J. 1991. Simple climatic indices for the tropical Atlantic Ocean and some applications. Journal of Geophysical Research, 96, 15137-15146.

Silva, M.; Araujo, M.; Servain, J.; Penven, P.; Lentini, C. 2009. High-resolution regional ocean dynamics simulation in the southwestern tropical Atlantic. Ocean Modeling, 30, 256-269.

Stramma, L. 1991. Geostrophic transport of the south equatorial current in the Atlantic. Journal of Marine Research, 49, 281-294.

Stramma, L.; Rhein, M.; Brandt, P.; Dengler, M.; Böning, C.; Walter, M. 2005. Upper ocean circulation in the western tropical Atlantic in boreal fall 2000. Deep Sea Research, 52, 221–240.

Stramma, L.; Schott, F. 1999. The mean flow field of the tropical Atlantic Ocean. Deep Sea Research, 46, 279–303.

Taylor, M. A.; Enfield, D. B.; Chen, A. A. 2002. Influence of the tropical Atlantic versus the tropical Pacific on Caribbean rainfall. Journal of Geophysical Research, 107 (C9), 3127, doi: 10.1029/2001JC001097

Uvo, C. B.; Repelli, C. A.; Zebiak, S. E.; Kushnir, Y. 1998. The relationships between tropical Pacific and Atlantic SST and northeast Brazil monthly precipitation. Journal of Climate, 11, 551-562.

Wagner, R. G.; da Silva, A. 1994. Surface conditions associated with anomalous rainfall in the Guinea coastal region. International Journal of Climatology, 14, 179-199.

Wang, C. 2001. Atlantic climate variability and its associated atmospheric circulation cells. Journal of Climate, 15, 1516-1536.

Wang, C; Enfield, D. B. 2001. The tropical western hemisphere warm pool. Geophysical Research Letters, 28 (8), 1635-1638.

Weingartner, T. J.; Weisberg, R. H. 1991. A description of the annual cycle in sea surface temperature and upper ocean heat in the equatorial Atlantic. Journal of Physical Oceanography, 21, 83-96.

Zebiak, S. E. 1993. Air-sea interaction in the equatorial Atlantic region. Journal of Climate, 6, 1567-1586.

OBJETIVOS E HIPÓTESES DE PESQUISA

1. Objetivo principal

O objetivo principal deste estudo é investigar a contribuição dos termos responsáveis pelo balanço de calor resultante no AT e suas implicações para o oceano e atmosfera. Para alcançar os objetivos, pretende-se avaliar os processos dinâmicos e termodinâmicos que determinam a variabilidade espaço-temporal desses termos nas escalas, sazonal e interanual. Ênfase será dada para o ATSO devido sua proximidade com a costa brasileira e a ocorrência da PQATSO que tem possível conexão com eventos extremos (precipitações) que vem ocorrendo na região nordeste do Brasil.

2. Objetivos específicos:

- Representar a variabilidade sazonal e interanual do oceano ATSO a partir de duas simulações numéricas, a primeira climatológica, e a última interanual;
- Comparar e validar a estrutura térmica representada numericamente utilizando dados de boias fundeadas do projeto PIRATA (Pilot Research Moored Array in the Tropical Atlantic);
- Verificar a existência e investigar a ocorrência e variabilidade da chamada "piscina quente do oceano Atlântico Sudoeste". Neste contexto será avaliado o melhor critério para sua determinação (temperatura limite), e o cálculo de variáveis particulares desse fenômeno (quantidade de calor, desenvolvimento ao longo do tempo e deslocamento espacial da piscina).
- Quantificar e analisar os fluxos de calor na interface oceano-atmosfera que ocorrem na borda oeste do oceano ATSO;
- Avaliar a importância relativa de cada um dos termos da equação de balanço de calor (entranhamento, difusão turbulenta, advecção e calor líquido na superfície) na determinação da TSM, dos fluxos de calor e quantidade de calor resultante, para o oceano ATSO;

- Analisar séries temporais dos termos da equação de balanço de calor, avaliando as escalas, sazonal e interanual. Essas avaliações com foco para as implicações termo a termo de fenômenos que se propagam na interface oceano-atmosfera irão contribuir para um melhor entendimento desses processos no oceano ATSO.

3. Hipóteses de pesquisa

Considerando que o balanço de calor nos oceanos pode ser modulado por diferentes processos e esses processos podem fazer com que ora os oceanos estejam sendo forçados pela atmosfera, ora estejam agindo como forçante para o outro meio. Espera-se que com a análise do balanço de calor, termo a termo, se entenda melhor como a energia térmica está sendo distribuída dinâmica e termodinâmica nos oceanos e na interface ar-mar, permitindo então elucidar questões sobre como diversos processos (oceanográficos e/ou atmosféricos) estão atuando efetivamente nesse balanço de calor, em especial no Atlântico Tropical Sudoeste. Tais considerações serão testadas para as escalas sazonal e inteanual.

Na região sudoeste do oceano Atlântico Tropical existe a possibilidade que o acúmulo de aguas quentes possa viabilizar a ocorrência de um fenômeno conhecido como piscina quente, que é amplamente reportado para as porções oeste dos oceanos no hemisfério norte. Espera-se que com os estudos de TSM, fluxo de calor líquido e conteúdo térmico armazenado na camada de mistura, focados para a porção tropical sudoeste do oceano Atlântico possam determinar a ocorrência e os processos físicos que controlam a evolução termodinâmica de tal fenômeno na região.

CAPÍTULO 1

Physical processes that drive the seasonal evolution of the Southwestern Tropical Atlantic Warm Pool

Processos físicos que controlam a evolução sazonal da Piscina Quente do Atlântico Tropical Sudoeste

Submetido e aceito à: **Dynamics of Atmospheres and Oceans**, ISSN (0377-0265), Fator de impacto = 1.6, Qualis CAPES = A2.

Marcio M. Cintra [a*], Carlos A. D. Lentini [b,c*], Jacques Servain [d,e*], Moacyr Araujo[f*], Eduardo Marone[a]

[a] Centro de Estudos do Mar, CEM, Universidade Federal do Paraná (UFPR), Av. Beira Mar s/n, 83255-000, Pontal do Paraná PR, Brazil

[b] Departamento de Física da Terra e do Meio Ambiente da Universidade Federal da Bahia (UFBA), Campus Ondina, 40170-280, Salvador BA, Brazil

[c] Current address: National Institute for Space Research (INPE), Remote Sensing Division, São José dos Campos - SP, 12227-010, Brazil

[d] LOCEAN-IRD/CNRS/UPMC/MNHN, UMR 7159, Université Pierre et Marie Curie, 4 Place Jussieu, 75252 Paris, France

[e] Visiting scientist at Fundação Cearense de Meteorologia e Recursos Hídricos (FUNCEME), Av. Rui Barbosa 1246, 60115-221 Fortaleza CE, Brazil

[f] Departamento de Oceanografia da Universidade Federal de Pernambuco – UFPE, Av. Arquitetura, s/n, 50740-550, Cidade Universitária, Recife PE, Brazil

*Grupo de Oceanografia Tropical - GOAT - www.goat.fis.ufba.br

Abstract

The thermodynamics of the seasonal evolution of the Southwestern Tropical Atlantic Warm Pool (hereafter SWTAWP), which is delimited by the 28°C isotherm, is investigated using the Regional Ocean Modeling System (ROMS). Results indicate that the net heat flux is responsible for the appearance and extinction of the SWTAWP. From March to May, the SWTAWP attains its maximum development and sometimes merges with equatorial warm waters towards the African continent, whose development follows the same period. Along the equator, the combination of oceanic terms (i.e., advection and diffusion) is important to promote the separation - when it occurs - of equatorial warm waters from southwestern tropical waters, which develops off the Brazilian coast. An analysis of the relative contribution of the temperature tendency terms of the mixed layer (ML) heat budget over the appearance, development and extinction of the SWTAWP is also done. The most important term for warming and cooling inside of the ML is the net heat flux at the sea surface. The ML is heated by the atmosphere between October and April, whereas the upper ocean cools down between May and September. The highest heat content values occur during the lower-temperature period (August to October), which is linked to the deepening of the ML during this time period. The horizontal advection along the equator is important, particularly at the eastern domain, which is influenced by the cold tongue. In this area, the vertical diffusive term is also significant; however, it presents values near zero outside the equator. These results contribute to a better understanding of the behavior of the heat budget within the tropical Atlantic, as previous studies over this region focused along the equator only.

Keywords: air-sea interactions, heat budget, mixed layer, net heat flux, seasonal cycle, tropical Atlantic, warm pool

Resumo

A termodinâmica do ciclo sazonal do oceano Atlântico tropical sudoeste (ATSO) superior é investigada usando o *Regional Ocean Modeling System (ROMS)*. Uma abordagem com alta resolução horizontal e vertical na camada superior do oceano foi empregada para diagnosticar as várias contribuições ao orçamento de calor na camada de mistura (CM). A simulação reproduz as principais características da circulação e estrutura térmica do ATSO. O termo mais importante

para o aquecimento e resfriamento na CM é o fluxo de calor líquido à superfície. A temperatura da CM é aquecida pela atmosfera entre Outubro e Abril, enquanto que entre Maio e Setembro o oceano superior se resfria. Os maiores valores de conteúdo térmico ocorreram durante o período de baixas temperaturas (Agosto a Outubro), o que foi atribuído ao aprofundamento da CM nesse período. O termo advectivo horizontal é importante ao longo do equador, especialmente na porção leste do domínio, sobre a influência da língua fria. Nessa região, o termo difusivo vertical também é significante, entretanto, apresenta valores próximos a zero fora do equador. O estudo foca na evolução do aquecimento da Piscina Quente do Atlântico Tropical Sudoeste (PQATSO), que é delimitada pela isoterma de 28°C dentro do ATSO. Nossos resultados indicam que o fluxo de calor líquido é o principal termo responsável pelo aparecimento e extinção da PQATSO. Ao longo do equador, a combinação dos termos oceânicos (advecção e difusão) é importante para separação das águas quentes.

Palavras chave: interações oceano-atmosfera; orçamento de calor; camada de mistura; fluxo de calor líquido; ciclo sazonal; Atlântico tropical; piscina quente;

1. 1. Introduction

In the western tropical Pacific and Atlantic Oceans, a phenomenon that is gaining attention in the scientific community is the western hemisphere warm pool, in which the sea surface temperature (SST) is warmer than 28°C, with occurrences practically all year round (Wang and Enfield, 2001, 2003; Enfield et al., 2006). These features undergo a large annual variation in their geographical extent and their presence has important implications for the regional climate in the surrounding continents. In the Atlantic basin, the aforecited studies essentially focus their attention over the northern parts (Gulf of Mexico and Caribbean) and the equatorial region of the warm pool. For instance, Enfield et al. (2006) find that warm waters over the equatorial Atlantic region constitute a separate feature over the northern tropical Atlantic warm pool due to its peculiar behavior in terms of dynamics and thermodynamics.

A southern part of the Atlantic warm pool exists immediately off the Brazilian coast in a region named here as the Southwestern Tropical Atlantic (SWTA). Up to now, little attention has been given to this region while it has been identified as a key area that contributes to strong

rainfall events that occur between February and July along the eastern Northeast Brazilian coast (Kouadio et al., 2012; Hounsou-gbo et al., 2015). Therefore, the main goal of this study is to analyze the relative contribution and importance of individual terms in the heat budget of the upper SWTA using a numerical simulation, whose focus is on the seasonal evolution of the Southwestern Tropical Atlantic Warm Pool (SWTAWP). An investigation of which physical mechanisms, among the net heat flux at the sea surface, ocean advection, or ocean eddy diffusivity are responsible not only for the SST seasonal variability in the region of interest but also for the behavior of the mixed layer (ML) heat content over the SWTA, is conducted. In order to achieve these objectives, a numerical simulation with a regional oceanic model, especially configured to reproduce the ocean's upper layer and its dynamics and thermodynamics, is done. The diagnostic outputs of the heat balance terms are analyzed with the main thermodynamic variables.

This article is outlined as follows: The main characteristics of the numerical model and the conditions of the climatological simulation are presented in the next section. Section 3 provides some details of the data set in the model validation, which comprises in situ observations from mooring buoys and reanalysis data. Section 4 describes the model evaluation, which includes comparisons between different data bases of the upper ocean temperature profiles, the heat content over the ML, the ML depth, the depth of the thermocline and the ocean currents inside the ML. In Section 5, we examine the seasonal evolution of the main heat budget terms over the SWTA. In Section 6, the seasonal evolution of the SWTAWP is presented and the summary and conclusions are provided in the last section.

1. 2. Model description

The numerical model in this study is the Regional Ocean Modeling System (ROMS), which was developed by Shchepetkin and McWilliams (2003; 2005; 2008). This model is a free surface ocean model that solves primitive equations in an Earth-centered rotating environment based on the classical Boussinesq approximation and hydrostatic vertical momentum balance (Shchepetkin and McWilliams, 2005). To prevent spurious diapycnal mixing, the rotated split upstream-biased advection scheme proposed by Marchesiello et al. (2009) is employed, with implementations proposed by Lemarié et al. (2012), which enable this scheme to rotate the

hyperdiffusive part in the neutral direction and increase its stability. Unresolved vertical subgrid-scale processes are parameterized by an adaptation of the nonlocal K-profile planetary boundary layer scheme (Large et al., 1994), which is modified by the scheme proposed by Shchepetkin (2005).

The model grid, forcing, and initial and boundary conditions were constructed using ROMSTOOLS (Penven et al., 2008). The model was forced by climatological seasonal wind stress and heat and freshwater fluxes derived from the Comprehensive Ocean-Atmosphere Data Set (COADS) with a horizontal resolution of 0.5° × 0.5° (da Silva et al., 1994). The COADS SST was replaced by the Pathfinder SST climatology field (approximately 9 km of horizontal resolution) to force the model at the surface (Casey and Cornillon, 1999). The initial and lateral boundary conditions were constructed using the temperature (Locarnini et al., 2010) and salinity (Antonov et al., 2010) derived from the World Ocean Atlas (WOA 2009) monthly climatology database with a horizontal resolution of 1° × 1°. Sea surface height and zonal and meridional velocities were obtained from geostrophic calculations.

Vertical discretization of the grid was constructed using a hybrid z – σ coordinate system that was obtained by relaxing the z-coordinate system toward the σ-coordinate (Shchepetkin and McWilliams, 2008; Lemarié et al., 2012).

The model domain ranged from 41° W to 12° W and 24° S to 8° N, which produces 260 × 285 points with a horizontal resolution of 1/9° (approximately 12 km) and 42 vertical levels. Bottom topography was based on the global topography data set at a 2′ resolution (Smith and Sandwell, 1997). Explicit lateral viscosity was null everywhere in the model, with the exception of sponge layers near the open boundaries, where it smoothly increased on ten grid points. Time integration of the simulation was performed with a time step of 800 s. The simulation begins from a state of rest and runs for ten years. Mixing of temperature and salinity is performed along isopycnals using a Laplacian operator, with a coefficient of 150 $m^2 s^{-1}$.

One of our goals is to measure the relative contribution of the temperature tendency terms over the appearance, development and extinction of the SWTAWP. We employed the temperature diagnostic outputs of the ROMS model to evaluate the heat budget terms. These outputs are initially expressed in $°C.s^{-1}$ and are presented in this section (Eq. 1). To facilitate this

discussion, we use quantities, which are summed or integrated over a month. The trends will be expressed in °C.month^{-1}.

$$\frac{\partial T}{\partial t} = \vec{u}\frac{\partial T}{\partial x} + \vec{v}\frac{\partial T}{\partial y} + \vec{w}\frac{\partial T}{\partial z} + K_h\left(\frac{\partial^2 T}{\partial x^2} + \frac{\partial^2 T}{\partial y^2}\right) + K_v\left(\frac{\partial^2 T}{\partial z^2}\right) + \Phi_T \qquad (1)$$

where T is the temperature, t is the time evolution, $\vec{u}$, $\vec{v}$ and $\vec{w}$ are the velocity components for the x, y and z directions, respectively, Φ_T represents the net heat flux used to force the model plus nudging, and K_h and K_v are the diffusion coefficients for the horizontal direction and vertical direction, respectively.

1. 3. The data sets for model validation

1. 3. 1. Mooring data

The Prediction and Research moored Array in the Tropical Atlantic (Servain et al., 1998; Bourlès et al., 2008) Southwestern Extension (PIRATA-SWE) data were employed to validate the model's performance in the upper surface layer over the SWTA. Since August 2005, these three moored buoys, which are located at 8°S-30°W, 14°S-32°W and 19°S-34°W (Fig. 1a,b), have provided daily time series of temperature and salinity (through the conductivity measurements) in the upper 500 m for temperature and the upper 120 m for salinity. Currently, from 0 to 140m depth, there are four levels with only temperature sensors (60 m, 80 m, 100 m and 140 m) and four levels with both temperature and conductivity sensors (1 m, 20 m, 40 m and 120 m). This array was conceived and implemented as a response to understanding and forecasting the Brazilian Climate, especially over the northeast Brazilian region. The PIRATA data can be downloaded at no cost from the NOAA/PMEL web site (www.pmel.noaa.gov/pirata).

Climatological seasonal data were computed using processed daily data (August 2005 to August 2014) and the flawed data were removed, which yielded monthly mean values. Vertical interpolations were processed using the PIRATA data when only one out of three consecutive temperature sensors along the moored line was dysfunctional.

1. 3. 2. Reanalysis data

The reanalysis data set consists of monthly mean climatological data that was constructed with a 30-year output (1978–2008) from the Simple Ocean Data Assimilation (SODA) reanalysis (Carton and Giese, 2008). The SODA system begins with a forecast state that is produced by an ocean general circulation model based on the Parallel Ocean Program numerics (Smith et al., 1992) with an average 0.25° × 0.4° of horizontal resolution and 40 vertical levels with 10 m spacing near the surface. The output (SODA – version 2.2.4) has 0.5° × 0.5° of horizontal resolution and 40 vertical levels. These data can be obtained at no cost from the Asia-Pacific Data Center web site (http://apdrc.soest.hawaii.edu/datadoc/soda_2.2.4.php).

1. 4. Model validation

An intercomparison between the model and the data sets is performed. They include the temperature over the ML, the surface currents inside the ML, the depth of the 20°C isotherm, which is representative of the thermocline depth (Molinari and Johns, 1994), the temperature vertical structure and the ML depth.

Comparison between the modeled mean upper ocean circulation and the SODA climatology during the austral autumn season (Fig. 1a,b) is realistic, with the westward cSEC well reproduced south of the equator. The numerical EUC presents similar velocities over the central region along equator, with velocities of approximately 0.3 $m.s^{-1}$. Along the western equatorial portion of the domain, the numerical EUC is decelerated and is not observed, while the SODA results showed an accelerated structure (0.5 $m.s^{-1}$) in a branch positioned to the north. The numerical reproduction of the NBC seems to be in good agreement, with resultant velocities of approximately 0.5 $m.s^{-1}$ at 4°S–37°W. The simulated NBC presents a narrower flow compared with the SODA data. According to Lumpkin and Garzoli (2005) in their drifter's analysis, the confluence of these currents indicates a strong acceleration in the NBC from 0.55 to 0.6 $m.s^{-1}$ at 4°S–36°W to 0.78 to 0.88 $m.s^{-1}$ at 3°S–39°W, which is completely compatible with our numerical results.

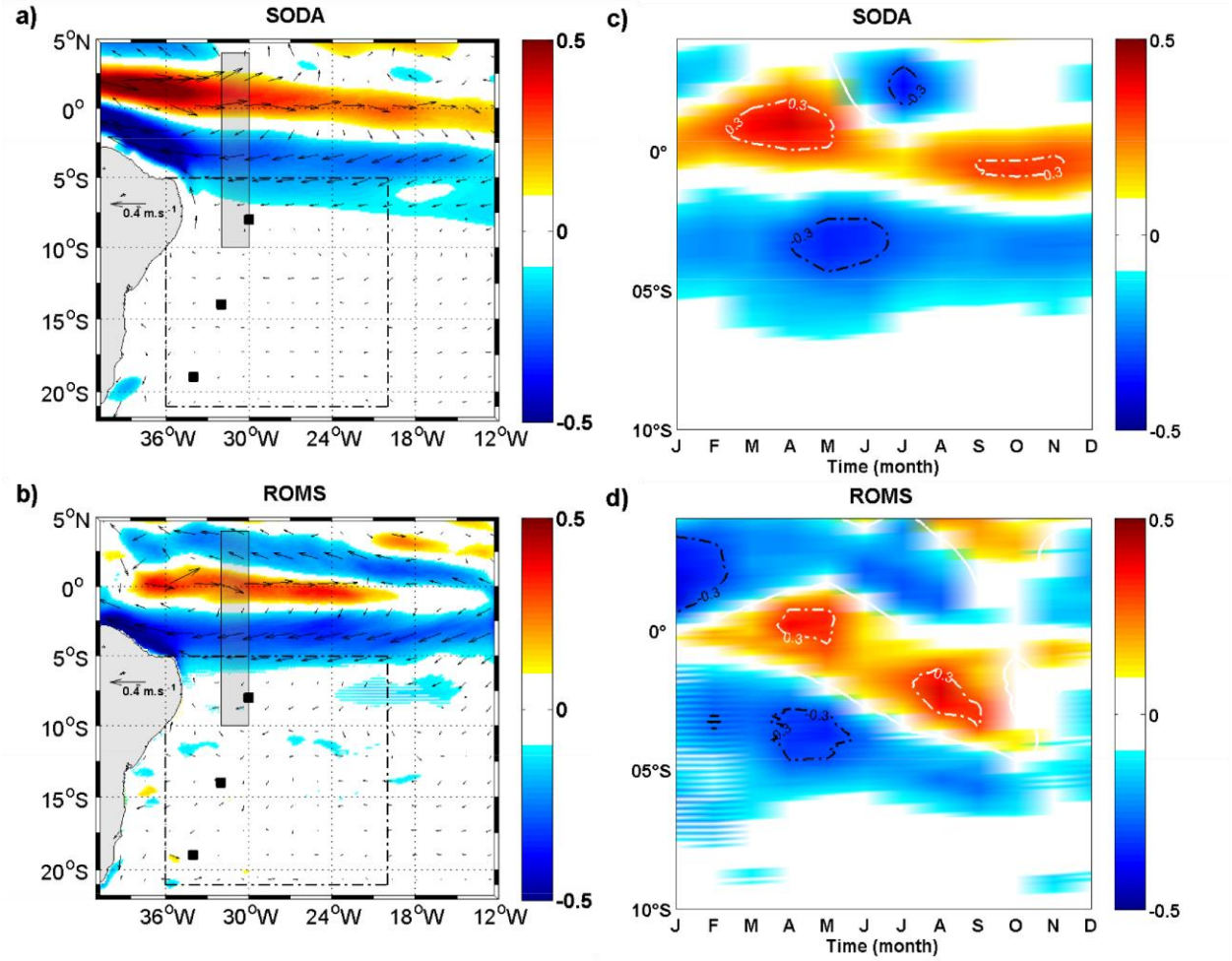

Figura 1. 1 Comparison of the currents (m.s^{-1}) averaged over the mixed layer (ML) from the SODA climatological mean and the model. (a) and (b) are the horizontal maps of the velocity zonal component during austral autumn (seasonal mean) of SODA and ROMS respectively, whereas (c) and (d) are the seasonal Hovmöller diagrams of the velocity zonal component averaged over the gray transparency area (zonal average between 30°W-31°W) of SODA and ROMS respectively. The black squares represent the PIRATA-SWE mooring positions and the dashed dotted line represents the SWTA limits seasonally evaluated.

The seasonal variation of the currents over the ML (Fig. 1c,d) was evaluated over a highlighted area (Fig. 1a,b gray transparency) and showed that the intensification of the cSEC attains maxima values in May-June to the SODA results, while to the numerical results this acceleration is observed during April-May. The EUC seasonality presents two maximums along the equator. In the SODA results, the first peak occurs in March-April while it occurs only in

April in the numerical results. The second EUC maximum is observed in September-October in the SODA results, whereas in the numerical results this acceleration occurs centered in August.

The first 200 m of the vertical temperature structure in the model corresponds with temperatures from the PIRATA-SWE measurements (Fig. 2). The reproduction of the 28°C isotherm, which defines the warm pool limits over this area, is well represented in the three PIRATA sites.

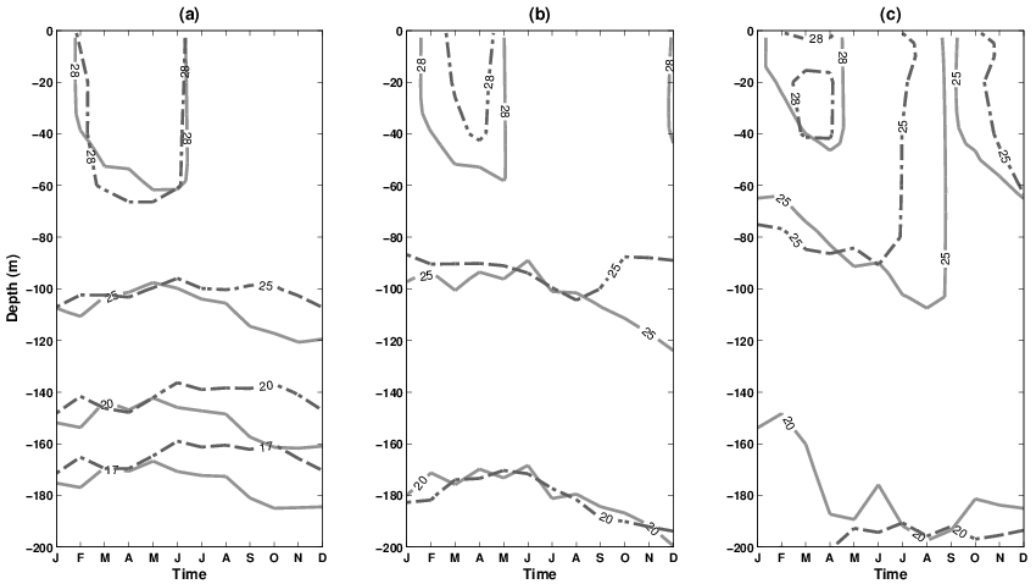

Figura 1. 2 Comparison of an annual monthly mean vertical temperature distribution (°C) for the first 200-m between ROMS (dark gray line) and PIRATA-SWE buoys (black dashed-dotted line) which are located at (a) 8°S-30°W, (b) 14°S-32°W and (c) 19°S-34°W mooring sites. The annual monthly mean of these PIRATA-SWE buoys comprises an average temperature for the period of August 2005 to August 2014.

At 8°S-30°W (Fig. 2a), the isotherms of 25°C, 20°C and 17°C correspond to the period from January to May and present a displacement of about 20 m in the subsequent months. At 14°S-32°W (Fig. 2b), the isotherms of 25°C and 20°C are in good agreement, while the numerical 28°C isotherm presents slightly overrated over time and with about 15m deeper. At 19°S-34°W, the 25°C isotherm presented an extended duration over the austral winter and the 20°C isotherm showed a strong displacement during the austral autumn (Fig. 2c). However, this

displacement at the base of the thermocline at 19°S-34°W does not compromise the good reproduction of the warmer isotherms above.

The modeled spatial distribution of the thermocline depth (Fig. 3a) corresponds well with the SODA climatology mean (Fig. 3b). The zonal and meridional slopes of the thermocline are similar between the model and the climatology fields: along the equator, the thermocline deepens from 100 m at 20°W to 140 m at 38°W. The deepest position of the thermocline (-180 m) is observed south of 10°S and west of 30°W in both data sets, which confirms the good reproduction of the vertical temperature structure.

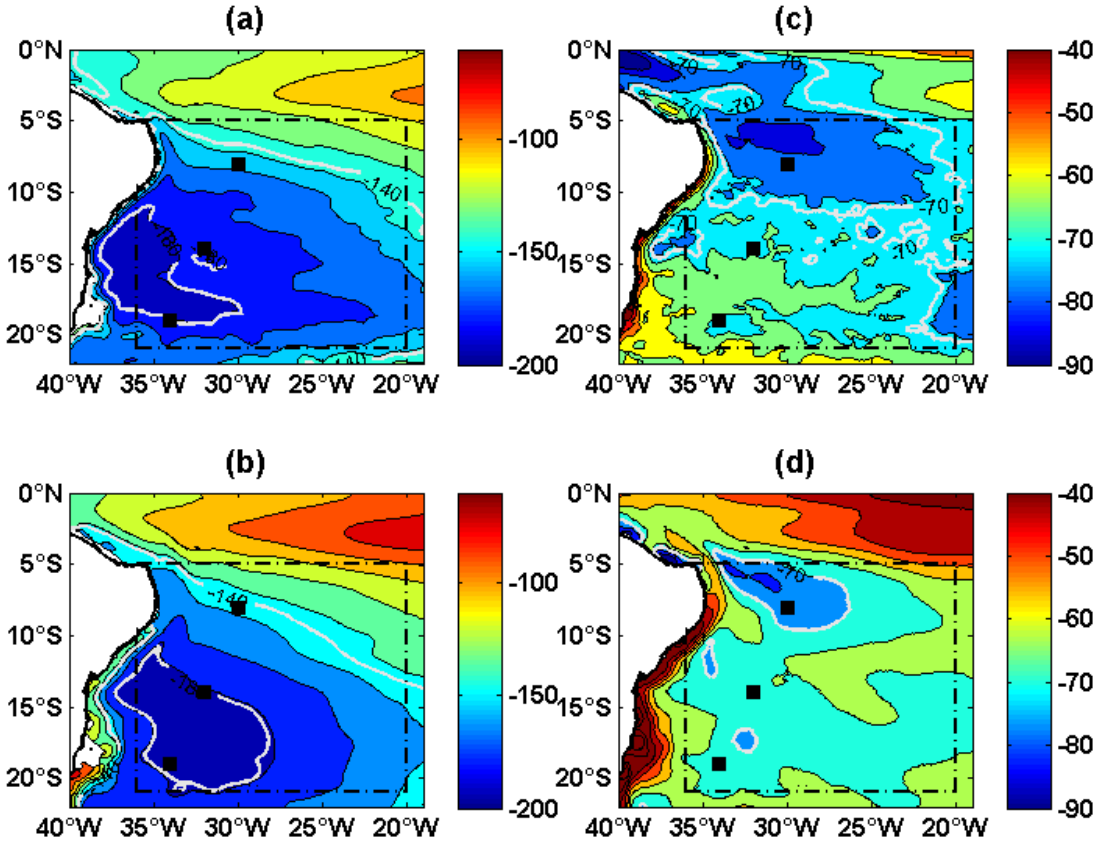

Figura 1. 3 Left panels: Horizontal maps of the time average of the 20°C isotherm depth for (a) ROMS (last year of simulation) and (b) SODA climatology mean. The white lines represent the depths of 140 m and 180 m. Right panels: Horizontal maps of the time average of the mixed layer depth (MLD) for (c) ROMS and (d) SODA climatology mean. The white line represents the depth of 70 m. The black squares represent the PIRATA-SWE mooring positions and the dashed dotted black line represents the SWTA limits evaluated seasonally.

The mixed layer depth (MLD) is calculated using the temperature threshold criterion with $\Delta T = -0.5°C$ compared with the SST. This method was successfully applied in the tropical Atlantic by Foltz et al. (2003) and was confirmed by de Boyer Montégut et al. (2004) as the best criterion method for use with averaged profiles. Deeper values of the MLD (Fig. 3c) are verified from west of 27°W to along the South American coast. The numerical results reveal that the deepest values are slightly widespread beginning from 23°W (Fig. 3d). A similar pattern of the MLD is observed between the model results and the reanalysis results, with the shallowest values in the northeastern part of the domain, deeper values southwestward and presenting the deepest values over 5°S-33°W. The shallower values over the continental shelf along the Brazilian coast were also well represented.

Figures 4a and 4b represent the temperature over the ML seasonal cycle from the model and SODA climatology, respectively. These variables consist of averages over the ML vertical extend and are presented in space-time Hovmöller diagrams considering an average along a meridional axis (5°S-21°S, Fig. 3 dashed dotted black line). From March to April, the temperature reaches maxima values (28.5°C in the model results against 28.1°C from SODA). The temperature decreases from April to September when its coolest values are attained (24.4°C in the model and 24°C in SODA) to the eastern part of our evaluated area. This cooling of the temperatures is in response to the strengthening of the trade winds during this time (austral winter). The temperature slowly increases from October to March with the highest values found in mid-March (austral autumn).

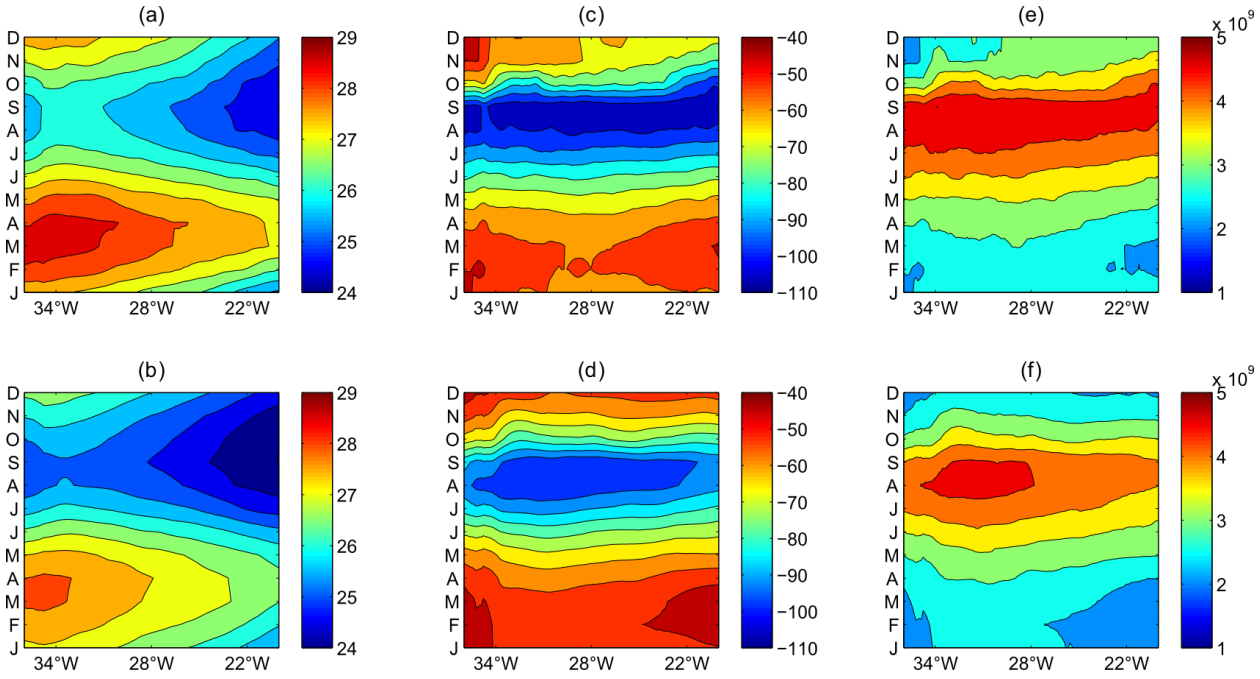

Figura 1. 4 Hovmöller diagrams in the SWTA (5°S-21°S, meridional mean), which present the annual mean temperature over the ML (°C) from (a) model and (b) SODA climatology; MLD (m) from (c) model and (d) SODA climatology and heat content (J m^{-2}) inside the ML from (e) model and (f) SODA climatology.

Figure 4c depicts the seasonal variations in the model MLD compared with the SODA climatology (Fig. 4d). Focusing on the SWTA (Fig. 3 dashed dotted black line), the zonal east-west gradient inside the tropical Atlantic cannot be verified but the seasonal evolution appears to be well linked to the pattern of wind variations. From March to April, the wind stress is very weak and the ocean remains highly stratified: the mixed layer is shallow and is approximately 50 m along 34°W for the numerical results compared with 45 m for the SODA data. During May and June, the sudden increase of the easterly wind stress rapidly deepens the mixed layer on both model and SODA climatologies. The MLD reaches its maximum depth in September: 108 m in the model and 98 m in the SODA data set. When the wind stress relaxes after November, the turbulent mixing decreases, the top of the upper ocean stratifies and the ML gets thinner. A comparison of the seasonal evolution of the heat content inside the ML between the model (Fig. 4e) and the SODA (Fig. 4f) data sets is also performed. Other than the atmospheric forcing, the heat content over the ML is influenced by the variation in the MLD. The highest temperatures are verified in the western part of the basin, which confer the highest values of heat content of

4.8×10^9 J m^{-2} at 30°W for the model (Fig. 4e) compared with 4.6×10^9 J m^{-2} for the SODA data for this region in August, when the MLD is deeper.

1. 5. Seasonal cycle of the heat budget terms in the SWTA

Rates of change in the heat budget terms are presented along the zonal limits of the SWTA, which are meridionally averaged between 5°S and 21°S (Fig. 5). The temperature rate of change (Fig. 5a) is substantially driven by the action of the surface forcing term (Fig. 5b) for both warming and cooling periods. The predominance of the surface forcing over the SWTA was previously noted by Yu et al. (2006) through the analysis of several net heat flux datasets at the Tropical Atlantic and confirmed by Silva et al. (2009), who analyzed the heat budget terms over the PIRATA sites. Foltz and McPhaden (2006) also pointed out the net heat flux predominance over the SWTA for the interannual timescale. The horizontal advection term (Fig. 5c) is relatively weak and acts as a secondary key player in balancing the surface forcing during the cooling period. This term contributes to 0.15°C.$month^{-1}$ in small fragmented regions between July and December, primarily in the western region which seems to be in response to the sSEC action.

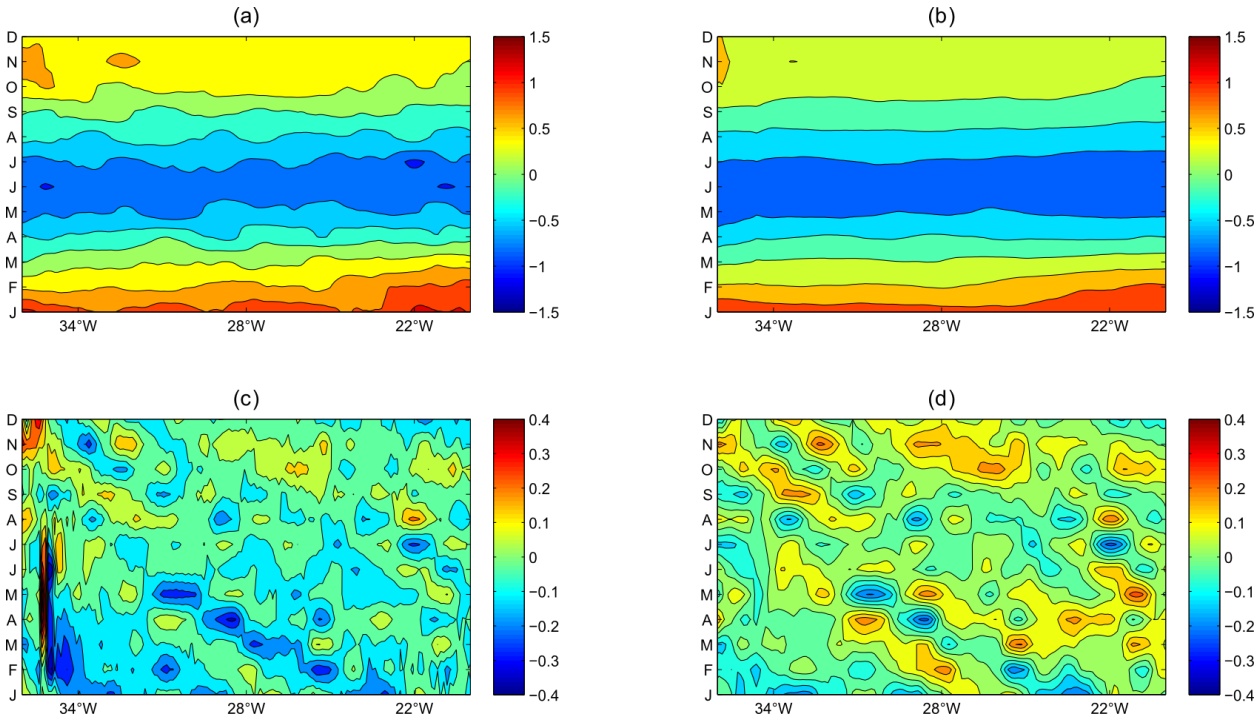

Figura 1. 5 Seasonal cycle of the most important heat budget terms over the mixed layer (°C month^{-1}) in the SWTA (5°S-21°S meridional mean). (a) temperature rate of change, (b) surface forcing (net heat flux + nudging), (c) horizontal advective term, (d) total oceanic terms (advective + diffusive). The colored scales are different and following a hierarchy distribution. (a) and (b) present the same scale (main role players); (c), and (d) also present the same scale (secondary role players).

The cooling period begins in April, reaches its minimum in June-July (temperature rate of change -0.7°C.month^{-1}) and ends in September, when the temperature tendency reverts to warming. The warming periods occur between October and March and provide energy to the upper ocean, which attains its highest temperature in April. The surface forcing accompanies this warming tendency with 0.5-0.6°C.month^{-1} during the austral spring. The highest rate of the surface forcing is observed in January (1.2°C.month^{-1}). During the cooling periods, the surface forcing reaches -0.75°C.month^{-1} in June (Fig. 5b). The total oceanic term (advection + diffusion) acts with 0.2°C.month^{-1} to balance the surface forcing during the cooling period (Fig. 5d) in some fragmented regions, which reflects the pattern of the horizontal advection over this area.

The vertical advective term (not shown) presents values of one or two orders of magnitude smaller than the horizontal advection, with negative values over the austral

winter. The vertical diffusive term (not shown) exhibits the less significant contribution. During the seasonal cycle, it presents values that are three orders of magnitude smaller than the horizontal advection.

Figure 6 presents the oceanic temperature tendency terms in two meridional mean values, which extend from 5°S to 21°S over 34°W (Fig. 6a) and 20°W (Fig. 6b) longitudes. They allow us to evaluate significant differences in these terms along the east-west gradient and the mean temperature over the ML for these two meridional transects (Fig. 6c).

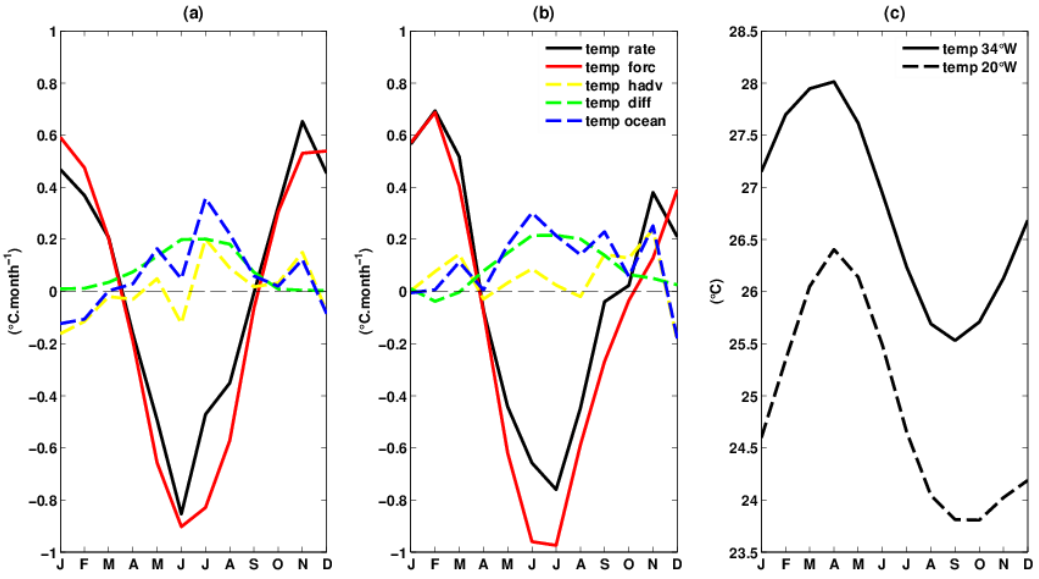

Figura 1. 6 Seasonal cycle of the temperature tendency terms in °C.month^{-1}. Plots show meridional climatological monthly mean values (5°S-21°S) for two different longitudes: (a) at 34°W and (b) at 20°W; (c) presents the mean temperature over the ML (in °C) for these two meridional transects. In (a) and (b), the colored lines represent the following terms: black, the rate of temperature change; red, the surface forcing; yellow, the horizontal advective term; green, the diffusive terms (horizontal + vertical); and blue, the total oceanic terms (advective + diffusive).

The mean temperature over the ML (Fig. 6c) shows the same pattern for the two evaluated transects; however, they differ in their amplitude, which is higher at 34°W (28°C in April) compared with 20°W (26.3°C in April). The seasonal evolution of the rate of temperature change also displays the same pattern for the two transects, which are primarily controlled by the surface forcing terms as previously described. At 34°W from January to March, the advective

terms balance the surface forcing; however, with approximately one third of their absolute amplitude (-0.2°C month^{-1} compared with 0.6°C month^{-1}, in January). From October–November, the advection contributes with 0.12°C month^{-1} as the main oceanic term and acts with the surface forcing to warm the ocean (Fig. 6a). Foltz and McPhaden (2006) investigated the role of horizontal oceanic heat advection in the tropical Atlantic and concluded that this nonlinear term dampens the surface flux-forced changes in the SST, particularly at the SWTA. In the 20°W section (Fig. 6b), the advection plays the main role of the oceanic terms during the warm period (October to April) and contributes with the surface forcing to maintain the heat tendency. The diffusive terms acts as the main oceanic forcing terms during the cooling tendency period (May to September) in both evaluated sections (Fig. 6a,b) and balance the surface forcing with approximately 0.2°C month^{-1}. At 34°W, the diffusion gains the significant contribution of the advection via the westward sSEC flow in July (Fig. 6a). The oceanic terms seem to be linked to the heat content seasonal evolution (Fig. 4e,f), whereas the temperature is primarily driven by the surface forcing. Servain and Lazar (2010) evaluated the relative contributions of the temperature tendency terms over the SWTA using the OGCM results (ORCA-05). Their results indicate that the warming period extends from October to March. Our numerical results showed a similar general pattern with the warming period extending until April.

1. 6. Seasonal evolution of the SWTAWP

In order to illustrate the seasonal evolution of the SWTAWP inside the SWTA, Figure 7 presents the occurrence of warm waters (temperatures > 28°C) in this area between February and June. In February, the existence of a warm pool over the SWTA is limited to two areas: a region along the Brazilian coast that extends from 20°S to 3°S and another portion north of the equator which extends in the west-east direction towards the African continent. During March, April and May, the equatorial Atlantic warm pool is highly developed and consists of an integrated region between the Brazilian and African coasts. In June, the warm waters over the SWTA are separated from the African portion and are positioned between 2°S and 8°S to the west of 24°W.

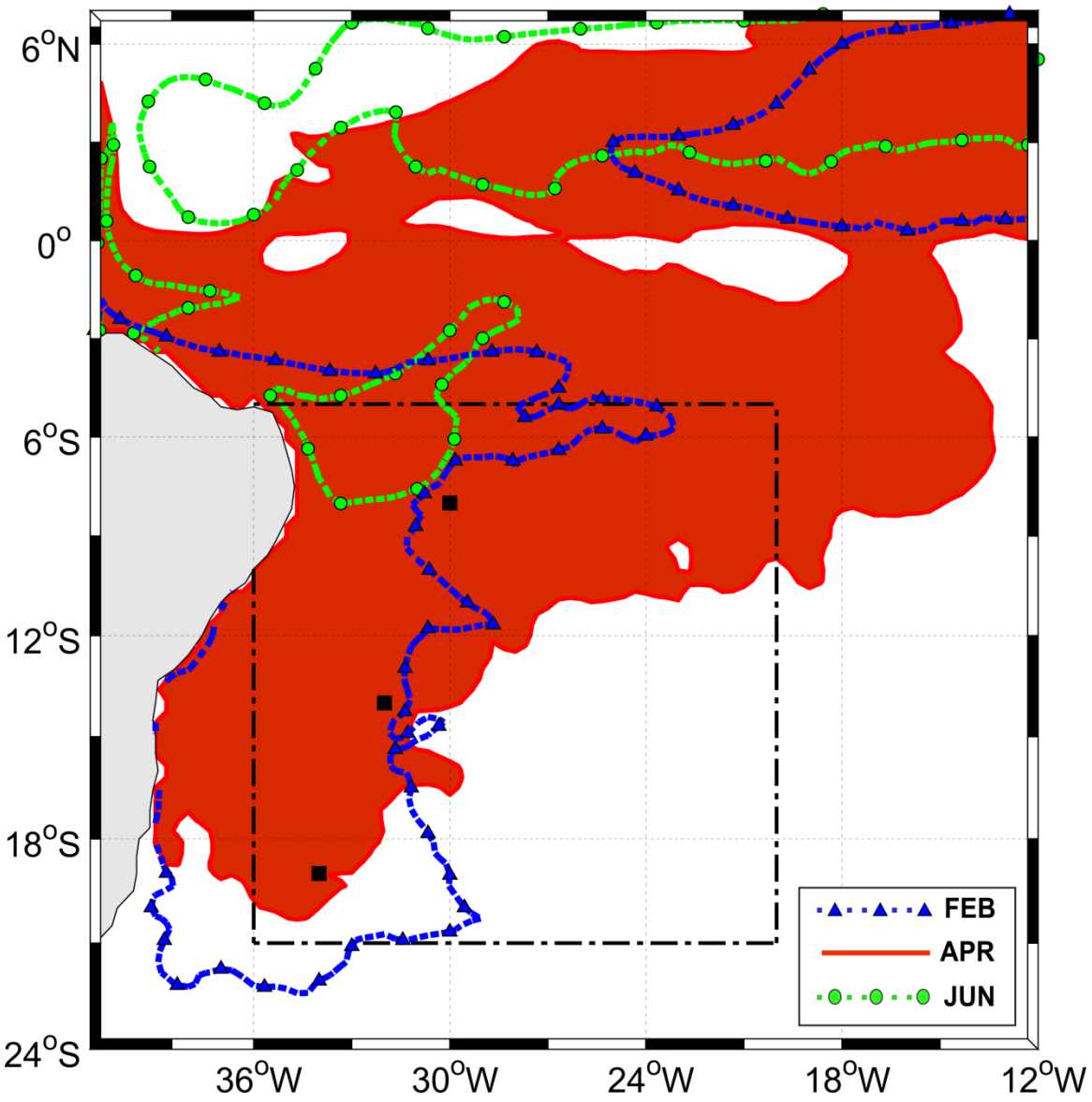

Figura 1. 7 Space-time seasonal evolution of the SST (monthly mean), considering highlighted the warm waters (T > 28 °C) inside the SWTAWP for the months of February (blue dotted line with triangles), April (continuous line filled in red) and June (green dotted line with circles). The black squares represent the PIRATA-SWE mooring sites and the dashed dotted line represents the SWTA limits.

During the austral autumn (Mar-Apr-May), the SWTAWP is highly developed along the Brazilian coast; the majority of the time, the warm waters merge with the equatorial warm pool and spread towards the African coast at the equator. The warm pool undergoes a seasonal parallel displacement from 10°S to the equator in austral autumn and from the equator to 10°N in

austral winter. This migration accompanies the ITCZ (not shown), which attains its lower latitude position between January and April. The ITCZ, which is usually located along the equator from March-April, displays large meridional seasonal excursions over the Atlantic sector. From March-April, its rainy band is located nearly on the equator onto which the trades converge. SST is uniformly warm in the equatorial zone of 5°N-10°S, which renders March-April the time period when the Atlantic ITCZ is very sensitive to even small changes in the inter-hemispheric SST gradient (Chiang and Sobel, 2002; Xie and Carton, 2004; Yu et al., 2006). This peculiar scenario with the warm pool presence over the SWTA significantly influences the climate and precipitation regime of northeastern Brazil (Moura and Shukla, 1981; Nobre and Shukla, 1996; Taylor et al., 2002; Hounsou-gbo et al., 2015). During June, the SWTAWP along the Brazilian coast shifts to the north, whereas a separate band of this warm pool is located along 6°N over the equator.

In order to evaluate the relative contribution of each term of the heat equation (Eq. 1) to the warm pool evolution over the SWTA, the horizontal distribution of the main heat budget terms in the ML, which is superimposed on the southwestern tropical Atlantic warm pool horizontal extension, is also investigated (Fig. 8). The temperature rate of change inside the warm pool region (Fig. 8, panels a–c) presents a general tendency to warming until April. In May, this tendency reverts to a cooling from the south towards the equator; in June, the cooling tendencies are predominant over the SWTA. That dominance of the surface forcing (Fig. 8, panels d–f) was previously mentioned by Yu et al., (2006) through correlations which evaluated the importance of the net flux over the SST climatological variability.

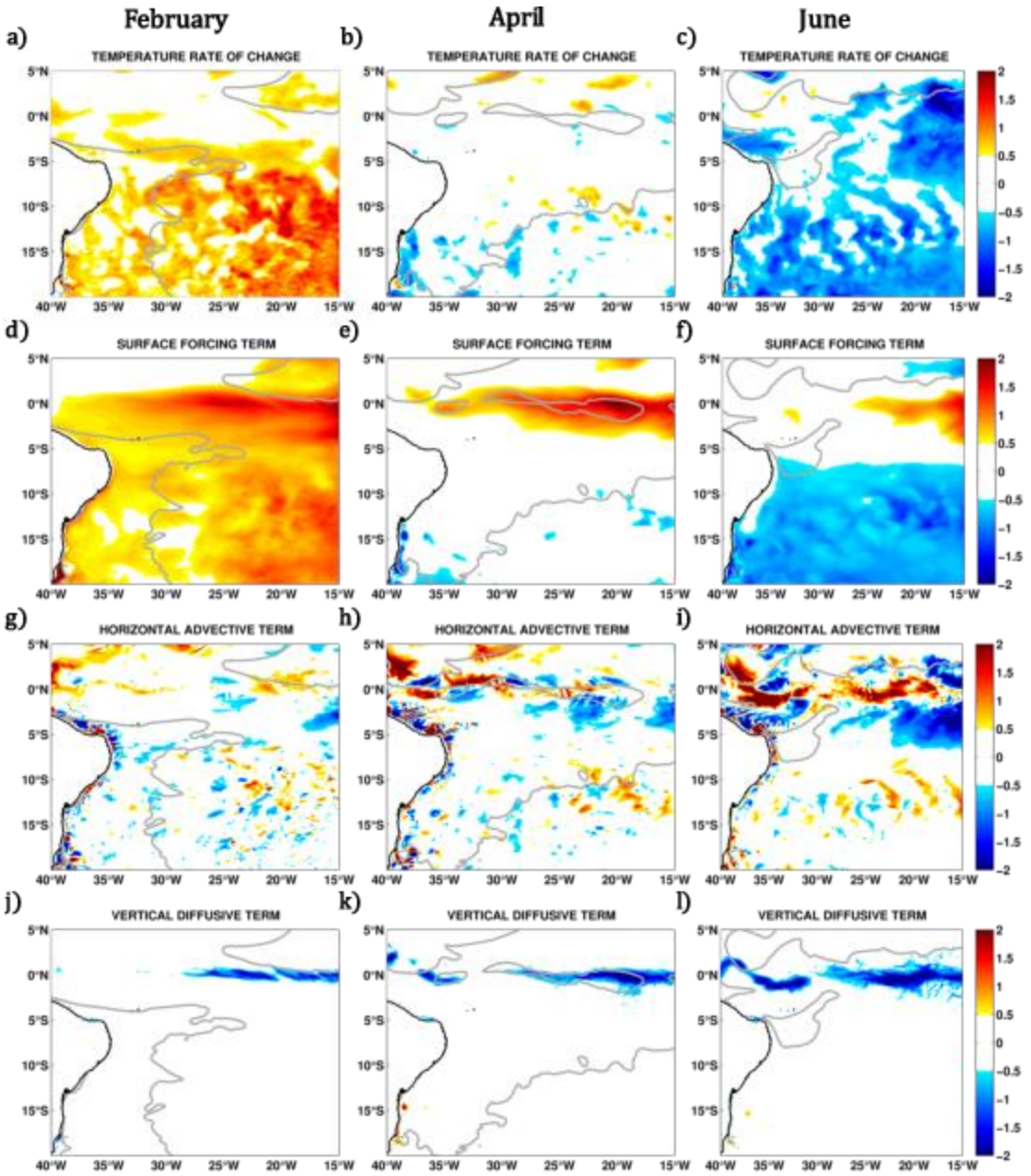

Figura 1. 8 Horizontal mean climatological maps of the temperature tendency terms over the mixed layer (°C.month^{-1}) to February (left), April (middle) and June (right). Letters a to l show the relative importance of the main terms described in equation 1: (a–c) is the temperature rate of change; (d–f) surface forcing; (g-i) horizontal advective term; (j-l) vertical diffusive term. The continuous gray line represents the SWTAWP area as previously illustrated in Figure 7.

The horizontal advective term (Fig. 8, panels g-i) is important near the equator, as noted by Peter et al. (2006). The westward flow of SEC branches contributes to a cooling tendency

(April, May and June), whereas the eastward flow of the EUC is responsible for the warming tendencies between the SEC branches in the same period. The horizontal shear of these currents promotes the strengthening of the vertical diffusive terms (Fig. 8, panels j–l) along the equator. This vertical term contributes to cooling the ocean in regions of more effective action of advection, particularly between these equatorial currents and counter-currents. Away from these regions, the diffusivity is less important and yields values near zero. In June, the general tendency of the rate of temperature change is to cool the ocean and accompany the imposed tendency of the predominant surface forcing term. At this time, the intensification of the trade winds in the tropical Atlantic encourages the advective terms to be stronger, and the westward flow of the SEC is more visible along 3°S. The acceleration of the advective terms in June directly reflects the response of the vertical diffusive term. The action of the diffusivity plus advection in the east-west direction approximately at 3°S seems to overlap the warming conditions imposed by the surface forcing. This finding suggests that the separation of the SWTA heated waters from the warm waters along the Gulf of Guinea is also a consequence of this response.

Therefore, the main responsible term for the seasonal appearance and extinction of the SWTAWP is the net heat flux, which is also the case for the equatorial Atlantic warm pool (Enfield and Lee, 2005) and several other regions in the tropical basin (Foltz et al., 2003; Yu et al., 2006; Servain and Lazar, 2010). The aforecited authors explain that the main contributors to this tendency are the latent heat loss and the energy input from the incoming shortwave radiation.

1. 7. Summary and conclusions

In this study, we considered the heat budget closure provided by a numerical diagnostics and presented a detailed assessment of the evolution of the temperature trends over the Southwestern Tropical Atlantic. A detailed investigation of the occurrence of the seasonal evolution of the Southwestern Tropical Atlantic Warm Pool (SWTAWP) was undertaken, which has a special interest for its involvement in the climate variability over the Northeastern part of Brazil.

The simulation was performed using the ROMS model in the tropical Atlantic, which includes the region of interest. This simulation was configured according to Lemarié et al. (2012), where the vertical resolution was increased to at least 18 levels above 150 m of depth in the upper ocean to provide a better reproduction of the mixed layer (ML) heat content.

From March to May, the SWTAWP attained its maximum development and sometimes merged with equatorial heated waters towards the African continent, whose development followed the same period. Along the equator, the combination of oceanic terms (i.e., advection and diffusion) was important to promote the separation - when it occurred - of equatorial warm waters from southwestern tropical waters, which developed off the Brazilian coast.

The predominance of the surface forcing over the remaining terms (horizontal advection and vertical diffusion) also played a main role in explaining the appearance and extinction of the SWTAWP. Warm waters over the equatorial Atlantic extended their area as far as the SWTA, which was a unique phenomenon along the Atlantic basin during austral autumn. These results contribute to a better understanding of the behavior of the heat content within the tropics, as previous studies over this region (Foltz et al., 2003; Enfield and Lee, 2005; Peter et al., 2006) focused along the equator only.

The seasonal variability of the mean temperature and heat content inside of the ML suggested the predominance of the surface forcing over other terms, such as advection and vertical/horizontal turbulent diffusion, which implied that the atmosphere played an important role over the oceanic terms in determining the temperature inside the ML. From early October to late March, the ML got warmer, whereas the upper ocean got cooler from April to September. The oceanic terms seemed to be opposite to the surface forcing, with the exception of near the ocean currents' core (i.e., SEC branches and EUC), where advective terms were likely to be significant. In other regions where advection was meaningful, the vertical turbulent diffusion was also important and they tend to balance each other. The heat content inside of the ML was higher when this layer was deeper, which seasonally occurred over the SWTA during austral winter. Therefore, the heat storage was modulated by the intensification/relaxation of the wind stress and the vertical transfer of momentum in the upper ocean.

Considering that the warm pool occurrence along the Atlantic equator and the SWTA has a significant impact over the African continent (e.g., Giannini et al., 2003) as well as over the Brazilian northeastern region (e.g., Nobre and Shukla 1996; Hastenrath, 2006; Hounsou-gbo et al., 2015), additional numerical investigations are recommended indeed. This can be achieved through a fully coupled ocean-atmosphere model to scrutinize the air-sea feedback variability over the tropical Atlantic warm pools from seasonal to decadal timescales.

Acknowledgements

We are grateful to the two anonymous reviewers for their useful comments. The first author was supported by a PhD scholarship provided by the Coordination for the Improvement of Higher Education Personnel (CAPES). The second author would like to thank CNPq for the research scholarship (PQ-2, grant #311835/2014-7) and FAPESP (grant #2015/09767-8). The third author is also grateful to CNPq for the grant *Pesquisador Visitante Especial (PVE)* associated with Project *Mudanças Climáticas no Atlântico Tropical (MUSCAT)*, Process 400544/2013-0. FUNCEME (Project BTT FUNCEME/FUNCAP, Edital 10/2013) is acknowledged for its support while J.S. visited Fortaleza, CE, Brazil. This paper is also a contribution to the Projetc *Pólo de Interação para o Desenvolvimento de Estudos Conjuntos em Oceanografia do Atlântico Tropical (PILOTE)*, CNPq-IRD grant 490289/2013-4.

References

Antonov, J.I., Seidov, D., Boyer, T.P., Locarnini, R.A., Mishonov, A.V., Garcia, H.E., Baranova, O.K., Zweng, M.M., Johnson, D.R., 2010. World Ocean Atlas 2009, Volume 2: Salinity. S. Levitus, Ed. NOAA Atlas NESDIS 69, U.S. Government Printing Office, Washington, D.C., 184 pp.

Bourlès, B., Lumpkin, R., McPhaden, M.J., Hernandez, F., Nobre, P., Campos, E., Yu, L., Planton, S., Busalacchi, A., Moura, A.D., Servain, J., Trotte, J., 2008. The Pirata Program: History, Accomplishments, and Future Directions. Bull. Am. Meteorol. Soc. 89, 1111–1125. doi:10.1175/2008BAMS2462.1

Carton, J.A., Giese, B.S., 2008. A Reanalysis of Ocean Climate Using Simple Ocean Data Assimilation (SODA). Mon. Weather Rev. 136, 2999–3017. doi:10.1175/2007MWR1978.1

Casey, K.S., Cornillon, P., 1999. A Comparison of Satellite and In Situ – Based Sea Surface Temperature Climatologies. J. Climate 12, 1848–1863.

Chiang, J.C.H., Sobel, A.H., 2002. Tropical tropospheric temperature variations caused by ENSO and their influence on the remote tropical climate. J. Climate 15, 2616–2631. doi:10.1175/1520-0442(2002)015<2616:TTTVCB>2.0.CO;2

da Silva, A.M., Young, C.C., Levitus, S.,1994. Atlas of surface marine data 1994, Vol. 1, Algotithms and procedures, NOAA Atlas NESDIS 6. U.S. Department of Commerce, NOAA, NESDIS, USA, 74 pp.

de Boyer Montégut, C., Madec, G., Fischer, A.S., Lazar, A., Iudicone, D., 2004. Mixed layer depth over the global ocean: An examination of profile data and a profile-based climatology. J. Geophys. Res. 109, C12003: 1–20. doi:10.1029/2004JC002378

Enfield, D.B., Lee, S.-K., 2005. The Heat Balance of the Western Hemisphere Warm Pool. J. Climate 18, 2662–2681.

Enfield, D.B., Lee, S.-K., Wang, C., 2006. How are large western hemisphere warm pools formed? Prog. Oceanogr. 70, 346–365. doi:10.1016/j.pocean.2005.07.006

Foltz, G.R., Grodsky, S.A., Carton, J.A., 2003. Seasonal mixed layer heat budget of the tropical Atlantic Ocean. J. Geophys. Res. 108. doi:10.1029/2002JC001584

Foltz, G.R., McPhaden, M.J., 2006. The role of oceanic heat advection in the evolution of tropical North and South Atlantic SST anomalies. J. Climate 19:6122–6138. doi: 10.1175/JCLI3961.1

Giannini, A., Saravanan, R., Chang, P., 2003. Oceanic forcing of Sahel rainfall on interannual to interdecadal time scales. Science 302, 1027–30. doi:10.1126/science.1089357

Hastenrath, S., 2006. Circulation and teleconnection mechanisms of Northeast Brazil droughts. Prog. Oceanogr. 70, 407–415. doi:10.1016/j.pocean.2005.07.004

Hounsou-gbo, G.A., Araujo, M., Bourlès, B., Veleda, D., Servain, J., 2015. Tropical Atlantic Contributions to Strong Rainfall Variability Along the Northeast Brazilian Coast. Adv. Meteorol. 1-13. doi:10.1155/2015/902084

Kouadio, Y.K., Servain, J., Machado, L.A. T., Lentini, C.A.D., 2012. Heavy Rainfall Episodes in the Eastern Northeast Brazil Linked to Large-Scale Ocean-Atmosphere Conditions in the Tropical Atlantic. Adv. Meteorol. 2012, 1–16. doi:10.1155/2012/369567

Large, W.G., McWilliams, J.C., Doney, S.C., 1994. Oceanic vertical mixing: A review and a model with a nonlocal boundary layer parameterization. Rev. Geophys. 32, 363–403.

Lemarié, F., Kurian, J., Shchepetkin, A.F., Jeroen Molemaker, M., Colas, F., McWilliams, J.C., 2012. Are there inescapable issues prohibiting the use of terrain-following coordinates in climate models? Ocean Model. 42, 57–79. doi:10.1016/j.ocemod.2011.11.007

Locarnini, R.A., Mishonov, A.V., Antonov, J.I., Boyer, T.P., Garcia, H.E., Baranova, O.K., Zweng, M.M., Johnson, D.R., 2010. World Ocean Atlas 2009, Volume 1: Temperature. S. Levitus, Ed. NOAA Atlas NESDIS 68, U.S. Government Printing Office, Washington, D.C., 184 pp.

Lumpkin, R., Garzoli, S.L., 2005. Near-surface circulation in the Tropical Atlantic Ocean. Deep Sea Res. Part I Oceanogr. Res. Pap. 52, 495–518. doi:10.1016/j.dsr.2004.09.001

Marchesiello, P., Debreu, L., Couvelard, X., 2009. Spurious diapycnal mixing in terrain-following coordinate models: The problem and a solution. Ocean Model. 26, 156–169. doi:10.1016/j.ocemod.2008.09.004

Molinari, R.L., Johns, E., 1994. Upper layer temperature structure of the western tropical Atlantic. J. Geophys. Res. 99 (C9): 18225-18233. doi: 10.1029/94JC01204

Moura, A.D., Shukla, J., 1981. On the Dynamics of Droughts in Northeast Brazil: Observations, Theory, and Numerical Experiments with a General Circulation Model. J. Atmos. Sci. 38, 2653–2675.

Nobre, P., Shukla, J., 1996. Variations of Sea Surface Temperature , Wind Stress and Rainfall over the Tropical Atlantic and South America. J. Climate 9, 2464–2479.

Penven, P., Marchesiello, P., Debreu, L., Lefèvre, J., 2008. Software tools for pre- and post-processing of oceanic regional simulations. Environ. Model. Softw. 23, 660–662. doi:10.1016/j.envsoft.2007.07.004

Peter, A.-C., Le Hénaff, M., du Penhoat, Y., Menkes, C.E., Marin, F., Vialard, J., Caniaux, G., Lazar, A., 2006. A model study of the seasonal mixed layer heat budget in the equatorial Atlantic. J. Geophys. Res. 111, C06014. doi:10.1029/2005JC003157

Servain, J., Lazar, A., 2010. Ocean Dynamics Contribution to Seasonal Mixed Layer Heat Budget in the Tropical Atlantic, In: Servain, J., Campos, J.N.B., Martins, E.S.B.R., Reis Jr, D.S. (Eds.), Clima do Atlântico Tropical e Impactos Sobre o Nordeste (CATIN). Editora Ronda, 392 pp.

Servain, J., Busalacchi, A.J., Mcphaden, M.J., Moura, A.D., Reverdin, G., Vianna, M., Zebiak, S.E., 1998. A Pilot Research Moored Array in the Tropical Atlantic (PIRATA). Bull. Amer. Meteor. Soc. 79, 2019–2031.

Shchepetkin, A.F., 2005. If-less KPP. ROMS/TOMS Workshop: Adjoint Modeling and Applications, La.Jolla, CA, October 24-28 http://www.myroms.org/Workshops/ROMS2005/Nonlinear/AlexanderShchepetkin.pdf.

Shchepetkin, A.F., Mcwilliams, J.C., 2003. A Method for Computing Horizontal Pressure-Gradient Force in an Oceanic Model with a Non-Aligned Vertical Coordinate. J. Geophys. Res. 108. doi:10.1 029/2001JC001047

Shchepetkin, A.F., McWilliams, J.C., 2005. The regional oceanic modeling system (ROMS): a split-explicit, free-surface, topography-following-coordinate oceanic model. Ocean Model. 9, 347–404. doi:10.1016/j.ocemod.2004.08.002

Shchepetkin, A.F., Mcwilliams, J.C., 2008. Computational Kernel Algorithms for Fine-Scale , Multi-Process , Long-Time Oceanic Simulations. Handb. Numer. Anal. 14, 121–183. doi:10.1016/S1570-8659(08)01202-0

Silva, M., Araujo, M., Servain, J., Penven, P., 2009. Circulation and heat budget in a regional climatological simulation of the southwestern tropical Atlantic. Trop. Oceanogr. 39, 41-57.

Smith, R.D., Dukowicz, J.K., Malone, R.C., 1992. Parallel ocean general circulation modeling. J. Phys. D: Appl. Phys. 60, 38–61.

Smith, W.H.F., Sandwell, D.T., 1997. Global seafloor topography from satellite altimetry and ship depth soundings. Science. 277, 1957-1962.

Taylor, M.A., Enfield, D.B., Chen, A.A., 2002. Influence of the tropical Atlantic versus the tropical Pacific on Caribbean rainfall. J. Geophys. Res. 107, 3127. doi:10.1029/2001JC001097

Wang, C., Enfield, D.B., 2001. The tropical Western Hemisphere warm pool. Geophys. Res. Lett. 28, 1635–1638.

Wang, C., Enfield, D.B., 2003. A Further Study of the Tropical Western Hemisphere Warm Pool. J. Climate 16, 1476–1493.

Xie, S.P., Carton, J. A., 2004. Tropical Atlantic variability: Patterns, mechanisms, and impacts. Geophys. Monogr. Ser. 147, 121–142. doi:10.1029/147GM07

Yu, L., Jin, X., Weller, R. A., 2006. Role of Net Surface Heat Flux in Seasonal Variations of Sea Surface Temperature in the Tropical Atlantic Ocean. J. Climate 19, 6153-6169

CAPÍTULO 2

Seasonal to interannual evolution of the Southwestern Tropical Atlantic Warm Pool and Equatorial Warm Pool

Evolução sazonal para interanual da piscina quente do Atlântico tropical sudoeste e piscina quente equatorial

Revista pretendida: **Ocean Modelling**, ISSN (1463-5003), Fator de impacto = 2.92, Qualis CAPES = A1

Marcio Cintra [a], Carlos A. D. Lentini [b], Eduardo Marone [a]

[a] Centro de Estudos do Mar, CEM, Universidade Federal do Paraná (UFPR), Av. Beira Mar s/n, 83255-000, Pontal do Paraná PR, Brazil

[b] Departamento de Física da Terra e do Meio Ambiente da Universidade Federal da Bahia (UFBA), Campus Ondina, 40170-280, Salvador BA, Brazil

Abstract

This study analyzes the thermodynamic development of the southwestern tropical Atlantic warm pool (SWTAWP) and the Equatorial warm pool (EQWP). A high resolution numerical simulation with the temperature diagnostic terms was used to describe the main features of these warm pools. The warm pools were delimited by the 28 °C isotherm over the tropical Atlantic. The SWTAWP has its development during the austral autumn and usually is observed merged with the EQWP in April. During this time, the southernmost position of the intertropical convergence zone (ITCZ) provides conditions to high values of sea surface temperature (SST) can be observed along the equator. We observed that the SWTAWP and the EWP are controlled through the dominance of the surface forcing term, which means that they result from the energy provided by the net heat flux at surface. Although the net heat flux plays a dominant role in the

development and extinction of the WPs over this region, they result from different compositions between the incoming solar radiation and the losses through the latent heat flux. In the austral autumn, the southwestern tropical Atlantic has intensified winds, which results in a deepening of the mixed layer and confers increased heat content inside this layer in relation to the shallower layer of the equator. The SWTAWP presented heat content values of about 45 $GW.m^{-2}$, and the analysis of the oceanic temperature trends over the mixed layer revealed that this stored heat is mainly drained through the action of the horizontal advection, especially near the Brazilian coast. In contrast, the dominant oceanic term over the EWP is the vertical oceanic term, which is mainly controlled by the vertical diffusion. We conclude that the SWTAWP and EWP are two different regions thermodynamically. These regions are differently forced by the atmosphere, and the oceanic response also indicates distinguished regions.

Keywords: air-sea interactions, interannual variability, temperature tendency terms, mixed layer, heat budget, warm anomalies,

Resumo

Este estudo analisa o desenvolvimento termodinâmico da piscina quente do Atlântico sudoeste (PQATSO) e da piscina quente Equatorial (PQE). Uma simulação numérica de alta resolução, com os termos de diagnóstico de temperatura, foi utilizada para descrever as principais características destas piscinas quentes. As PQs foram delimitadas pela isoterma de 28 °C sobre o Atlântico tropical. A PQATSO tem o seu desenvolvimento durante o outono austral e em Abril, geralmente é observada fundida com a PQE. Durante este período, a posição mais ao sul da zona de convergência intertropical (ZCIT) proporciona condições para que altos valores de temperatura da superfície do mar (TSM) possam ser observados ao longo do equador. Nós observamos que a PQATSO e a PQE são controladas pelo domínio do forçante superficial, o que significa que elas resultam da energia fornecida pelo fluxo de calor líquido à superfície. Embora o fluxo de calor líquido desempenhe um papel dominante no desenvolvimento e extinção das PQs sobre esta região, estas resultam de uma composição diferente entre a radiação solar incidente e as perdas através do fluxo de calor latente. No outono austral, os ventos se intensificam no Atlântico tropical sudoeste, o que resulta em um aprofundamento da camada de

mistura e confere o aumento do conteúdo térmico no interior dessa camada em relação à camada equatorial, mais rasa. A PQATSO apresentou valores de conteúdo térmico de cerca de 45 $GW.m^{-2}$, bem como a análise das tendências de temperatura oceânica sobre a camada de mistura revelou que este calor armazenado é drenado principalmente através da ação da advecção horizontal, especialmente perto da costa brasileira. Em contraste, o termo oceânico dominante sobre a PQE é o termo oceânico vertical, que é controlado principalmente pela difusão vertical. Nós concluímos que a PQATSO e a PQE são duas regiões diferentes termodinamicamente. Estas regiões são forçadas diferentemente pela atmosfera, e a resposta oceânica também indica áreas distintas.

Palavras chave: interações oceano-atmosfera, variabilidade interannual, termos de tendência da temperatura, camada de mistura, orçamento de calor, anomalias quentes

2. 1. Introduction

The north–south displacement of the Atlantic intertropical convergence zone (ITCZ) reaches its maximum variance during the austral autumn. Its impact in the autumn [March to May (MAM)] brings consequences to rainfall over the Brazilian northeast region (Nobre and Shukla, 1996; Taylor et al., 2002). A recent study of Hounsou-gbo et al. (2015) pointed out that the presence of a warm pool (WP) over the southwestern tropical Atlantic has strong impact over the Brazilian northeast region rainfall. During the austral autumn, the western equatorial Atlantic basin is characterized by the presence of the WP, a zone where sea surface temperatures (SST) exceed 28°C. The so-called Southwestern Tropical Atlantic Warm Pool (SWTAWP) (Huang et al. 1995; Silva et al. 2009, Hounsou-gbo et al. 2015, Cintra et al. 2015) extends off the Brazilian coast to middle basin and from about 15°S to the north hemisphere. These warm waters were also reported by other authors (Enfield and Lee 2005; Enfield et al. 2006) as the equatorial warm pool (EQWP). In the months when this phenomenon is best developed, the warm waters from southwestern Atlantic merge with the heated waters of the eastern equatorial Atlantic, extending throughout the basin. Enfield and Lee (2005) highlighted the importance of the western hemisphere warm pools (WHWP) as a player in the Walker and Hadley circulations of the western hemisphere. The WHWP contributes to replacing the austral summer convective center over tropical South America as the winter heat source for the western hemisphere tropics.

Previous studies have pointed out that the WP has a significant annual cycle and interannual variation in the area and the intensity. The annual and interannual variations of the WP are associated with the seasonal changes in tropospheric moisture, stability and heat, resulting in the various air–sea interaction systems (Wang and McPhaden, 2000; Enfield et al. 2006; Lin et al. 2011).

Considering the lack of data over the Southwestern Tropical Atlantic (SWTA) we decided to use a numerical approach to investigate the thermodynamics of this region focusing on the analysis through the heat budget terms responsible to the onset and decay of the SWTAWP. Possible thermodynamic distinctions of the SWTAWP to the EQWP will be discussed, if they exist. An interannual simulation over the TA was used to provide the temperature tendency terms which are analyzed through the mixed layer of the upper ocean. After describing the used model and model configuration (Section 2), in Section 3 we present some details of the data set in the model validation, which comprises in situ observations from mooring buoys, satellite data and diagnostic model output. Section 4 provides the model evaluation, which includes the validation of the surface currents inside the mixed layer, SST, subsurface temperature and mixed layer depth. The SWTAWP and its main thermodynamic features are presented in Section 5. In the last Section we summarize and present the conclusions.

2. 2. Model description

The numerical model in this study is the Regional Ocean Modeling System (ROMS), which was developed by Shchepetkin and McWilliams (2003; 2005; 2008). This model is a free surface ocean model that solves primitive equations in an Earth-centered rotating environment based on the classical Boussinesq approximation and hydrostatic vertical momentum balance (Shchepetkin and McWilliams, 2005). To prevent spurious diapycnal mixing, the rotated split upstream-biased advection scheme proposed by Marchesiello et al. (2009) is employed, with implementations proposed by Lemarié et al. (2012), which enable this scheme to rotate the hyperdiffusive part in the neutral direction and increase its stability. Unresolved vertical subgrid-scale processes are parameterized by an adaptation of the nonlocal K-profile planetary boundary

layer scheme (Large et al., 1994), which is modified by the scheme proposed by Shchepetkin (2005).

The model grid, forcing, and initial and boundary conditions were constructed using ROMSTOOLS (Penven et al., 2008).The model grid, forcing, initial and boundary conditions were built using the ROMSTOOLS (Penven et al., 2008). The model was forced by inter-annual wind stress, heat and freshwater fluxes derived from the NCEP/NCAR reanalysis products (R-2). These datasets (Kanamitsu et al., 2002) are available at 1.875°×1.875° resolution and at 6-hourly timescale. The data can be obtained from http://www.esrl.noaa.gov/psd/data/gridded/data.ncep.reanalysis2.gaussian.html. The parameters obtained from NCEP are air temperature at 2m height, zonal and meridional components of winds at 10m height, specific humidity of air at 2m, and net short-wave and long-wave radiation at sea surface. These data were connected to the model through a bulk flux parameterization (Liu et al., 1979) and the COARE algorithm of Fairall et al. (1996). The SST was defined in the model with the new prognostic scheme developed by (Zeng and Beljaars, 2005).

The initial and lateral boundary conditions (temperature, salinity, sea surface high, zonal and meridional velocities) were imposed from a monthly mean (2000-2010) data of Simple Ocean Data Assimilation (SODA – version 2.2.4) reanalysis which has 1/2 of horizontal resolution (Carton and Giese, 2008). Despite of we are using reanalysis data, a flag (obc_volcons) was used to ensure the conservation of mass inside do simulated domain. This flag computes the integral of mass flux at the open boundaries which is needed to enforce global mass conservation constraint through a correction in barotropic mass flux. The vertical discretization of the grid was constructed using a hybrid z – σ coordinate system obtained by relaxing the z- coordinate system toward the σ – coordinate (Shchepetkin and McWilliams, 2008; Lemarié et al., 2012).

The model domain ranged from 43^{o} W to 5^{o} W and 20^{o} S to 28^{o} N, resulting in 297 X 227 points with 1/6° (~18 km) in horizontal resolution and 40 vertical levels (θ_s = 10 , θ_b = 2, hc = 200). Explicit lateral viscosity is null everywhere in the model, except in sponge layers near the open boundaries where it increases smoothly on 10 grid points. We perform the time integration of the simulation with a time step of 800s, starting at year of 2000 and finishing at 2010. The model run for 2 years to reach a spin-up state, after that, the model integration was considered in

steady state, when the total kinetic energy oscillated quasi-periodically around an equilibrium state (not shown).

One of our goals is to measure the relative contribution of the temperature tendency terms over the onset and decay of the SWTAWP. We employed the temperature diagnostic outputs of the ROMS model to evaluate the heat budget terms. These outputs are initially expressed in °C.s^{-1} and are presented in this section (Eq. 1). To facilitate this discussion, we use quantities, which are summed or integrated over a month. The trends will be expressed in °C.month^{-1}.

$$\frac{\partial T}{\partial t} = \vec{u}\frac{\partial T}{\partial x} + \vec{v}\frac{\partial T}{\partial y} + \vec{w}\frac{\partial T}{\partial z} + K_h\left(\frac{\partial^2 T}{\partial x^2} + \frac{\partial^2 T}{\partial y^2}\right) + K_v\left(\frac{\partial^2 T}{\partial z^2}\right) + \Phi_T \qquad (1)$$

where T is the temperature, t is the time evolution, $\vec{u}$, $\vec{v}$ and $\vec{w}$ are the velocity components for the x, y and z directions, respectively, Φ_T represents the net heat flux used to force the model plus nudging, and K_h and K_v are the diffusion coefficients for the horizontal direction and vertical direction, respectively.

2. 3. The data sets for model validation

2. 3.1. Mooring data

The Prediction and Research moored Array in the Tropical Atlantic -PIRATA (Servain et al., 1998; Bourlès et al., 2008) data was used to validate the model's temperature in the first 200 m of depth. The PIRATA program is an ocean-meteorological observing system which contributes to the operational climate survey of the global ocean. Three buoys of this project are positioned at the southwestern tropical Atlantic and are called PIRATA-SW, whose the main goal is helping in the forecast of the Brazilian climate, especially over the Northeast Brazilian region. We choose 9 buoys to perform this validation (Fig. 2), being 3 located at the South Atlantic (8 S 30 W, 14 S 32 W, 10 S 10 W), 3 from the equator (0 10 W , 0 23 W and 0 35 W) and 3 positioned at the north Atlantic (8 N 38 W, 15 N 38 W and 12 N 23 W). The comparisons were performed from 2000 to 2010. The PIRATA data can be downloaded at no cost from the NOAA/PMEL website (www.pmel.noaa.gov/pirata). All-time series of these data were processed as monthly means, where the flawed data were removed. Vertical interpolations were

processed on the PIRATA data when only one out of three consecutive temperature sensors along the moored line was dysfunctional.

2.3.2. Satellite data

For the SST and SWTAWP coverage area inter-comparisons we used the L4 product from the National Oceanic and Atmospheric Administration (NOAA) Optimum Interpolation SST (OISST) version 2 data set (Reynolds et al., 2007). These data have been made available by the NOAA Earth System Research Laboratory Physical Science Division (ESRL/PSD) through their web site at http://www.esrl.noaa.gov/psd/ . These are daily SST records (one daily value for each pixel), with spatial resolution of 0.25 × 0.25°, based on the Advanced Very High Resolution Radiometer (AVHRR) infrared satellite measurements (Pathfinder data in September 1981 through December 2005; operational AVHRR from January 2006). The final data set has been derived using satellite SST retrievals, SST observations from ships and buoys, and proxy SSTs generated from sea ice concentrations. Full description of data processing methods and comparisons between the NOAA OISST SST and in situ data can be found in Reynolds et al. (2007) and at www.ncdc.noaa.gov/sst/description.php. In this study we perform comparisons between the model and the OISST considering the simulation time (2000-2010).

2. 3. 3. Surface currents comparison data set

In this study, we employed surface velocities from the SCUD (Maximenko and Hafner, 2010) program provided by the Asia Pacific Data Research Center/International Pacific Research Center (APDRC/IPRC). The Surface CUrrents from Diagnostic Model (SCUD) data set comprises nearly global and daily surface velocities as a result of a simple diagnostic model that combines three sources of scientific information: (i) geostrophic components produced by the sea level anomaly from the Archiving Validation and Interpretation of Satellite Data in Oceanography (AVISO) project (www.aviso.oceanobs.com/duacs/) and mean dynamic ocean topography from Maximenko et al. (2009); (ii) wind-driven components using satellite daily winds from the Quick Scatterometer (QuikSCAT - http://www.remss.com/missions/qscat); and (iii) drifter trajectories, which provide consistent data for tuning the diagnostic model. SCUD

surface velocities are daily gridded with 1/4° of spatial resolution. This data set can be downloaded at no cost from the Asia-Pacific Data Center web site http://apdrc.soest.hawaii.edu/datadoc.scud.php.

2. 4. Model validation

An intercomparison between the model and the data sets is performed. They include the surface currents, the SST, the temperature vertical structure and the ML depth.

Autumn mean surface currents from the SCUD dataset (Fig. 2.1a), was compared with the ROMS numerical currents (Fig. 2.1b). The spatial structure of the surface currents are in good agreement, the numerical results were able to reproduce the westward weak flows of the North Equatorial Current (NEC) around 16 N and the southern branch of the South Equatorial Current (SEC) over 16 S. The classical equatorial surface current system is well defined in our numerical results. From north to south, there are the flows of the eastward North Equatorial Countercurrent (NECC) and the westward SEC. The SEC is clearly separated into northern and central branches with a minimum over the equator.

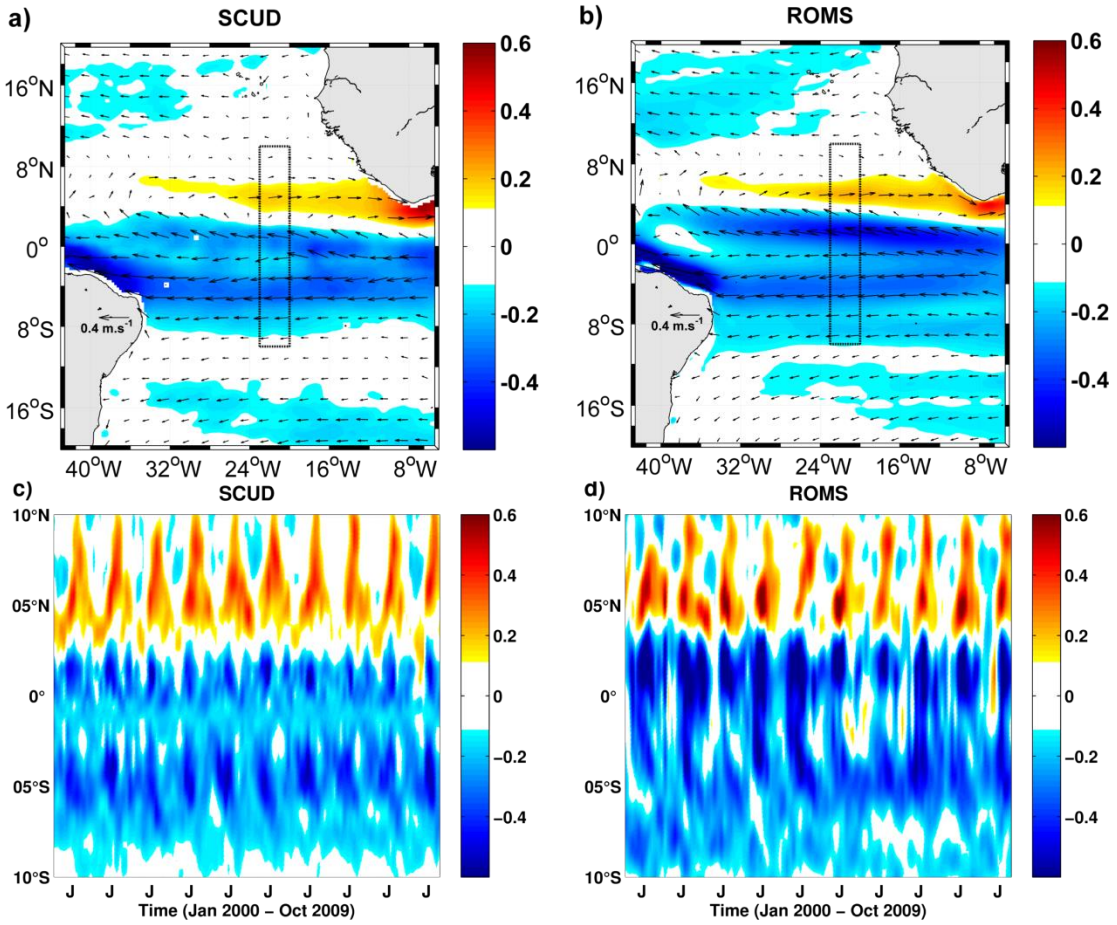

Figure 2. 1 Comparison of the surface currents. a) autumn mean (2000-2009) of the zonal component of velocity (m.s^{-1}) from SCUD and b) from ROMS model. The dashed dotted black line represents the position where a longitudinal mean were processed (3° of longitude) to present the Hovmoller diagrams in c) from (SCUD) and in d) from ROMS model

The interannual variations of the main equatorial surface currents (e.g. NECC and SEC) were evaluated over a delimited area (10°S – 10°N, 20°W – 23°W) at the TA. The time evolution (2000 - 2009) of these currents presented slightly accelerated in numerical results (Fig. 2.1d) in comparison with the surface currents of the SCUD program (Fig. 2.1c). The largest errors, around |0.4| m.s^{-1}, occurred between 0° and 2°N inside the northern branch of SEC and are associated with the austral winter acceleration of the surface currents in response to winds intensification. However, the relaxations/intensifications during the analyzed period were in acceptable match.

The numerical SST was evaluated through comparison with the NOAA OISST satellite derived dataset. The SST numerical errors (ROMS - OISST) and the WP limits (SST > 28 °C)

over the TA (Fig. 2.2) were evaluated along the entire simulated period (2000 to 2010) considering only the April's month, because the WP is generally best developed at this time of year.

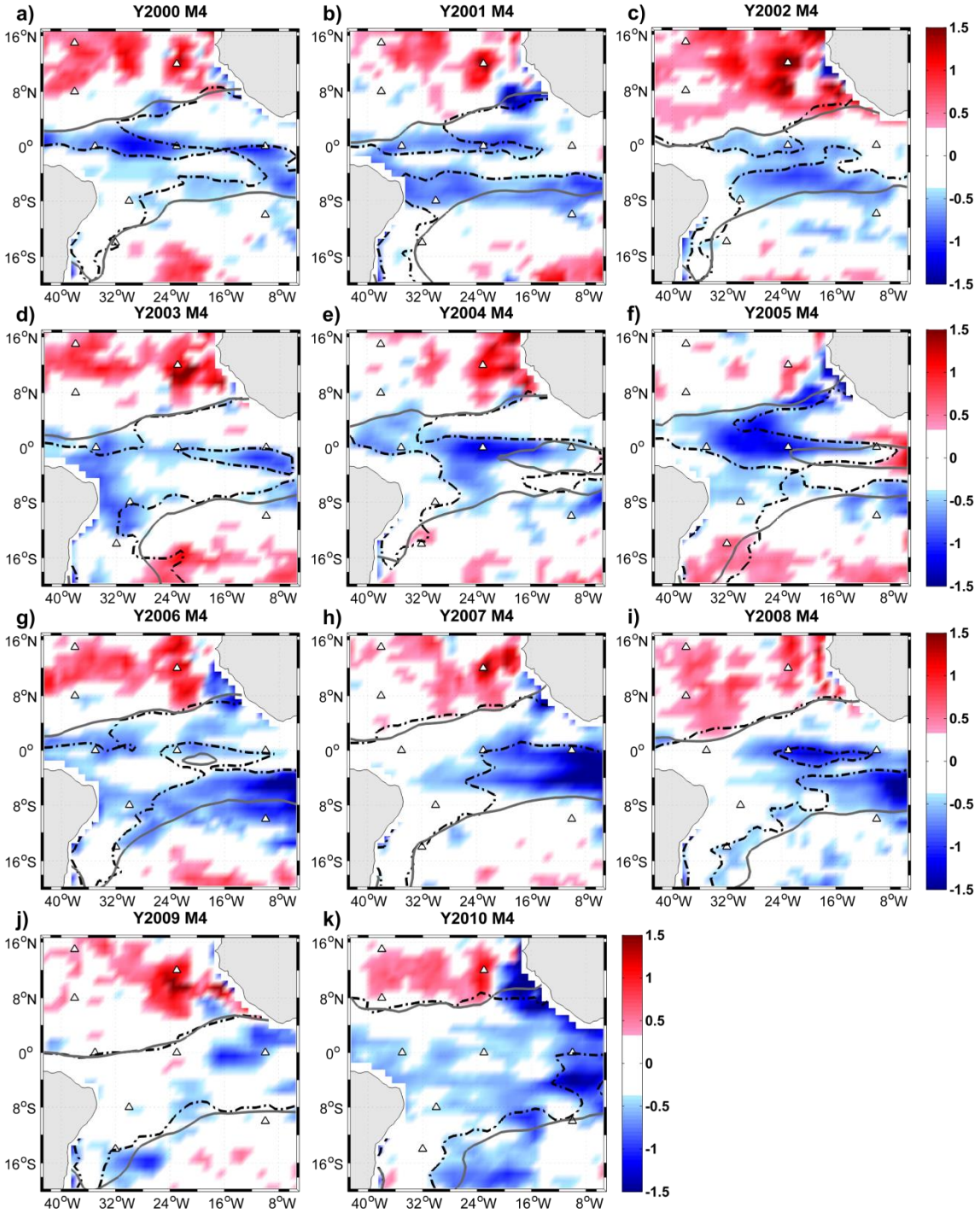

Figure 2. 2 SST error (ROMS – NOAA OISST) superimposed of the SWTAWP limits (temperature > 28 °C). The gray continuous line represents the WP limit from NOAA OISST while the dashed black line is from ROMS model. The white triangles represent the PIRATA moored positions used to evaluate the subsurface temperature

Generally, the numerical SST spatial distribution was well represented over the TA, however near the equator, the modeled SST presented colder than the satellite measurements, resulting in an underestimation of the WP area over this region. The largest errors over the WP reproduction were seen around the eastern boundary of the simulated domain, near the cold tongue region, especially for the years of 2006 to 2008 (Fig. 2.2, panels g-i). Positive SST errors were often observed to the north of 6°N and occasionally near the south boundary of the domain, but in both cases, outside the WP limits.

Figure 2.3 presents the first 200 m of the vertical temperature structure in the model in association with temperatures from the PIRATA measurements. The numerical results were able to reproduce the tightening of the thermocline for the equatorial PIRATA sites (Fig. 2.3 d, e, f) as well as the sinking and relaxation of the vertical gradient in response to displacement away from the equator for the southwestern areas (Fig. 2.3 g, h) and northwestern areas (Fig. 2.3 a, b).

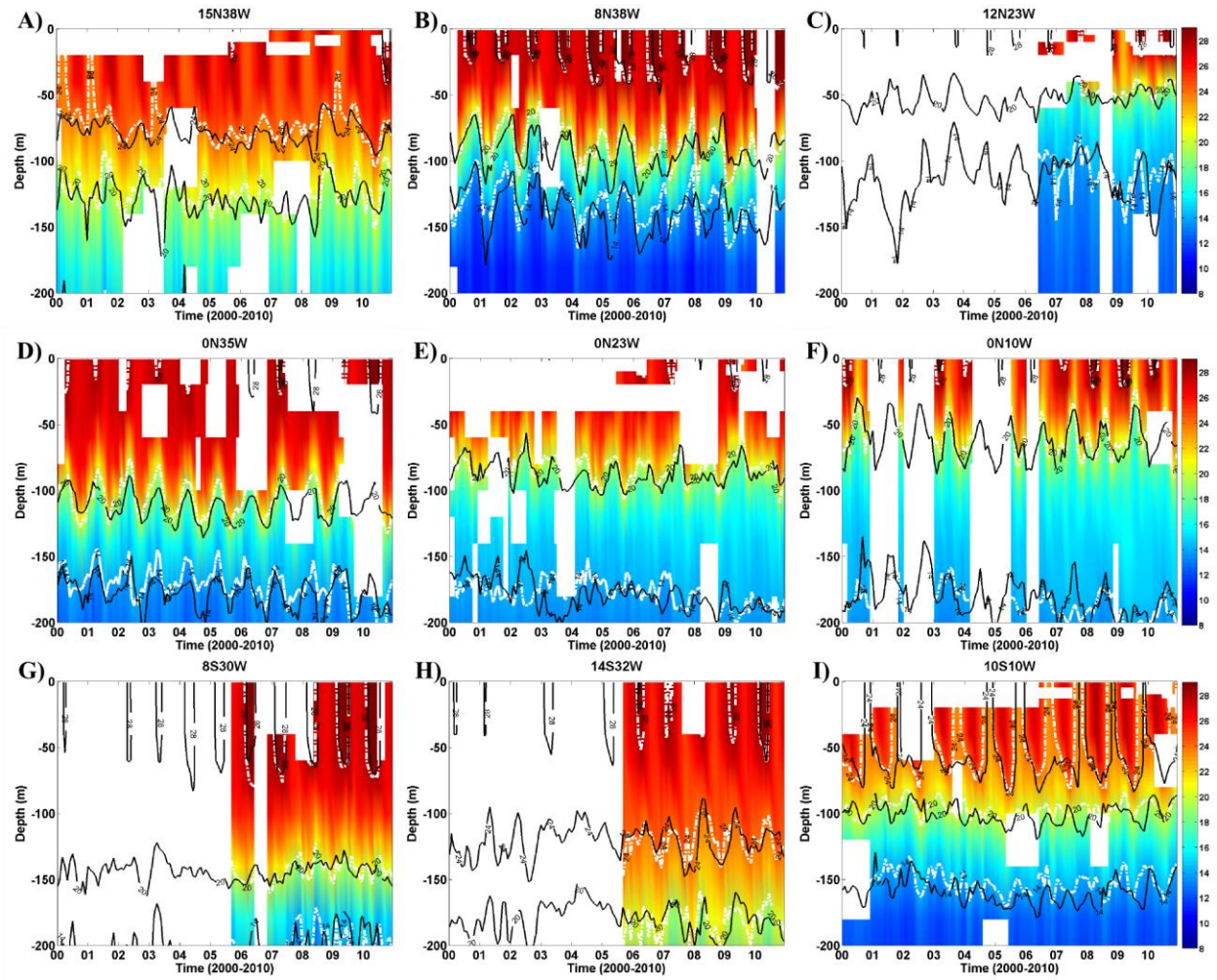

Figure 2. 3 Subsurface temperature comparisons between numerical (ROMS) and observed (PIRATA) data. The comparisons comprise the upper 200m of depth from January 2000 to December 2010. The model-derived temperature is represented by black contours and the PIRATA observed temperature appears as white contours and shaded colors. Panels A) to C) are the north Atlantic comparisons, being 15°N 38°W, 8°N 38°W and 12°N 23°W respectively. Panels D) to F) are the equatorial Atlantic comparisons, being 0° 35°W, 0° 23°W and 0° 10°W, respectively. Panels G) to I) are the south Atlantic comparisons, being 8°S 30°W, 14°S 32°W and 10°S 10°W, respectively

In 8°N 38°W (Fig. 2.3b) and in 8°S 30°W (Fig. 2.3g) the time evolution of the 28°C isotherm was very well reproduced by the model. The 20°C isotherm had variations around 100m of depth at the 0° 35°W and these variations (seasonal and inter-annual signs) submerge until reach the 180m of depth at 14°S 32°W (Fig. 2.3h). Although the largest errors were observed in the thermocline zone (reaching 2.5°C in some displacements), this region and its variations reach a satisfactory numerical reproduction.

Considering that the main variables analyzed in this work (e.g. heat budget terms) consist of mean inside the mixed layer (ML), we validated the numerical mixed layer depth (MLD) performing a comparison between the ROMS and PIRATA (Fig. 2.4). The MLD was defined using the temperature threshold criterion with ΔT = -0.5 °C compared to the SST. This method was successfully used in a wide range of timescales (Foltz et al. 2003; Zhang and McPhaden 2010) and was also used for WP evaluation by (Enfield and Lee 2005, Cintra et al., 2015).

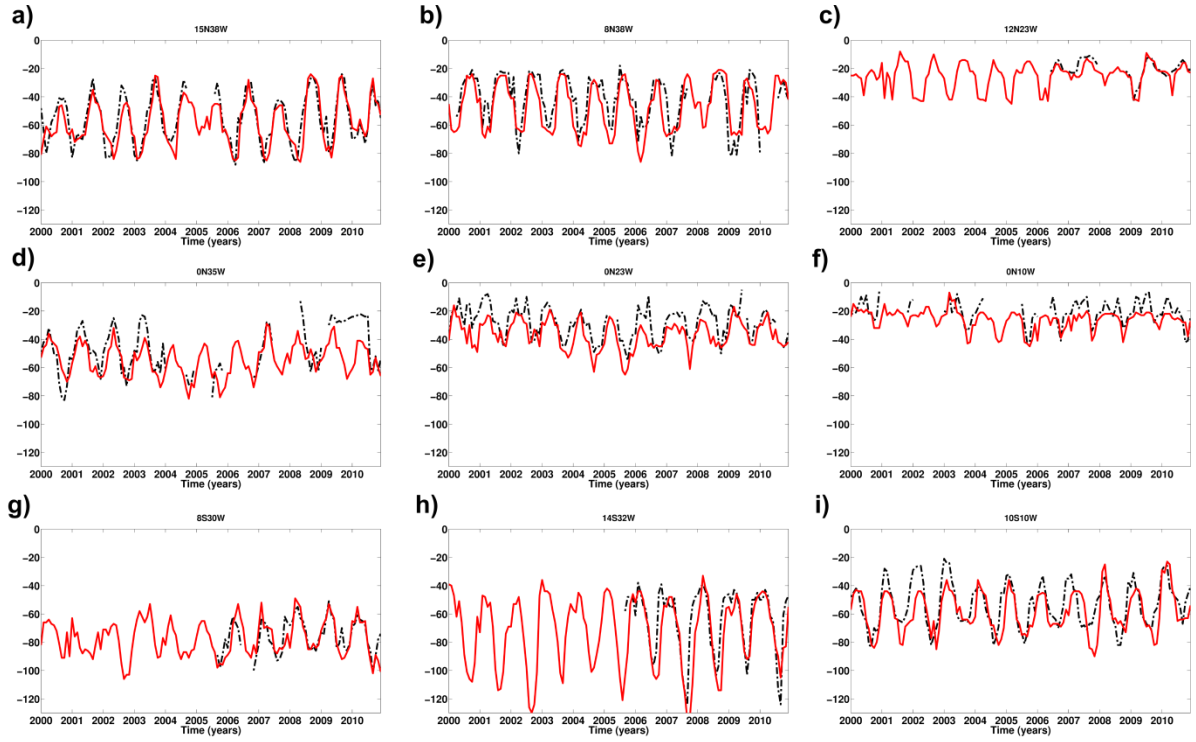

Figure 2. 4 MLD comparisons between ROMS (red solid line) and PIRATA (black dash dotted line). Panels a) to c) are the north Atlantic comparisons, being 15°N 38°W, 8°N 38°W and 12°N 23°W respectively. Panels d) to f) are the equatorial Atlantic comparisons, being 0° 35°W, 0° 23°W and 0° 10°W, respectively. Panels g) to i) are the south Atlantic comparisons, being 8°S 30°W, 14°S 32°W and 10°S 10°W, respectively

The vertical position of the ML was well represented numerically. Assessing the comparisons made in the 38°W positions (Fig. 2.4 a,b), a very good reproduction of the MLD can be verified. At the three PIRATA sites over the equator, the shallower MLD at the eastern basin in contrast with the westward deepening was well reproduced by the model (Fig. 2.4, panels d-f). While at 0° 10°W the MLD oscillated around 25m of depth at 0° 35°W its variation was around the 60m of depth. At the PIRATA sites where it wasn't possible to evaluate the

entire simulated period (e.g. 8°S 30°W; 14°S 32°W; 12°N 23°W), comparisons with the numerical data were also satisfactory, taking into account the average position of oscillation of MLD. Some numerical MLD displacements (10m) relative to observed data were found in the equatorial positions (Fig. 2.4 panels d-f) and in 10°S 10°W (Fig. 2.4i), most verified between August and December, however without compromising the proper validation of numerical data.

2.5. Thermodynamic features and time evolution of the SWTAWP and EQWP

Considering that the SWTAWP and EQWP has its occurrence linked to the seasonal variations over the TA which results in its best development over the austral autumn, we began with an examination of the autumn mean SST, MLD, depth of the 20°C isotherm, latent heat and short wave radiation fluxes and winds in the tropical Atlantic. SST reaches a maximum just north of the equator with a poleward decrease that is strongest in the eastern half of the basin (Fig. 2.5a).

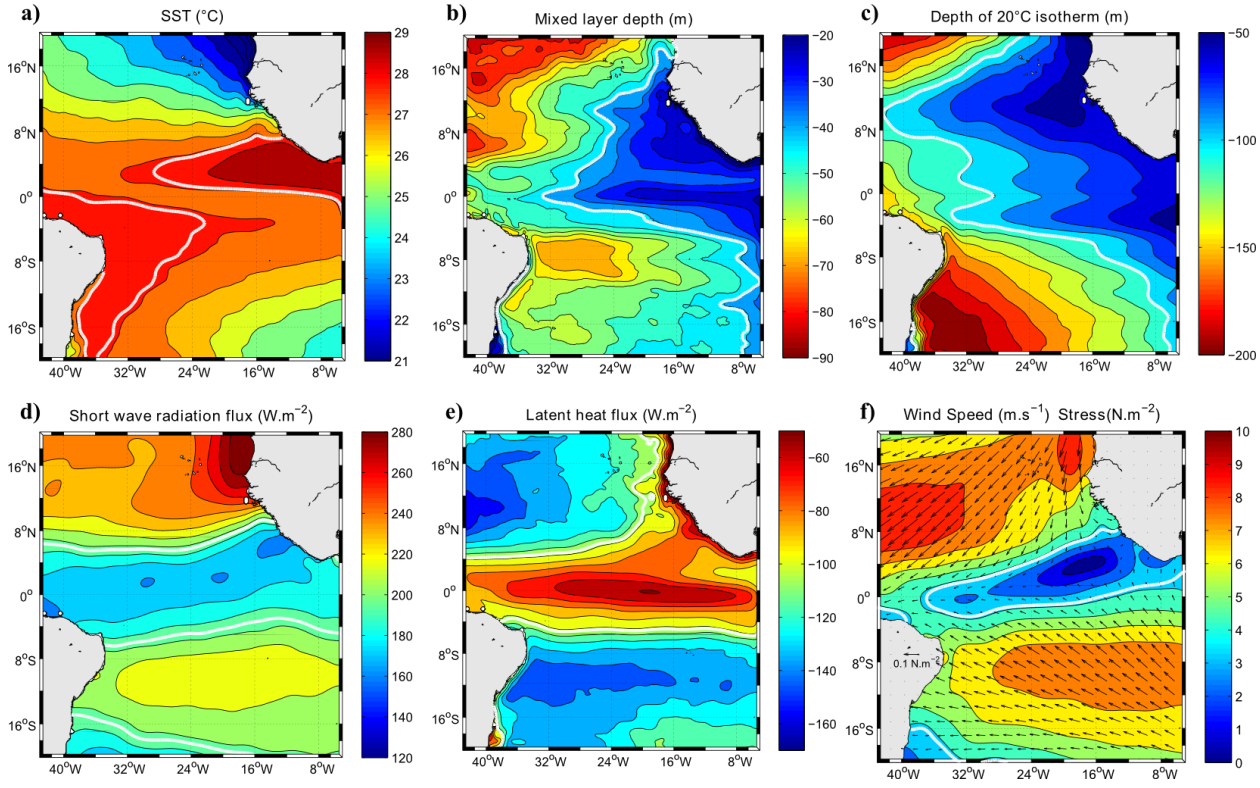

Figure 2. 5 Autumn mean (2000–2010) of a) SST; b) MLD; c) Depth of the 20°C isotherm; d) Surface shortwave radiation (> indicates heat gain by the ocean); e) Latent heat flux (< indicates heat loss by the ocean) and f) wind speed (contours) and stress (vectors)

The SWTAWP comprehends the warm waters (e.g. temperatures > 28°C) off the Brazilian coast from 20°S to equator, while the EQWP is also identified at the seasonal mean exhibit heated waters from the Guinea Gulf over the equator to 30°W.

The MLD and the depth of the isotherm of 20°C, which is representative of the thermocline depth (Molinari and Johns, 1994), presented similar patterns as expected (Fig. 5 b, c). To the south of 20°N, the gradient in East-West direction predominates in the basin, with shallower values verified near the African coast and on the equator, more specifically in the region of actuation of the cold tongue. In contrast, the deepest values were verified poleward of 10° N at the western domain. The MLD presented a single pattern over the southern tropical Atlantic, where the deepest values occurred over a region between 5°S to 10°S, off the Brazilian coast.

The net surface heat flux consists of the balance of the energy which comes from the sun through shortwave radiation (Q_{sw}) and the losses through net longwave radiation (Q_{lw}) emitted from the sea surface and latent and sensible heat fluxes (Q_{lat} and Q_{sen}, respectively). The lowest values of Q_{sw} were observed along the equatorial region (Fig. 2.5d), possibly connected with the mean position of the ITCZ during the austral autumn (Fig. 2.5f). The Q_{sw} values grow to 220 Wm^{-2} in the region between 10°N and 20°N as well as between 5°S and 20°S. The highest values were observed north of 12°N near the African coast. The Q_{lat} distributions (Fig. 2.5 e), showed less intense flows inside the cold tongue region, with lower value of -35 Wm^{-2}, however these flows are intensified outside the equatorial region reaching -160 Wm-2 in the central southern tropical gyre. Figure 5f presents the austral autumn patter (March-April-May mean) of the winds at surface. The zone of convergence of winds (ITCZ) can be easily noted from the African coast to mid-basin around 2-5°N. This region presented weaker winds over the eastern basin with more intense winds at the western basin. At the STA intensified southeast trades are present bring moisture to the South America continent. The presence of the ITCZ maintains a zone of weaker winds and strong convergence (the doldrums) at the junction between the south-easterly trade winds, which affect the southern part of the basin, and the north-easterly trade winds in the northern part. The seasonal migration of the ITCZ results in a seasonal reinforcement of the south-easterlies in austral summer, when the ITCZ reaches its northernmost position.

Conversely, a reinforcement of the north-easterlies is observed in the northern hemisphere when the ITCZ reaches its southernmost position (Barreiro et al. 2004).

Although the seasonal cycle of the atmospheric and oceanic forcings prevails over the TA, the interannual variations cannot be neglect. We perform area integration over the WP region without any distinction between EQWP and SWTAWP. Figure 2.6 presents the WP variations of area along the austral autumn (February to June) considering the studied period (2000-2010). The lowest coverage areas (3-4 millions of Km^2) were noted in the years of 2001, 2002 and 2004 with a strong positive peak in-between these years (year of 2003). After the year of 2007 a tendency to increase the WP coverage area can be observed, presenting the highest area on the last analyzed year (7-8 millions of Km^2, April 2010).

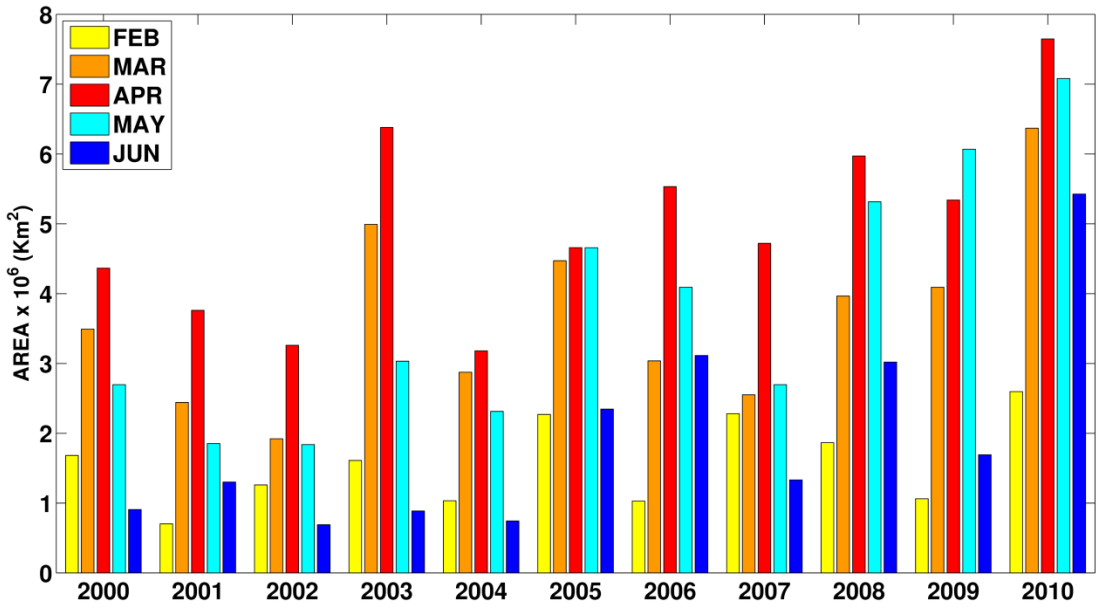

Figure 2. 6 Coverage area (10^6 Km^2) of the WP (SST > 28°C over 20°S – 20°N, 5°W – 43°W) during the analyzed period (2000-2010)

To evaluate the onset and decay of the SWTAWP along the simulated period (2000-2010) and its variability, we selected two years which represent extreme opposite conditions along the 11 years analyzed. Figure 7 depicts the time evolution, from February to July, of the

SWTAWP along the year of 2001, where the cold anomalies prevail over the WP area resulting in an occurrence below the climatological average.

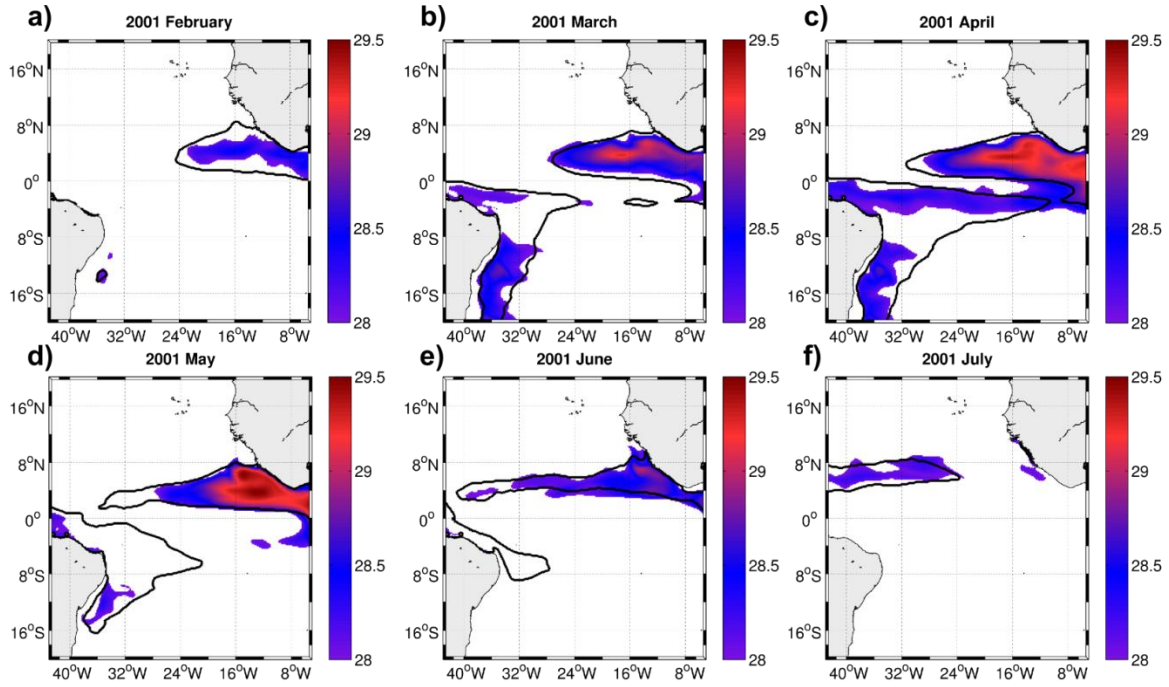

Figure 2. 7 Space-time evolution of the WP in 2001. a) to f) represent the time evolution from February to July. The black continuous line is the seasonal boundary of the WP for each month and the shading colors are the boundaries of the WP considering both, seasonal and interannual signs

In February (Fig. 2.7a), the presence of the SWTAWP off the Brazilian coast was observed as a very small region that could be disregarded, while over the eastern equatorial region, from the gulf of Guinea spreading to 24°W the EQWP was observed. From March to May (Fig. 2.7b,c,d), waters warmer than 29°C could be detected only over the eastern equatorial region, while over the SWTA the WP occurrence was marked by a weak presence, considering both, temperature and coverage area. Just in April (Fig. 2.7c), month which usually denotes the best development of the WP over this region, was possible to observe the warm waters from both hemispheres, merged over the basin. In May (Fig. 2.7d), only a small area spread through the Brazilian coast was responsible by the WP incidence over the SWTA. At the WP decay period, the SWTAWP doesn't occur at the SWTA, while at the north hemisphere, the EQWP can be observed at the eastern domain in June (Fig. 2.7e) moving to western domain in July (Fig. 2.7f).

In contrast with the findings of the aforementioned results, during the year of 2010 (Fig. 2.8) the WP occurrence over the TA exhibited the predominance of warm anomalies, which resulted in the larger coverage of the WP of the entire studied period.

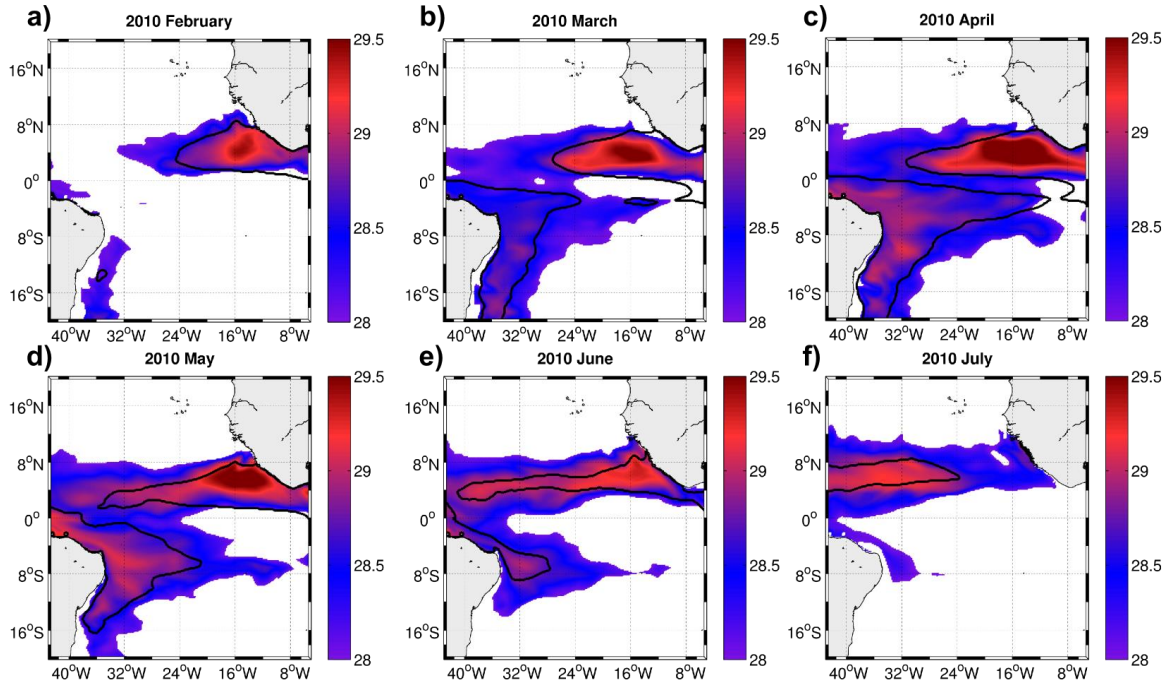

Figure 2. 8 Same as Figure 2.7 but for the year of 2010

In February (Fig. 2.8a) it's possible to note the presence of the SWTAWP spreading off the Brazilian coast from 20°S to 8°S and a small region apart, located near the South America north coast. At this time, the EQWP cover the region off the African coast to 32°W along 5°N. From March to July (Fig. 2.8 b-f), the SWTAWP and EQWP are depicted merged. Two regions presenting the highest temperatures (e.g. temperatures > 29°C) are revealed inside the climatological position of these two WPs. As a consequence of the warm anomalies at this year, even during the decay months (e.g. June and July), was possible to verify the SWTAWP and the EQWP merged over the TA.

The WP undergoes a seasonal parallel displacement from 10° S to the equator in austral autumn and from the equator to 10° N in austral winter. According with Barreiro et al. (2004) the SST anomaly is created south of 10° S, but moves northwestward by means of the Wind-Evaporation-SST (WES) feedback mechanism. As a result, the SST anomaly induces a strong atmospheric response in the austral autumn, shifting the ITCZ toward anomalously warm waters.

This migration accompanies the ITCZ which reaches its lower latitude position between January and April (on average, it is located on the equator in March - April). The ITCZ and its associated band of continental convection display large seasonal excursions over the Atlantic sector. In March-April, the rain band is located nearly on the equator onto which the trades converge from both hemispheres. SST is uniformly warm in the equatorial zone of 10°S-5°N, making March-April the time when the Atlantic ITCZ is very sensitive to even small changes in interhemispheric SST gradient (Chiang et al. 2002, Xie and Carton 2004). This peculiar scenario with the WP presence over the SWTA strongly influences the climate and precipitation regime of the northeastern Brazil (Moura and Shukla 1981, Nobre and Shukla 1996, Taylor et al. 2002, Hounsou-gbo et al. 2015).

During June, the SWTAWP off the Brazilian coast is shifting to the north, while a band of warm waters of the EQWP is located along the equator around 6° N. Exception are made to 2009 (not shown) and 2010, when the waters from the SWTAWP and EQWP still merged.

Figure 2.9 shows maps of the isotherm depth (T=28 °C, D28) contrasting with the maps of MLD and also presents maps of the heat content inside the MLD for the two extreme conditions aforementioned.

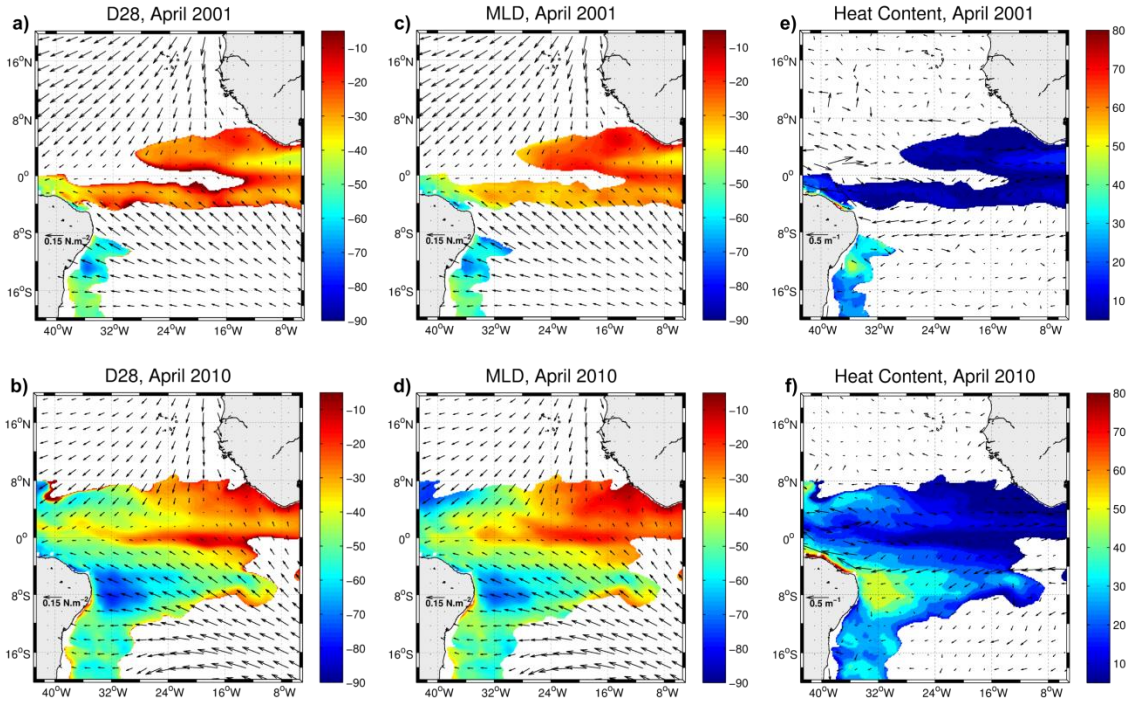

Figure 2. 9 Depth of the isotherm of 28°C (left panels); MLD (middle panels); Heat content inside the ML (right panels). Top panels are for the year of 2001 and bottom panels are from the year of 2010

Two distinct areas are well visible, an area extending from African coast to mid-basin over the equator (EQWP) with similar depths of D28 (Fig. 2.9a,b) and MLD (Fig. 2.9c,d) and another region, extending from the Brazilian coast to 20° W, from 18° S to the equator (SWTAWP) over the SWTA, where these variables deepen and generally reach depths down to 50m. These two regions are under control of different dynamics of the atmosphere, the first (EQWP) is under the ITCZ, while the SWTAWP is under the intensified southeastern trade winds. Despite the doldrums, the winds are, on annual average, much stronger over the western Atlantic than over the eastern Atlantic. This results in a mixed layer deeper all year long in the western Atlantic. The wind stress over the TA (Fig. 2.9 a,b,c,d) presented differences of one order of magnitude between the wind stress under the ITCZ (about 0.01 $N.m^{-2}$) against 0.1 $N.m^{-2}$ south of 4° S, especially at the SWTA. The deepest D28 and MLD (about – 75m) were verified over the center of the SWTAWP. As a reflex of the MLD horizontal distribution, the heat content inside the mixed layer over these two WPs (Fig. 2.9e,f) follow the same pattern of distinction. The EQWP region not exceeded 30 $GW.m^{-2}$ while the SWTAWP presents values that range from 35 $GW.m^{-2}$ to 50 $GW.m^{-2}$ and over the northern South America, values higher than 55 $GW.m^{-2}$ were observed near the coast. Kouadio et al. (2012) suggest that an active synoptic system of atmospheric easterly waves, associated with positive anomalies in the heat content over the south equatorial Atlantic, may favor conditions that cause strong rainfall occurrences over eastern northeast Brazil.

The discrepancies between the years of 2001 and 2010 had great impact over the area of the WPs but also had influence over the heat stored inside the ML. While in 2001 (Fig. 2.9e) highest values were restricted to a small portions over the SWTA, in 2010 (Fig. 2.9f) a region with values of about 45 $GW.m^{-2}$ can be noted off the Brazilian coast to 28° W between 4° and 10° S of latitude.

The temperature trends over the SWTAWP and EQWP are mainly driven by the seasonal cycle, where the role of the net heat flux is preponderant over the other temperature forcings

(Cintra et al., 2015). However, the role of the temperature terms on interannual time scale presents higher variability over the space-time distributions and a detailed evaluation was performed. Figure 2.10 presents the space distribution of the interannual anomalies of the main temperature trends for the year of 2001. Monthly anomalies of the variables are derived by subtracting the monthly climatological mean values (11 yr) from the original values. All derived anomalies are then detrended by subtracting the linear trend from the anomalies, and are smoothed with a 5-month running mean to emphasize variability on interannual time scale.

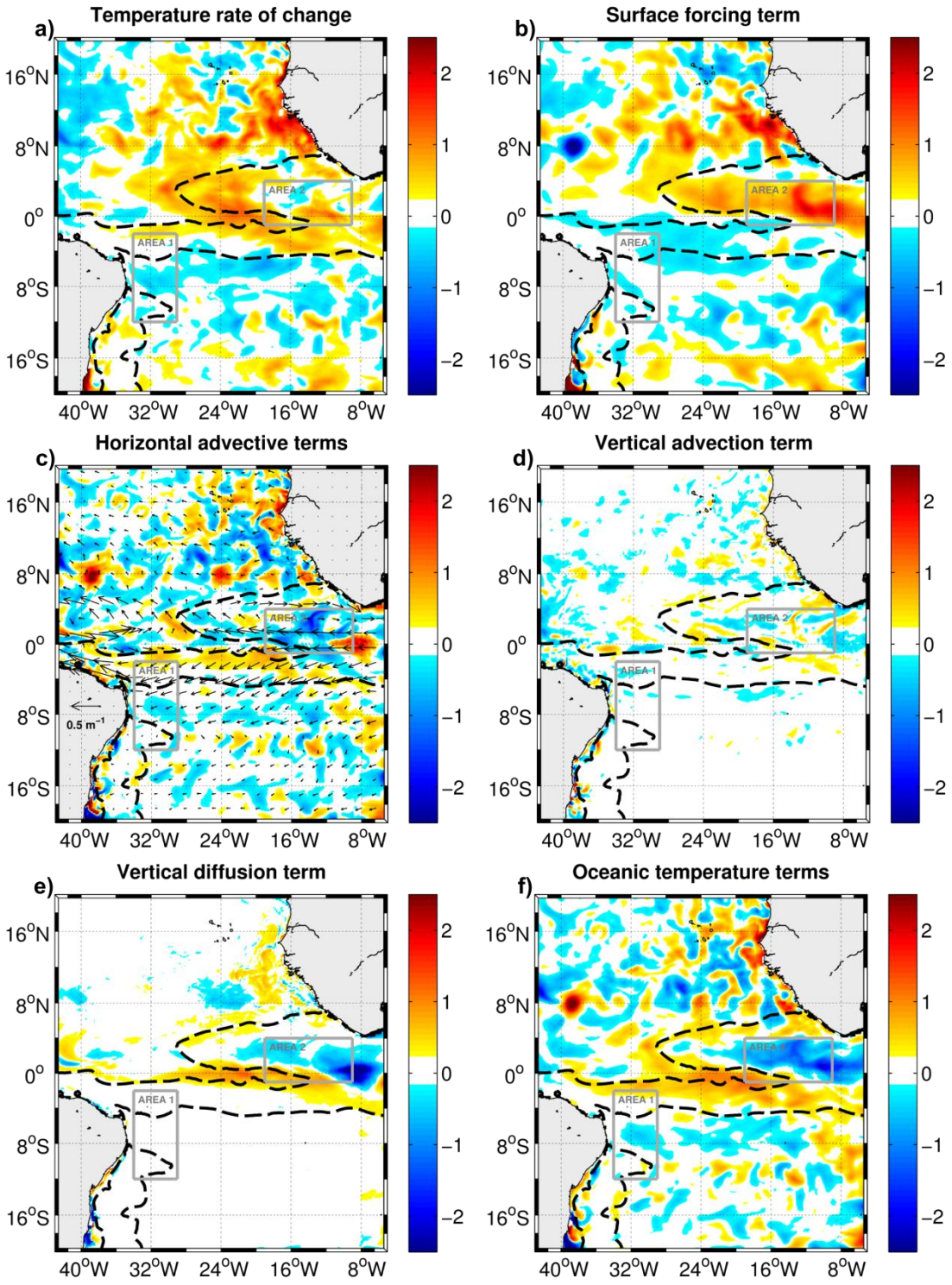

Figure 2. 10 Spatial distribution of the main temperature terms interannual anomalies (°C.month^{-1}) for April of 2001. The black dotted line is the WP boundary for the period. a) Temperature rate of change; b) Surface forcing; c) Horizontal advective term; d) Vertical advection term; e) Vertical diffusion term; f) Total oceanic terms (Vertical + Horizontal advection + Vertical diffusion)

` The interannual temperature rate of change (Fig. 2.10a) presents two regions dominated by the warm anomalies. The first one, extends from the southern domain to 12°S while the second one, from the 3°S until 16°N, with the warm anomalies prevailing at the east domain. A band where prevails the cold anomalies was verified between 12°S and 3°S occupying the entire east-west domain. Generally, the temperature rate of change spatial distribution can be explained by the dominance of the surface forcing (Fig. 2.10b). Exception may be considered inside our area of control over the EQWP region (e.g. Area 2). Over this area, the horizontal advection (Fig. 2.10c) and the vertical diffusion (Fig. 2.10e) are the main contributors of the oceanic terms (Fig. 2.10f), which are preponderant over the atmospheric forcing in some discontinued regions. The vertical advection (Fig. 2.10d) had a secondary role in the determination of the temperature trends and its more significant contributions can be verified just over the equator to the north tropical Atlantic.

In contrast, the space distribution of the interannual anomalies of the main temperature trends for the year of 2010 is presented in the Figure 2.11. The warm anomalies responsible for the enlarged WP of April 2010 are primarily a consequence of the trends distribution patterns in previous months, where prevails the warm anomalies. However, the spatial distribution of temperature change rate in April (Fig. 2.11a) helps to understand how the maintenance and decay of this phenomenon lasted more during this year.

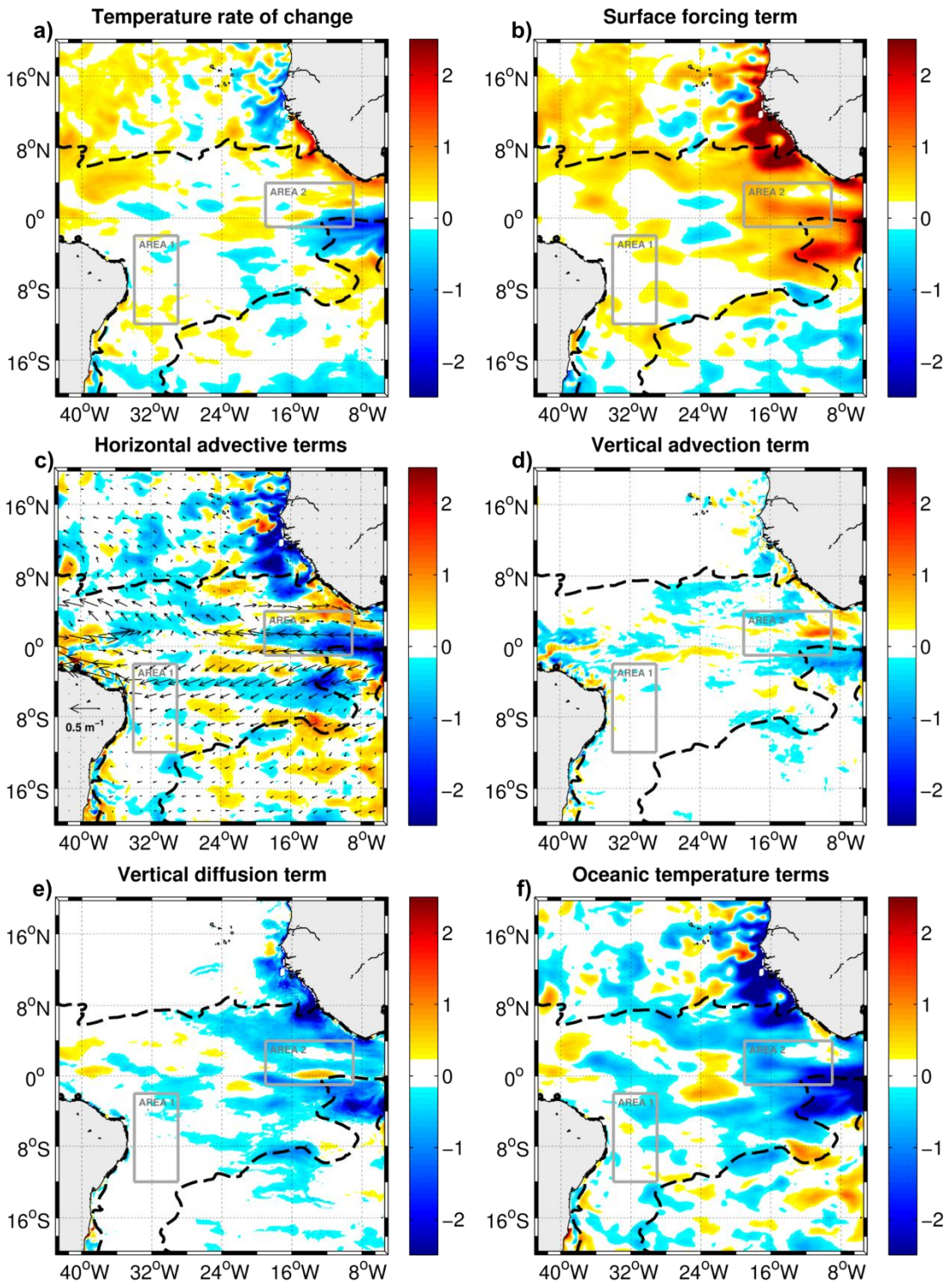

Figure 2. 11 Same as Figure 2.10 but for the April of 2010

The surface forcing (Fig. 2.11b) inside the WP presented the dominance of warm anomalies, especially in two regions where the trends are intensified. The region off the African coast along 8°N undergoes the influence of the Canary Current system, which is a system that contains coastal upwelling, filaments, and eddies, being a very complex region dynamically. The second region is under the influence of the cold tongue at the eastern domain and also presents intensified positive atmospheric contributions that reach 2°C.month^{-1}. These strong contributions of the surface forcing are in opposition to the negative temperature trends of the horizontal advection (Fig. 2.11c) and the vertical diffusion (Fig. 2.11e) over these regions. The total oceanic terms (Fig. 2.11f) presents a general tendency to balance the surface forcing term. Considering these two aforementioned regions, the surface forcing prevails at the upwelling system inside the north boundary of the WP near the African coast. While over the region influenced by the cold tongue, the negative anomalies of the oceanic terms exceed the atmospheric forcings, resulting in a restriction of the WP area over this region. As occurred in 2001, the vertical advection term played a secondary role in magnitude, performing positive/negative contributions associated with regions of convergence/divergence of the surface currents.

Our results (e.g. SST, Heat content inside ML, MLD and D28) suggest that although the areas representing the SWTAWP and EQWP are being frequently observed merged at surface through the SST, their distinct physical forcings imply in different areas of thermodynamic features. To investigate more properly these differences, the Figure 2.12 presents the main temperature trends terms over two controls areas, one positioned inside the SWTAWP region (2°S – 12°S, 29°W – 34°W) and another located at the EQWP region (1°S – 4°N, 9°W – 19°W). The comparisons of the temperature terms were performed considering the seasonal (e.g. monthly mean of the simulated period, [Fig. 2.12 a,b]) development and the interannual anomalies (e.g. 2000-2010, [Fig. 2.12 c,d]).

a)

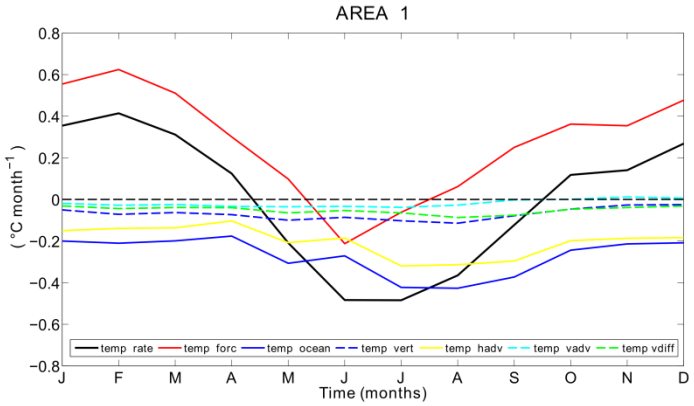
AREA 1
(°C month⁻¹)
Time (months)
J F M A M J J A S O N D
temp rate
temp forc
temp ocean
temp vert
temp hadv
temp vadv
temp vdiff

b)

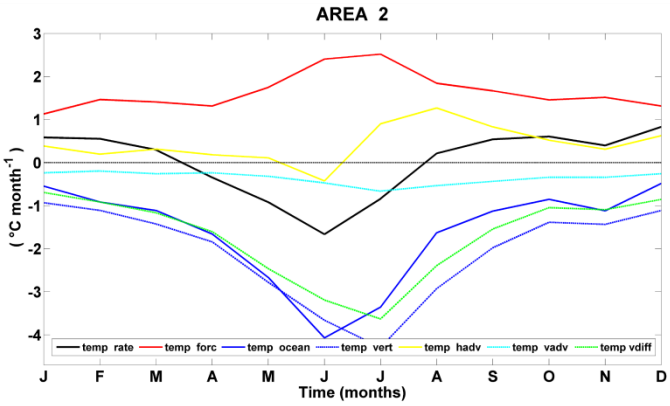
AREA 2
(°C month⁻¹)
Time (months)
J F M A M J J A S O N D
temp rate
temp forc
temp ocean
temp vert
temp hadv
temp vadv
temp vdiff

c)

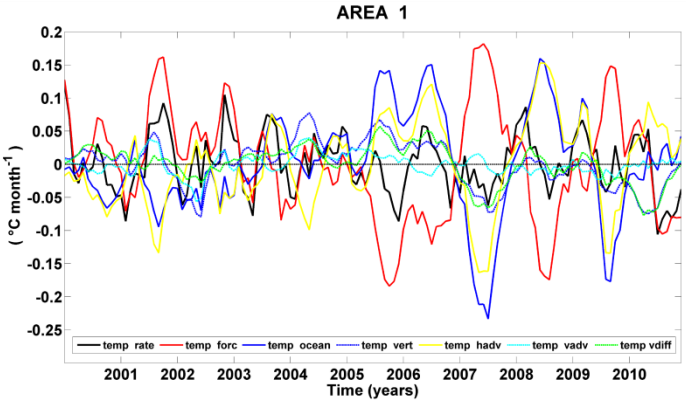
AREA 1
(°C month⁻¹)
Time (years)
2001 2002 2003 2004 2005 2006 2007 2008 2009 2010
temp rate
temp forc
temp ocean
temp vert
temp hadv
temp vadv
temp vdiff

d)

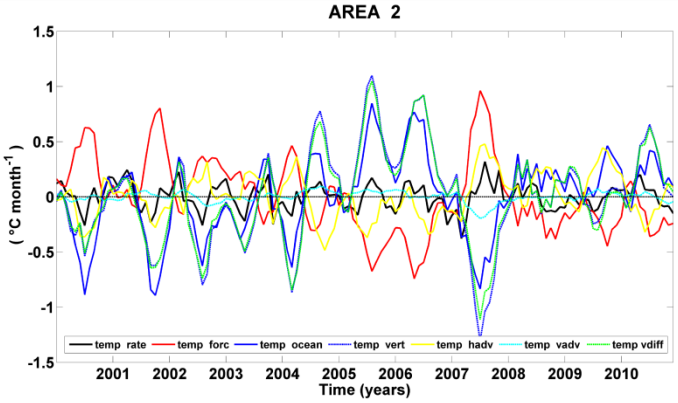
AREA 2
(°C month⁻¹)
Time (years)
2001 2002 2003 2004 2005 2006 2007 2008 2009 2010
temp rate
temp forc
temp ocean
temp vert
temp hadv
temp vadv
temp vdiff

Figure 2. 12 Time evolution of the main temperature tendency terms in °C.month^{-1}. a) and b) are the seasonal comparisons between two control boxes (Area 1, 2°S – 12°S, 29°W – 34°W) and (Area 2, 1°S – 4°N, 9°W – 19°W) respectively. c) and d) the same comparison of areas (Areas 1 and 2, respectively) considering the interannual anomalies (2000-2010); the colored lines represent the following terms: black, the rate of temperature change; red, the surface forcing; continuous blue, the total oceanic terms (advective + diffusive); dotted blue, vertical oceanic terms (vertical advection + diffusion); yellow, the horizontal advective term; cyan, the vertical advective term and green, the vertical diffusive term

Seasonally, the SWTAWP region (Fig. 2.12a) presented a total dominance of the surface forcing over the other temperature components, being responsible to reach positive contributions of 0.6°C.month^{-1} in February. The main oceanic term was the horizontal advection, which played a secondary role, contributing with negative rates during the all year long. The other analyzed terms (e.g. vertical advection and vertical diffusion) presented a tertiary role, whose negative increments never exceeded -0.1°C.month^{-1}. The EQWP region (Fig. 2.12b), presented temperature trends values ranging about three times more in magnitude than the SWTAWP region. The surface forcing contributes with positive values during all year long which the highest values occurred in austral winter. The oceanic terms play the main role over this region, being the vertical oceanic trends (e.g. vertical advection and diffusion) the main contributors of the oceanic trends. The vertical oceanic trends oppose the atmospheric contributions during all year long prevailing during the austral winter. Although the role of the horizontal advection is minor in magnitude, exerts a decisive role in determining the rate of temperature variation. The appearance and maintenance of the WP during the austral autumn over this region is in response of the surface forcing and horizontal advection positive contributions, while the WP decay results of the vertical diffusion preponderance after mid-March. The seasonal predominance of the surface forcing term away from the equator and the enhancement of importance of the horizontal advection and vertical diffusion over the equator, especially at the eastern portion had already been previously verified by other authors (e.g. Foltz et al. 2003, Peter et al. 2006, Yu et al. 2006, Cintra et al. in press).

Analyzing the interannual anomalies, the same pattern of distribution of the trends roles can be observed. Over the SWTAWP region (Fig. 2.12c) the horizontal advection is the main oceanic term during most of the analyzed period. These results confirm the findings of Foltz and McPhaden (2006) which pointed out that the horizontal advection acts damping the surface

forcing over the SWTA. Over the EQWP region (Fig. 2.12d) the vertical diffusion is the main oceanic temperature trend. The major difference considering the seasonal and interannual variations is that the temperature trends anomalies cannot maintain the stability of the terms roles distributions presented in the seasonal variations. Although a pattern of distributions can be observed in general way, the role of the temperature individual terms can invert and/or interact in different ways during short periods of time, being necessary a detailed evaluation over each period of interest when the interannual anomalies were being considered.

The negative anomalies of the SST which results in a restricted coverage area of the SWTAWP in 2001 (Fig. 2.7) were in response of the negative anomaly of the surface forcing prevailing over the positive oceanic contributions of the horizontal advection. In contrast, the warm SST anomalies over the WP area in 2010 (Fig. 2.8) presented different contributions to each evaluated area. While in the SWTAWP this warming result from the combination of the horizontal advection and surface forcing, over the EQWP region the vertical advection term exerts a preponderant role.

2.6. Summary and conclusions

We used in this study the ROMS model in a basin scale domain, configured to present increased number of vertical levels at the upper ocean. This approach allows a well reproduction of the mixed layer and more reliability in the numerical diagnosis of the temperature terms used to study the SWTAWP and the EQWP during the austral autumn. We took advantage of the reliable closure of the temperature tendency terms and the good coverage of the high resolution simulation to explore how these terms can provide an insight about the thermodynamics features of these WPs.

During the austral autumn the SWTAWP and EQWP reach their maximum development and sometimes are merged through the SST over the TA. We perform comparisons of the main thermodynamic features of these two regions that pointed out some distinctions which we would like to highlight.

Although the warm pools during the austral autumn were mainly controlled by the seasonal signs propagation into the atmosphere and ocean, we showed that the interannual signs

cannot be neglected. The interannual anomalies of the temperature trends must be considered as an important modulator of the warm pool coverage area and duration time to each year. Comparisons of two years where the interannual anomalies interfere in opposite conditions over the warm pool evolution were performed. In 2001, the predominance of the cold anomalies, issued a limited coverage area of the warm pool which also resulted in limited duration of the phenomenon (e.g. SWTAWP complete extinguished in June 2001). In contrast, the predominance of the warm anomalies in 2010 resulted in the largest coverage area of the analyzed period (2000-2010) and the SWTAWP remained occurring along the north-northeast Brazilian coast until July. Our findings suggest that the interannual anomalies that precede the best development month (e.g. before April) are determinant to define the spatial structure of the warm pool.

The comparisons of the MLD and warm pool depth (D28) showed similar spatial distribution over the TA, indicating that the MLD can be also used to vertical delimit the WP over this region. However, the SWTAWP always presented deeper than the EQWP. In consequence of the greater depths, the SWTAWP maintain more heat stored in its mixed layer and this is one of the most important thermodynamic features of distinction of these two areas.

The net heat flux at surface seems to control the onset of the warm pool for both seasonal and interannual time scales. Inside the ocean, the main terms responsible to balance the surface forcing over the warm pool presented different constitutions to each studied area. While over the SWTAWP the horizontal advection plays the main role to equalize the atmospheric forcing, over the EQWP the vertical diffusion term exerts this function. At the EQWP particularly, the secondary roles of the vertical and horizontal advection should also be considered, since they are important in the final constitution of the total oceanic trends. This hierarchy pattern of the temperature terms over the analyzed warm pools can be considered seasonally and as a general interannual tendency. However, the interannual temperature trends should be carefully analyzed, once the roles of each anomaly of terms can invert and/or significantly vary in a short period of time, leaving the general pattern observed.

The main thermodynamic characteristics of these two WPs were described focusing on identify distinctions when possible. Considering that the EQWP has significant impacts over the equator and to the African continent (e.g. Giannini et al. 2003) and the SWTAWP is also an

important region which bring impacts to the Brazilian northeastern region (e.g. Nobre and Shukla 1996; Hastenrath 2006; Hounsou-gbo et al. 2015), we recommend further investigation in these regions with a coupled ocean-atmospheric model to investigate possible WES feedback and other impacts that could result from the air-sea interactions over the WPs.

References

Barreiro, M., Giannini, A., Chang, P., Saravanan, R., 2004. On the Role of the South Atlantic Atmospheric Circulation in Tropical Atlantic Variability. Earth's Clim. 143–156. doi:10.1029/147GM08

Bourlès, B., Lumpkin, R., McPhaden, M.J., Hernandez, F., Nobre, P., Campos, E., Yu, L., Planton, S., Busalacchi, A., Moura, A.D., Servain, J., Trotte, J., 2008. The Pirata Program: History, accomplishments, and future directions. Bull. Am. Meteorol. Soc. 89, 1111–1125. doi:10.1175/2008BAMS2462.1

Carton, J. a., Giese, B.S., 2008. A Reanalysis of Ocean Climate Using Simple Ocean Data Assimilation (SODA). Mon. Weather Rev. 136, 2999–3017. doi:10.1175/2007MWR1978.1

Chiang, J.C.H., Sobel, A.H., 2002. Tropical tropospheric temperature variations caused by ENSO and their influence on the remote tropical climate. J. Clim. 15, 2616–2631. doi:10.1175/1520-0442(2002)015<2616:TTTVCB>2.0.CO;2

Dash, P., Ignatov, A., Martin, M., Donlon, C., Brasnett, B., Reynolds, R.W., Banzon, V., Beggs, H., Cayula, J.F., Chao, Y., Grumbine, R., Maturi, E., Harris, A., Mittaz, J., Sapper, J., Chin, T.M., Vazquez-Cuervo, J., Armstrong, E.M., Gentemann, C., Cummings, J., Piollé, J.F., Autret, E., Roberts-Jones, J., Ishizaki, S., Høyer, J.L., Poulter, D., 2012. Group for High Resolution Sea Surface Temperature (GHRSST) analysis fields inter-comparisons-Part 2: Near real time web-based level 4 SST Quality Monitor (L4-SQUAM). Deep. Res. Part II Top. Stud. Oceanogr. 77-80, 31–43. doi:10.1016/j.dsr2.2012.04.002

Enfield, D., Lee, S., 2005. The Heat Balance of the Western Hemisphere Warm Pool. J. Clim. 18, 2662–2681.

Enfield, D.B., Lee, S.K., Wang, C., 2006. How are large western hemisphere warm pools formed? Prog. Oceanogr. 70, 346–365. doi:10.1016/j.pocean.2005.07.006

Fairall, C.W., Bradley, E.F., Rogers, D.P., Edson, J.B., Young, G.S., 1996. Bulk parameterization of air-sea fluxes for Tropical Ocean-Global Atmosphere Coupled-Ocean Atmosphere Response Experiment. J. Geophys. Res. 101, 3747–3764.

Foltz, G.R., 2003. Seasonal mixed layer heat budget of the tropical Atlantic Ocean. J. Geophys. Res. 108, 1–13. doi:10.1029/2002JC001584

Giannini, A, Saravanan, R., Chang, P., 2003. Oceanic forcing of Sahel rainfall on interannual to interdecadal time scales. Science 302, 1027–1030. doi:10.1126/science.1089357

Hastenrath, S., 2006. Circulation and teleconnection mechanisms of Northeast Brazil droughts. Prog. Oceanogr. 70, 407–415. doi:10.1016/j.pocean.2005.07.004

Hounsou-gbo, G.A., Araujo, M., Bourlès, B., Veleda, D., Servain, J., 2015. Tropical Atlantic Contributions to Strong Rainfall Variability Along the Northeast Brazilian Coast. Adv. Meteorol. 2015, 13.

Huang, B., Carton, J., Shukla, J., 1995. A Numerical Simulation of the Variability in the Tropical Atlantic Ocean, 1980-88. J. Phys. Oceanogr.

Kanamitsu, M., Ebisuzaki, W., Woollen, J., Yang, S.-K., Hnilo, J.J., Fiorino, M., Potter, G.L., 2002. NCEP–DOE AMIP-II Reanalysis (R-2). Bull. Am. Meteorol. Soc. 83, 1631–1643. doi:10.1175/BAMS-83-11-1631

Lemarié, F., Kurian, J., Shchepetkin, A.F., Jeroen Molemaker, M., Colas, F., McWilliams, J.C., 2012. Are there inescapable issues prohibiting the use of terrain-following coordinates in climate models? Ocean Model. 42, 57–79. doi:10.1016/j.ocemod.2011.11.007

Large, W.G., McWilliams, J.C., Doney, S.C., 1994. Oceanic vertical mixing: A review and a model with a nonlocal boundary layer parameterization. Rev. Geophys. 32, 363–403.

Lin, C.Y., Ho, C.R., Zheng, Q., Kuo, N.J., Chang, P., 2011. Warm pool variability and heat flux change in the global oceans. Glob. Planet. Change 77, 26–33. doi:10.1016/j.gloplacha.2011.02.006

Liu, W.T., Katsaros, K.B., Businger, J.A., 1979. Bulk Parameterization of Air-Sea Exchanges of Heat and Water Vapor Including the Molecular Contraints at the Interface. J. Atmos. Sci. 36, 1722–1735.

Marchesiello, P., Debreu, L., Couvelard, X., 2009. Spurious diapycnal mixing in terrain-following coordinate models: The problem and a solution. Ocean Model. 26, 156–169. doi:10.1016/j.ocemod.2008.09.004

Maximenko, N., Hafner, J., 2010. SCUD: Surface Currents from Diagnostic model 17p.

Maximenko, N., Niiler, P., Rio, M.H., Melnichenko, O., Centurioni, L., Chambers, D., Zlotnicki, V., Galperin, B., 2009. Mean dynamic topography of the ocean derived from satellite and drifting buoy data using three different techniques. J. Atmos. Ocean. Technol. 26, 1910–1919. doi:10.1175/2009JTECHO672.1

Moura, A. D., Shukla, J., 1981. On the dynamics of droughts in northeast Brazil - Observations, theory and numerical experiments with a general circulation model. doi:10.1175/1520-0469(1981)038<2653:OTDODI>2.0.CO;2

Nobre, P., Shukla, J., 1996. Variations of sea surface temperature, wind stress, and rainfall over the tropical Atlantic and South America. J. Clim.

Penven, P., Marchesiello, P., Debreu, L., Lefèvre, J., 2008. Software tools for pre- and post-processing of oceanic regional simulations. Environ. Model. Softw. 23, 660–662. doi:10.1016/j.envsoft.2007.07.004

Servain, J., Busalacchi, A.J., McPhaden, M.J., Moura, A.D., Reverdin, G., Vianna, M., Zebiak, S.E., 1998. A Pilot Research Moored Array in the Tropical Atlantic (PIRATA). Bull. Am. Meteorol. Soc. 79, 2019–2031. doi:10.1175/1520-0477(1998)079<2019:APRMAI>2.0.CO;2

Shchepetkin, A.F., 2005. If-less KPP. ROMS/TOMS Workshop: Adjoint Modeling and Applications, La.Jolla, CA, October 24-28 http://www.myroms.org/Workshops/ROMS2005/Nonlinear/AlexanderShchepetkin.pdf.

Shchepetkin, A.F., McWilliams, J.C., 2005. The regional oceanic modeling system (ROMS): A split-explicit, free-surface, topography-following-coordinate oceanic model. Ocean Model. 9, 347–404. doi:10.1016/j.ocemod.2004.08.002

Shchepetkin, A.F., McWilliams, J.C., 2009. Computational Kernel Algorithms for Fine-Scale, Multiprocess, Longtime Oceanic Simulations. Handb. Numer. Anal. 14, 121–183. doi:10.1016/S1570-8659(08)01202-0

Silva, M., Araujo, M., Servain, J., Penven, P., Lentini, C. a D., 2009. High-resolution regional ocean dynamics simulation in the southwestern tropical Atlantic. Ocean Model. 30, 256–269. doi:10.1016/j.ocemod.2009.07.002

Taylor, M.A., Enfield, D.B., Chen, A.A., 2002. Influence of the tropical Atlantic versus the tropical Pacific on Caribbean rainfall. J. Geophys. Res. 107, 3127. doi:10.1029/2001JC001097

Wang, W., McPhaden, M.J., 2000. The Surface-Layer Heat Balance in the Equatorial Pacific Ocean. Part II: Interannual Variability*. J. Phys. Oceanogr. 30, 2989–3008. doi:10.1175/1520-0485(2001)031<2989:TSLHBI>2.0.CO;2

Xie, S.P., Carton, J. a., 2004. Tropical Atlantic variability: Patterns, mechanisms, and impacts. Geophys. Monogr. Ser. 147, 121–142. doi:10.1029/147GM07

Zeng, X., Beljaars, A., 2005. A prognostic scheme of sea surface skin temperature for modeling and data assimilation. Geophys. Res. Lett. 32, 1–4. doi:10.1029/2005GL023030

Zhang, X., McPhaden, M.J., 2010. Surface layer heat balance in the eastern equatorial pacific ocean on interannual time scales: Influence of local versus remote wind forcing. J. Clim. 23, 4375–4394. doi:10.1175/2010JCLI3469.1

CAPÍTULO 3

Numeric diagnosis of the interannual temperature tendency terms over the Tropical Atlantic

Diagnóstico numérico dos termos de tendência da temperatura interanuais sobre o Atlântico tropical

Revista pretendida: **Ocean Dynamics**, ISSN (1616-7341), Fator de impacto (JCR 2013) = 1.94, Qualis CAPES = A2

Marcio Cintra [a], Carlos A. D. Lentini [b], Eduardo Marone [a]

[a] Centro de Estudos do Mar, CEM, Universidade Federal do Paraná (UFPR), Av. Beira Mar s/n, 83255-000, Pontal do Paraná PR, Brazil

[b] Departamento de Física da Terra e do Meio Ambiente da Universidade Federal da Bahia (UFBA), Campus Ondina, 40170-280, Salvador BA, Brazil

Abstract

The Regional Ocean Modeling System (ROMS) is used to investigate the relative magnitudes of the thermodynamics components which contribute in the setting up of the interannual mixed layer heat budget in the tropical Atlantic (28° N – 20° S; 43° W – 5° W). The analysis is carried out mainly inside boxes (areas) having a rather homogeneous dynamics. This analysis was conducted using the model temperature diagnostics outputs and through monthly means inside the mixed layer, which varies in space and time. The monthly means had the seasonal sign detrend and the interannual anomalies were analyzed from 2000 to 2010 considering seven areas in the tropical Atlantic. A spatial correlation between the temperature rate of change and the main terms of the heat budget showed that oceanic terms dominate the equatorial area, while the furthest away of the equator regions (to north and south) are dominated by the surface forcing

(net heat flux). The spatial analysis of the standard deviation revealed two regions of enhanced variability, the cold tongue region and an area north of 5° N, from 25° W to the African coast. The analysis of the individual terms inside the regions showed that the northern oceanic region, the southwest region and the southern oceanic region, presented the dominance of the surface forcing term. While in the other regions, this term continuously opposes to the oceanic trends, with a similar range of variation. In the cold tongue region (6^o S – 2^o N, 20^o W -5^o W), a warm anomaly reached 0.9 °C.month^{-1} in 2008. In this region the vertical diffusion and the horizontal advection seems to play similar role considering the oceanic components which contribute to the interannual mixed layer heat budget. While the surface forcing term presents an identifiable occurrence pattern in relation the distance of equator, the oceanic trends presented a more complex spatial distribution, and each area should be considered with its peculiar characteristics along the analyzed period. The main oceanic trends are in general controlled by the vertical diffusion and the horizontal advection, but their roles can vary substantially inside each region

Resumo

O modelo *Regional Ocean Modeling System (ROMS)* foi utilizado para investigar as magnitudes relativas dos componentes termodinâmicos que contribuem para definir o orçamento de calor interanual da camada de mistura no Atlântico tropical (28° N – 20° S; 43° W – 5° W). A análise foi realizada principalmente dentro de caixas (áreas) com uma dinâmica bastante homogênea. Esta análise foi conduzida utilizando as saídas de diagnóstico de temperatura do modelo através de médias mensais dentro da camada de mistura, que varia no espaço e no tempo. As médias mensais tiveram o sinal sazonal retirado e as anomalias interanuais foram analisadas de 2000 a 2010 considerando sete áreas no Atlântico tropical. Uma correlação espacial entre a taxa de variação da temperatura e os principais termos do orçamento de calor mostrou que os termos oceânicos dominaram a região equatorial, enquanto que as regiões mais afastadas do equador (para norte e sul) foram dominadas pelo forçante superficial (fluxo de calor líquido). A análise espacial dos desvios padrões revelou duas regiões de intensa variabilidade, a região da língua fria e a área ao norte de 5° N, de 25° W até a costa Africana. A análise dos termos individuais dentro de cada região mostrou que a região oceânica norte, a região sudoeste e a região oceânica sul apresentaram a dominância do termo forçante superficial. Enquanto que em outras regiões, este termo se opõe continuadamente as tendências oceânicas, com uma taxa similar de variação. Na região da língua fria (6^o S – 2^o N, 20^o W -5^o W), uma anomalia quente alcançou 0.9 °C.month^{-1} em 2008. Nessa região a difusão vertical e a advecção horizontal parecem desempenhar papeis

similares considerando os componentes oceânicos que contribuem para o orçamento de calor interanual na camada de mistura. Enquanto o termo forçante superficial apresenta um padrão de ocorrência identificável em relação à distância do equador, as tendências oceânicas apresentaram uma distribuição espacial mais complexa, e cada área deve ser considerada com suas características peculiares ao longo do período analisado. As principais tendências oceânicas são em geral controladas pela difusão vertical e advecção horizontal, porém seus papéis podem variar substancialmente dentro de cada região.

Palavras chave: variabilidade do Atlântico tropical, interações oceano-atmosfera, orçamento de calor, camada de mistura, variabilidade interannual

Keywords: tropical Atlantic variability, air-sea interactions, heat budget, mixed layer, interannual variability

3.1. Introduction

From the atmospheric perspective, the circulation over the tropics is extremely sensitive to fluctuations in temperature fields of the sea surface, which is an extremely important oceanic variable to study the air-sea interaction processes, as well for weather and climate studies (Foltz et al. 2003). From the oceanographic point of view, the tropical Atlantic (TA) is an important region for the large-scale circulation and the global climate. This is due to inter-hemispheric flow of mass and heat net flows associated with the thermohaline circulation (Fratantoni et al. 2000; Lazar et al. 2001). According to Brandt et al. (2011) some aspects of intrinsic ocean dynamics, such as year-to-year variations in the strength of tropical instability waves, are similarly identified as causes of interannual sea surface temperature (SST) variability, and may be responsible to force variability in the atmosphere.

The SST variability is controlled by various mechanisms of comparable influences, from both regional ocean–atmosphere interaction as well as remote forcings. Although, the seasonal cycle is by far the largest source of climate variability in the tropical Atlantic (Servain 1991), the interannual components cannot be neglected (Servain et al. 2003; Huang et al. 2004).

Considering the tropical Atlantic variability (TAV), a similar interannual phenomenon, but weaker than the Pacific El Niño also occurs in the Atlantic. This phenomenon is also called

Atlantic Niño or Equatorial mode of variability. The largest near-equatorial SST anomalies occur in the equatorial eastern Atlantic. The warm events reach their maximum strength during austral winter, with manifestations focused primarily near the equator (e.g., Zebiak 1993; Carton and Huang 1994; Wu et al. 2004; Xie and Carton 2004). During the warm anomaly phase, the trade winds in the equatorial western Atlantic are weak and SST is high in the equatorial eastern Atlantic. Although the connections between the equatorial Atlantic variability and the rainfall regime has been more studied considering the interhemispheric mode, implications for the local climate resulting from the equatorial mode have been reported by Carton and Huang (1994) and Kouadio et al. (2002).

Several studies have been conducted to identify physical processes underlying SST variations in the Atlantic Ocean, most of them focusing in the equatorial region. Some of these were observationally based empirical studies (Wang 2001) while others occurred through modeling efforts using different models and configurations (Carton et al. 1996; Chang et al. 2000; Lazar et al. 2000), as well as there are studies based on comparisons of model and observational data (Huang and Shukla 2005). Moreover, because of the lack of observations data, many observation-based heat balance analyses cannot achieve a closure of heat budget without making assumptions that are difficult to validate (Wang and McPhaden 1999; Zhang and McPhaden 2010).

Taking into account the subjects above, we decide to use numerical diagnostic outputs of a high resolution TA simulation to describe and evaluate physically the relative contributions of the temperature tendency terms over the upper ocean mixed layer. Comparisons between the main temperature tendency terms which are dominant in different regions with the previous works will be done always as possible, even considering different time scales of evaluation. Then, the temperature anomalies over the mixed layer will be discussed with main focus to the interannual variations.

The remainder of this paper is organized as follows. In section 2, the used model, its configuration, the simulation domain and the datasets used to force the model are presented. Section 3 describes the comparison datasets . Section 4 the temperature tendency equation and the numerical diagnostics outputs are described. Section 5 consists of model validation through surface velocities, mixed layer depth and temperature vertical structure. Section 6 presents the

interannual temperature tendency terms over the tropical Atlantic, followed by summary and discussion in section 7.

3.2. Model and model configuration

The numerical model used in this study was the Regional Ocean Modeling System (ROMS). This model is a free surface ocean model that solves the primitive equations in an earth-centered rotating environment based on the classical Boussinesq approximation and hydrostatic vertical momentum balance (Shchepetkin and McWilliams, 2005). To prevent the spurious diapycnal mixing we use the rotated split upstream-biased advection scheme proposed by Marchesiello et al. (2009), with the implementations proposed by Lemarié et al. (2012) that allow this scheme to rotate the hyperdiffusive part in the neutral direction as well as to increase its stability. Unresolved vertical subgrid-scale processes are parameterized by an adaptation of the non-local K-profile planetary boundary layer scheme (Large et al., 1994) with the implementations of the kpp scheme proposed by Shchepetkin, (2005).

The model grid, forcing, initial and boundary conditions were built using the ROMSTOOLS (Penven et al., 2008). The model was forced at surface by inter-annual wind stress, heat and freshwater fluxes derived from the NCEP/NCAR reanalysis products (R-2). These datasets (Kanamitsu et al., 2002) are available at 1.875°×1.875° resolution and at 6-hourly timescale. The data can be obtained from http://www.esrl.noaa.gov/psd/data/gridded/data.ncep.reanalysis2.gaussian.html. The parameters obtained from NCEP are air temperature at 2 m height, zonal and meridional components of winds at 10 m height, specific humidity of air at 2 m, and net short-wave and long-wave radiation at sea surface. These data were connected to the model through a bulk flux parameterization (Liu et al., 1979) and the COARE algorithm of Fairall et al. (1996). The SST was defined in the model with the new prognostic scheme developed by (Zeng and Beljaars, 2005).

The initial and lateral boundary conditions (temperature, salinity, sea surface high, zonal and meridional velocities) were imposed from a monthly mean (2000-2010) data of Simple Ocean Data Assimilation (SODA – version 2.2.4) reanalysis which has 1/2 of horizontal

resolution (Carton and Giese, 2008). Despite of we are using reanalysis data, a flag (obc_volcons) was used to ensure the conservation of mass inside do simulated domain. This flag computes the integral of mass flux at the open boundaries which is needed to enforce global mass conservation constraint through a correction in barotropic mass flux. The mean density over the entire domain (Fig. 3.1 c) oscillated around the value of 1029.35 kg.m^3, keeping a steady state. The vertical discretization of the grid was constructed using a hybrid z – σ coordinate system obtained by relaxing the z- coordinate system toward the σ – coordinate (Shchepetkin and McWilliams, 2008; Lemarié et al., 2012).

The model domain (Fig. 3.1 a) ranged from 43^o W to 5^o W and 20^o S to 28^o N, resulting in 297 X 227 points with 1/6° (~18 km) in horizontal resolution and 40 vertical levels (θ_s = 10 , θ_b = 2, hc = 200). The bottom topography is based on the global topography dataset at 2′ resolution (Smith and Sandwell, 1997). Explicit lateral viscosity is null everywhere in the model, except in sponge layers near the open boundaries where it increases smoothly on 10 grid points. We perform the time integration of the simulation with a time step of 800s, starting at year of 2000 and finishing at 2010. The model run for 2 years to reach a spin-up state (not shown), after that, the model integration was considered in steady state (Fig. 3.1 b), when the total kinetic energy oscillated quasi-periodically around an equilibrium state.

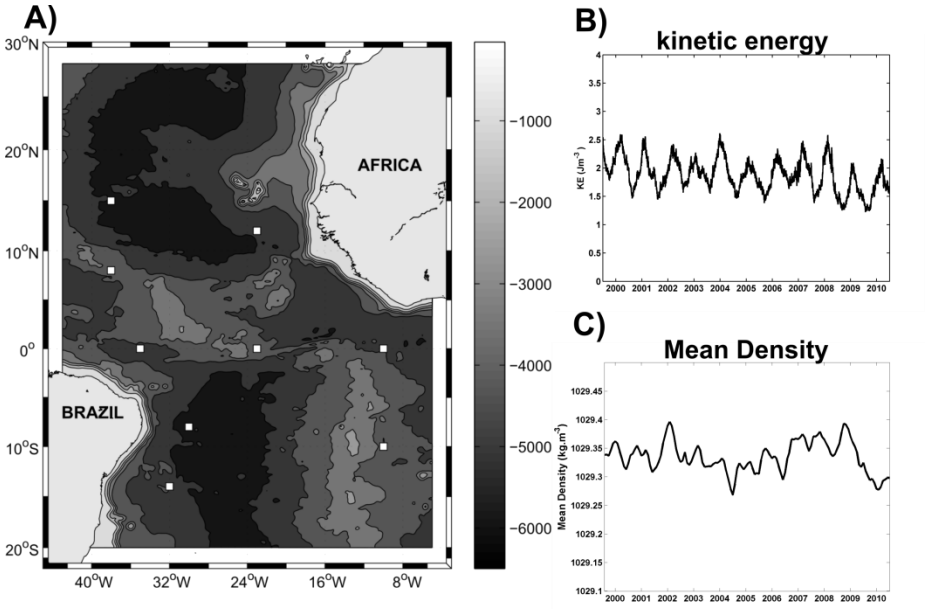

Figure 3. 1 A) Model domain and bathymetry, the white squares are the points of comparison between model and PIRATA buoys data (depths are indicated in m in the gray scale at the right side). B) Kinetic energy (J.m-3) integrated over the model domain. C) Mean density (kg.m-3) over the model domain.

3.3. The data sets for model validation

In order to validate our numerical results, we used data from moored buoy (vertical comparisons) and diagnostic model data (surficial currents comparison).

3.3.1. Mooring data

The PIRATA (Bourlès et al., 2008) data was used to validate the model's temperature in the first 200 m of depth. We choose 9 buoys to perform the this validation (Fig. 3.1), being 3 located at the South Atlantic (8^o S 30^o W, 14^o S 32^o W and 10^o S 10^o W), 3 from the equator (0^o 10^o W , 0^o 23^o W and 0^o 35^o W) and 3 positioned at the North Atlantic (8^o N 38^o W, 15^o N 38^o W , 12^o N 23^o W).

The comparison is done for the year 2000 to 2010, with exception for the two PIRATA-SWE extension buoys, which are operational since August 2005 and for the buoy site at 12^o N 23^o W, operational since June 2006. The PIRATA data can be downloaded freely from the NOAA/PMEL website (www.pmel.noaa.gov/pirata).

All-time series of these data were processed as monthly means, where the flawed data were removed. Vertical interpolations were processed on the PIRATA data when only one out of three consecutive temperature sensors along the moored line was dysfunctional.

3.3.2. Surface currents

In this study we used surface velocities from the SCUD (Maximenko and Hafner, 2010) program provided by the Asia Pacific Data Research Center/International Pacific Research Center (APDRC/IPRC). The SCUD (Surface CUrrents from Diagnostic Model) data set comprises nearly global, daily surface velocities as a result of a simple diagnostic model that combines three sources of scientific information: (i) geostrophic components produced by the sea level anomaly from the AVISO (Archiving Validation and Interpretation of Satellite Data in

Oceanography) project and mean dynamic ocean topography from Maximenko et al. (2009); (ii) wind-driven components using satellite daily winds from QuikSCAT 1/4°; and (iii) drifter trajectories, which provide consistent data for tuning the diagnostic model. The SCUD project considers 8058 drifters drogued at 15 m depth covering a time period from February 1979 through September 2008. SCUD surface velocities are daily gridded with 1/4° of spatial resolution. This data set can be freely downloaded from http://apdrc.soest.hawaii.edu/datadoc.scud.php. Due to the availability of the SCUD data, the comparison is done for the years 2000 to 2009, using monthly mean data.

3.4. The temperature tendency equation and diagnostics outputs

Our objective is to measure the relative contribution of the oceanic terms entering in the interannual variation of the mixing layer heat budget at the TA. To reach that, we used the temperature diagnostics outputs of the ROMS model to evaluate the temperature tendency terms. These outputs are expressed in $^{o}C.s^{-1}$ and are presented below in the advective form (Equation 1). To facility the discussion we will use quantities which are summed or integrated over a monthly duration. The trends will be thus expressed in °C.month^{-1}.

$$\frac{\partial T}{\partial t} = \vec{u}\frac{\partial T}{\partial x} + \vec{v}\frac{\partial T}{\partial y} + \vec{w}\frac{\partial T}{\partial z} + AK_t\left(\frac{\partial^2 T}{\partial x^2} + \frac{\partial^2 T}{\partial y^2}\right) + AK_v\left(\frac{\partial^2 T}{\partial z^2}\right) + \Phi_T \qquad (1)$$

Where, T is temperature, t is time evolution, $\vec{u}, \vec{v}\ and\ \vec{w}$ are the velocity components for the x, y and z directions respectively. Φ represents the net heat flux used to force the model plus nudging. AK_t and AK_v *are* the eddy viscosity coefficients for the horizontal and vertical directions, respectively.

The average temperature and temperature tendency terms of the mixed layer have been calculated by taking means from the top level to the depth of the mixed layer ($\overline{ML}$), which is defined using the temperature threshold criterion with ΔT = -0.5 ^{o}C compared to the SST. This method was used with success in the TA by Foltz et al. (2003) and was confirmed by de Boyer Montégut et al. (2004) as the best criterion method for use with averaged profiles. Monthly anomalies of the variables are derived by subtracting the monthly climatological mean values (11 yr) from the original values. All derived anomalies are then detrended by subtracting the linear trend from the anomalies, and are smoothed with a 5-month running mean to emphasize variability on interannual time scale.

3.5. Model validation

The dynamics of the model was evaluated through the surface currents comparison. The annual mean of SCUD zonal component of the velocity (Fig. 3.2 a) shows the occurrence of the South Equatorial Current (SEC) westward flow divided in three branches (south, central and north) as well as the more diffuse westward flow of North Equatorial Current (NEC) north of 10^{o} N. The numerical NEC reproduction (Fig. 3.2 b) presents good agreement with the SCUD data, with maximum velocities of about - 0.15 $m.s^{-1}$ near 15^{o} N of latitude. The numerical annual mean of the SEC branches also were quite well represented by the model, with the Southern branch (sSEC) weaker than the others (- 0.12 $m.s^{-1}$ near 15^{o} S). The annual mean of the central and northern braches of SEC (cSEC and nSEC) presented similar velocities (- 0.32 $m.s^{-1}$) and were founded near 3^{o} S and 2^{o} N respectively. The SCUD nSEC showed a more fragmented zonal flow when compared with the SCUD cSEC, while both of their numerical reproductions presented a more continuous westward flow. When the cSEC reaches the Brazilian coast, it merges with the North Brazilian Current (NBC) presenting an intensified flow along the South American shelf. The numerical reproduction of the NBC presenting zonal velocities stronger (- 0.7 $m.s^{-1}$) than the SCUD program (-0.55 $m.s^{-1}$), however, the horizontal structure was well reproduced. The eastward flow of the North Equatorial Counter Current (NECC) along of 5^{o} N of latitude was good represented numerically. At 5^{o} N - 24^{o} W, the velocity of the SCUD program was 0.15 $m.s^{-1}$ (against 0.14 $m.s^{-1}$ ROMS) and presents an eastward intensification reaching 0.5 $m.s^{-1}$ at 6^{o} W (against 0.44 $m.s^{-1}$ ROMS) near the African coast. The time evolution (2000 - 2010) of the nSEC, NBC and NECC were compared between SCUD program and ROMS model over a mean section inside these currents (Fig. 3.2 c, d, e). The comparison of the resultant velocity showed good representation of surface currents by the numerical results, mainly at in the reproduction of the NBC and nSEC, while at the NECC numerical results were stronger than SCUD data. A strong review of the main currents over the upper TA can be obtained consulting Stramma and Schott (1999); Goni and Baringer (2002); Lumpkin and Garzoli (2005).

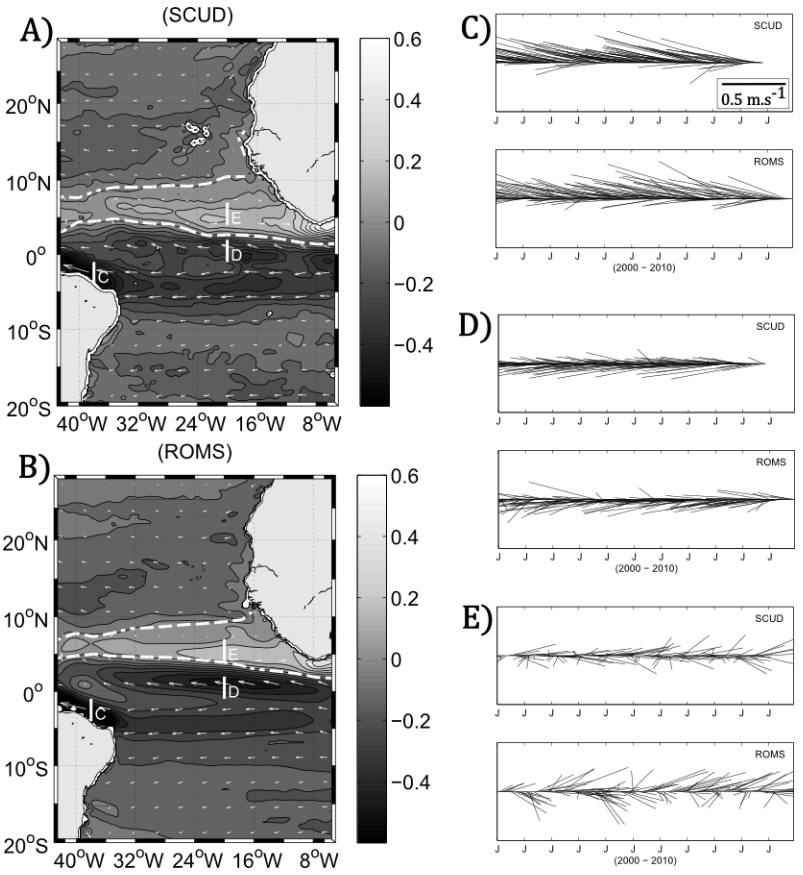

Figure 3. 2 Comparison between SCUD (A) and ROMS (B) of the annual mean (2000 - 2010) of the zonal component of velocity (gray shading). The white vectors are the resultant velocity. The white bars represent the sections used to evaluate the time evolution (monthly mean) of NBC (C), nSEC (D) and NECC (E).

Considering that the main variables analyzed in this work consist of mean inside the mixed layer, we validated the numerical MLD performing a comparison between the ROMS and PIRATA (Fig. 3.3). In general way, the vertical position of the mixed layer was well represented numerically. When evaluating the three PIRATA sites at the equator, the shallower MLD at the eastern basin in contrast with the westward deepening was well reproduced by the model. While at 0^o 10^o W the MLD oscillated around 25m deep at 0^o 35^o W its variation was around the depth of 60m. When we evaluate the comparisons made in the 38^o W positions, a very good reproduction of the numerical MLD can be verified. At the PIRATA sites where it was not possible to evaluate the entire modeled period (8^o S 30^o W; 14^o S 32^o W, 21^o N 23^o W), comparisons with the numerical data were also satisfactory, taking into account the average position of oscillation of MLD. Some numerical MLD displacements relative to observed data

were found in 10° S 10° W and 14° S 32° W, most verified between August and December, however without compromising the proper validation of numerical data.

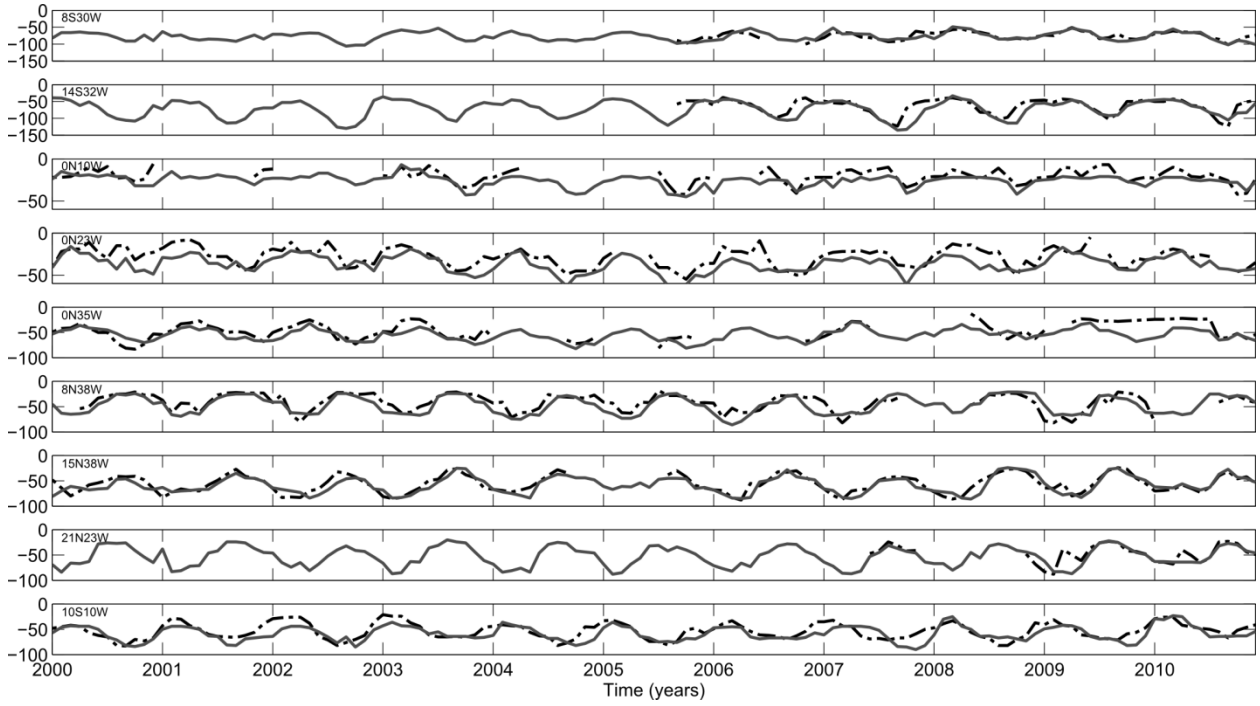

Figure 3. 3 Comparison between ROMS (gray solid line) and PIRATA (black dash dotted line) MLD.

To validate the vertical temperature structure of the simulation, nine selected monthly mean temperature profiles (0–200m) computed from ROMS outputs are compared to the observational data derived from the PIRATA moorings for the same months (Fig. 3.4). Two isotherms were analyzed in particularly, 28 °C and 20 °C. According with Graham and Barnett (1987) when SST reaches a critical value (27.5 °C) it promotes a dramatic change in convection regime, favoring the occurrence of deep convection. In the sharp thermocline underneath, temperatures drop from 25 to 15°C over about 50m in the vertical and the 20 °C isotherm is often taken as a lower boundary of the tropical surface water. This isotherm is closely related to the isopycnal σ_θ= 25:8 kg.m^{-3} which is used here as the lower boundary (Stramma and Schott, 1999; Stramma et al., 2005).

At the surface and inside the superficial mixed layer the numerical results were in good agreement with the buoys data. In 8° S 30° W (Fig. 3.4 g) the seasonal appearance of the 28 °C isotherm (February - May) was very well reproduced by the model.

The numerical results were able to reproduce the tightening of the thermocline for the equatorial PIRATA sites (Fig. 3.4 d, e, f) as well as the sinking and relaxation of the vertical gradient in response to displacement away from the equator for the southwestern areas (Fig. 3.4 g, h) and northwestern areas (Fig. 3.4 a, b). The 20°C isotherm had variations around 100m of depth at the 0° 35° W and these variations (seasonal and inter-annual signs) submerge until reach the 180m of depth at 14° S 32° W (Fig. 3.4 h). Although the largest errors were observed in the thermocline zone (reaching 2.5°C in some displacements), this region and its variations reach a satisfactory numerical reproduction.

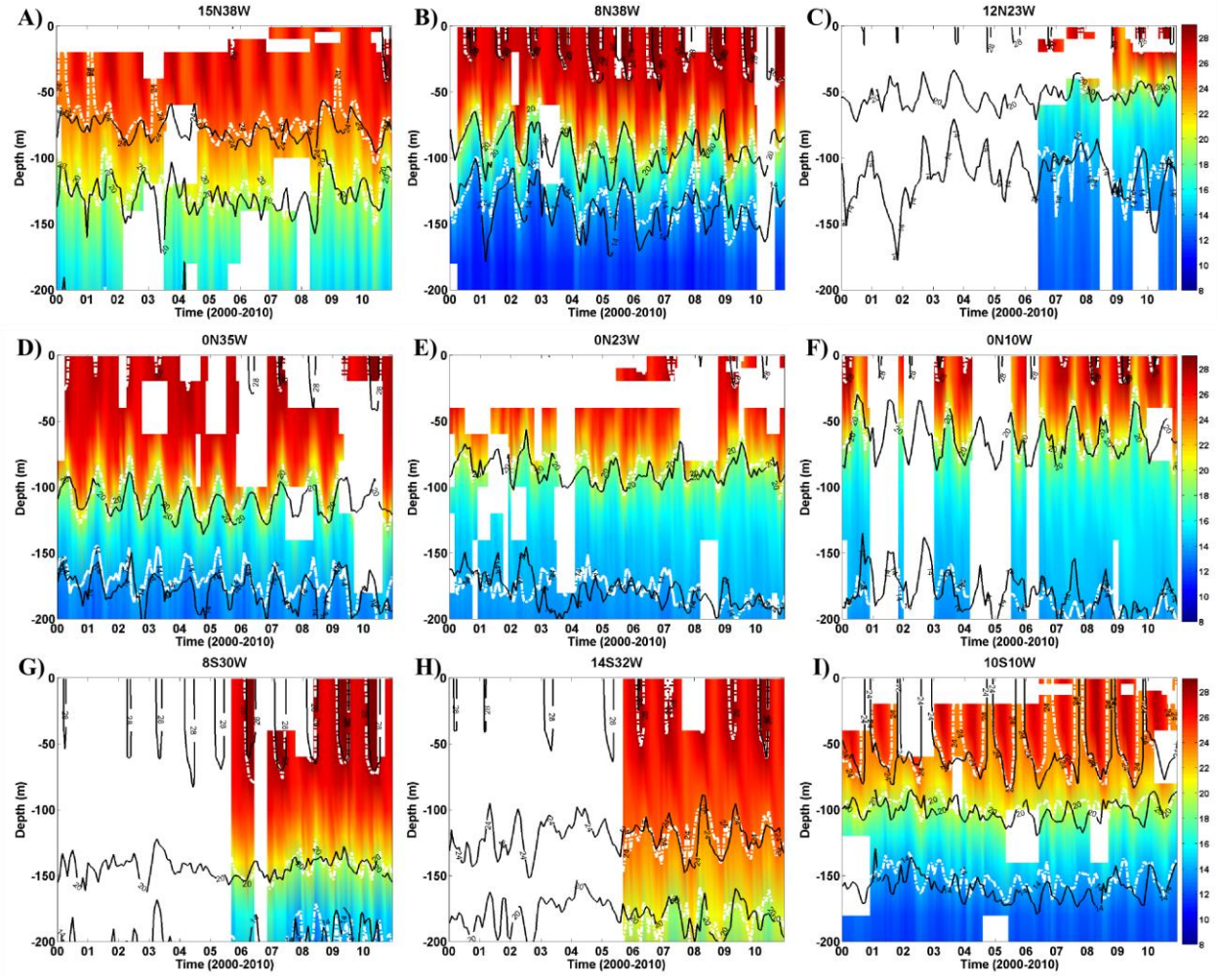

Figure 3. 4 Comparison between simulated and observed temperature (°C) variations for the upper 200m from January 2000 to December 2010 for the PIRATA locations presented at Fig. 3.1. Model-

derived temperature is represented by black contours and the PIRATA observed temperature appears as white contours and shaded colors.

3.6. Results

In order to gain better insight into the main variables which have influence in thermodynamics of the upper ocean, we perform a verification of the annual mean SST, mixed layer depth, depth of the 20 ^{o}C isotherm, latent heat and short wave radiation fluxes and winds in the tropical Atlantic. SST reaches a maximum just north of the equator with a poleward decrease that is strongest in the eastern half of the basin (Fig. 3.5 a). The MLD and the depth of the isotherm of 20 ^{o}C (used here as the thermocline depth) have similar patterns as expected (Fig. 3.5 b, c). To the south of 20^{o} N, the gradient in East-West direction predominates in the basin, with shallower values verified near the African coast and on the equator, more specifically in the region of actuation of the cold tongue. In contrast, the highest values were verified poleward of 10^{o} N-S at the western basin.

The net surface heat flux consists of the balance of the energy which comes from the sun through shortwave radiation (Q_{sw}) and the losses through net longwave radiation (Q_{lw}) emitted from the sea surface and latent and sensible heat fluxes (Q_{lat} and Q_{sen}, respectively). The lowest values of Q_{sw} were observed along the equatorial region (Fig. 3.5 d), more specifically on the mean position of the ITCZ (throughout 5^{o} N) near the African coast (155 Wm^{-2}) and reaching 170 Wm^{-2} westward. The Q_{sw} values grow to 220 Wm^{-2} in the region between 10^{o} N and 20^{o} N as well as between 5^{o} S and 20^{o} S. The highest values were observed north of 12^{o} N near the African coast.

Regarding the Q_{lat} distributions (Fig. 3.5 e), the less intense flows were observed inside the cold tongue region, with lower value of -35 Wm^{-2}, however these flows are intensified outside the equatorial region reaching -160 Wm^{-2} in the central southern tropical gyre.

The mean surface winds converge over the warmest SST and are strongest in the western basin. Here the wind stress acquires a strong zonal component, in contrast to the predominantly meridional component of wind stress in the east (Fig. 5 f).

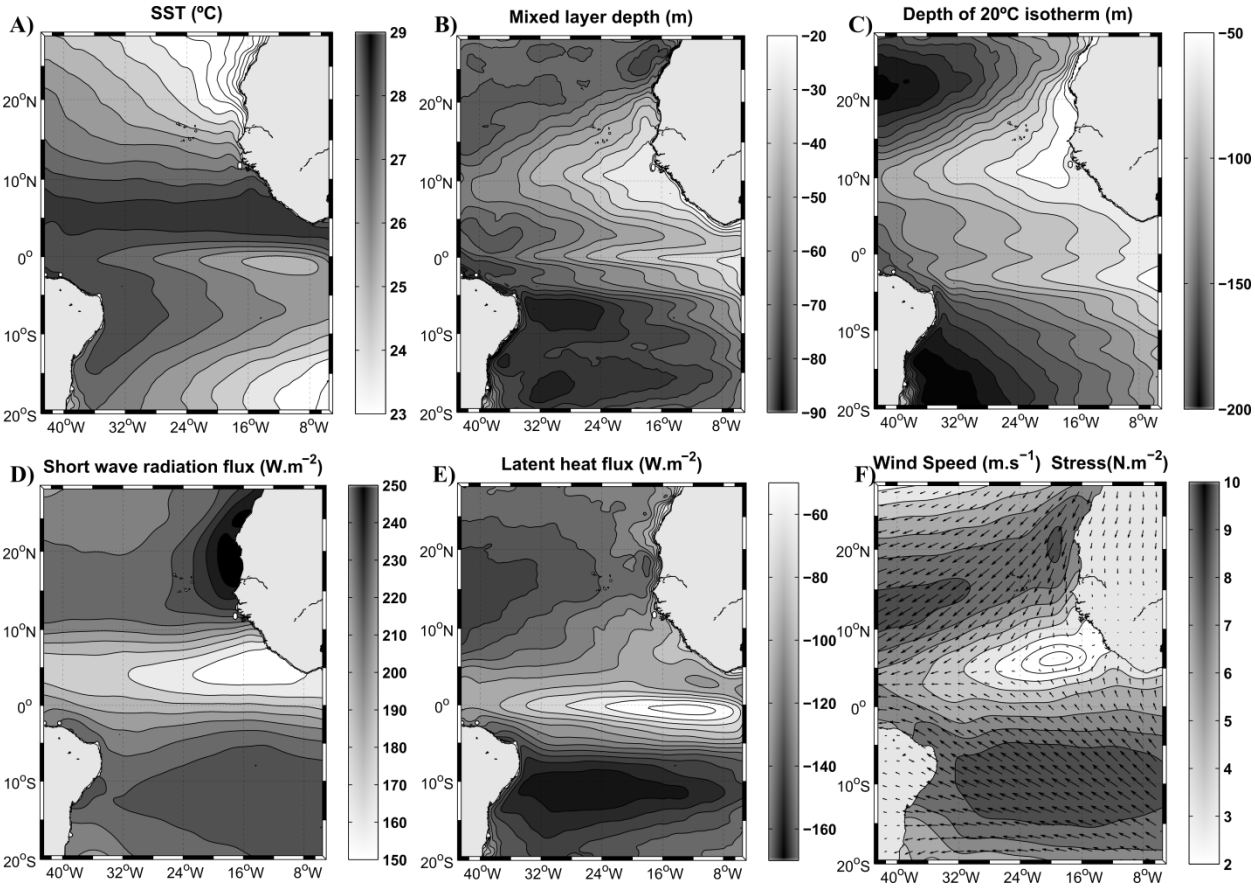

Figure 3. 5 Annual mean (2000–2010) of (A) SST, (B) MLD, (C) Depth of the 20C isotherm, (D) Surface shortwave radiation (> indicates heat gain by the ocean), (E) Latent heat flux (< indicates heat loss by the ocean), and (F) wind speed (contours) and stress (vectors).

Next, we consider the variability of SST and mixed layer temperature rate of change (Temp rate). It was verified two areas of SST enhanced variability (standard deviation > 0.4 °C), located in the eastern tropical North Atlantic and the eastern equatorial region (Fig. 3.6 a). The SST pattern is ratified by the variability of the Temp rate over the mixed layer (Fig. 3.6 b), were the same areas exhibit enhanced variability (standard deviation > 0.15 °C.month^{-1}).

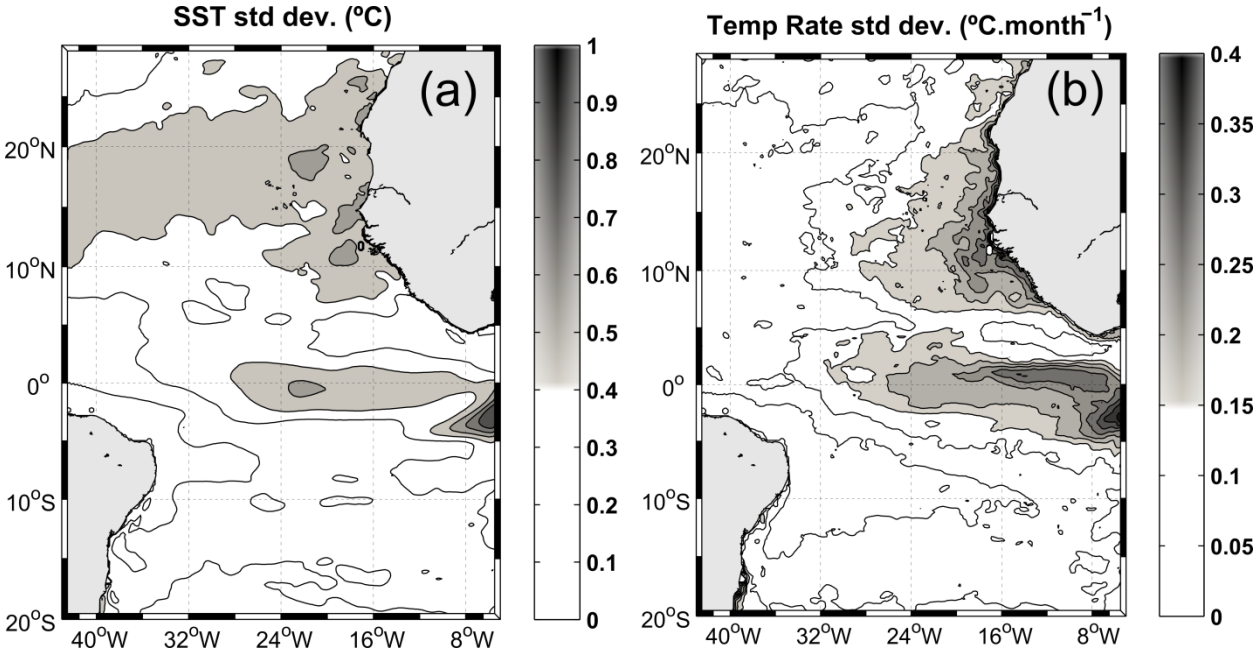

Figure 3. 6 Interannual standard deviations (std. dev.) of the SST (a) and Temperature rate of change over the mixed layer (b). The standard deviations were calculated from monthly anomalies from the seasonal cycle, smoothed with a 5-month running mean.

This study is limited here at north by 28° N, at south by 20° S, at east by 5° W, and at west by 43° W. For a greater legibility of the results we carry out the analysis from isolated areas. These areas are regarded as representative of the principal regional characteristics associated to oceanic dynamics entering in the setting up of the heat budget of the mixing layer and are similar of the delimited boxes already used with success by Servain and Lazar (2010) in the seasonal evaluation of the relative contributions of the temperature trends terms over the TA. The delimited areas present here (Fig. 3.7) also are representative of the differences between the spatial correlations of the temperature rate of change and the main temperature trend terms of atmospheric and oceanic sources. The equatorial area (area 3) showed a strong influence (correlation > 0.5) of the oceanic terms in determination of temperature (Fig. 3.7 a). The most remote areas away from the equator (areas 1 and 6), presented enhanced correlations between the temp rate and atmospheric forcing (Fig. 3.7 b). The southwest region of the TA (area 4) also presented strong correlation with atmospheric forcing in determination of the temperature, however at this region the oceanic terms also exerts influence, mainly represented by the horizontal advection (Fig. 3.7 c) along the continental shelf. The horizontal advective term

(Temp hadv) also presented correlation > 0.5 along the African Coast (area 2), at equator (area 3) and between areas 5 and 6. This relative contribution of the horizontal advection from equator to the south seems to be relative to the actuation of the SEC branches over these areas. The relative contributions of the vertical oceanic terms (temp vert) are presented in Fig. 3.7 d. Well-marked contributions in temperature determination along the equator (correlation > 0.3), seems to be in response of the currents and counter-currents interactions over the equatorial region.

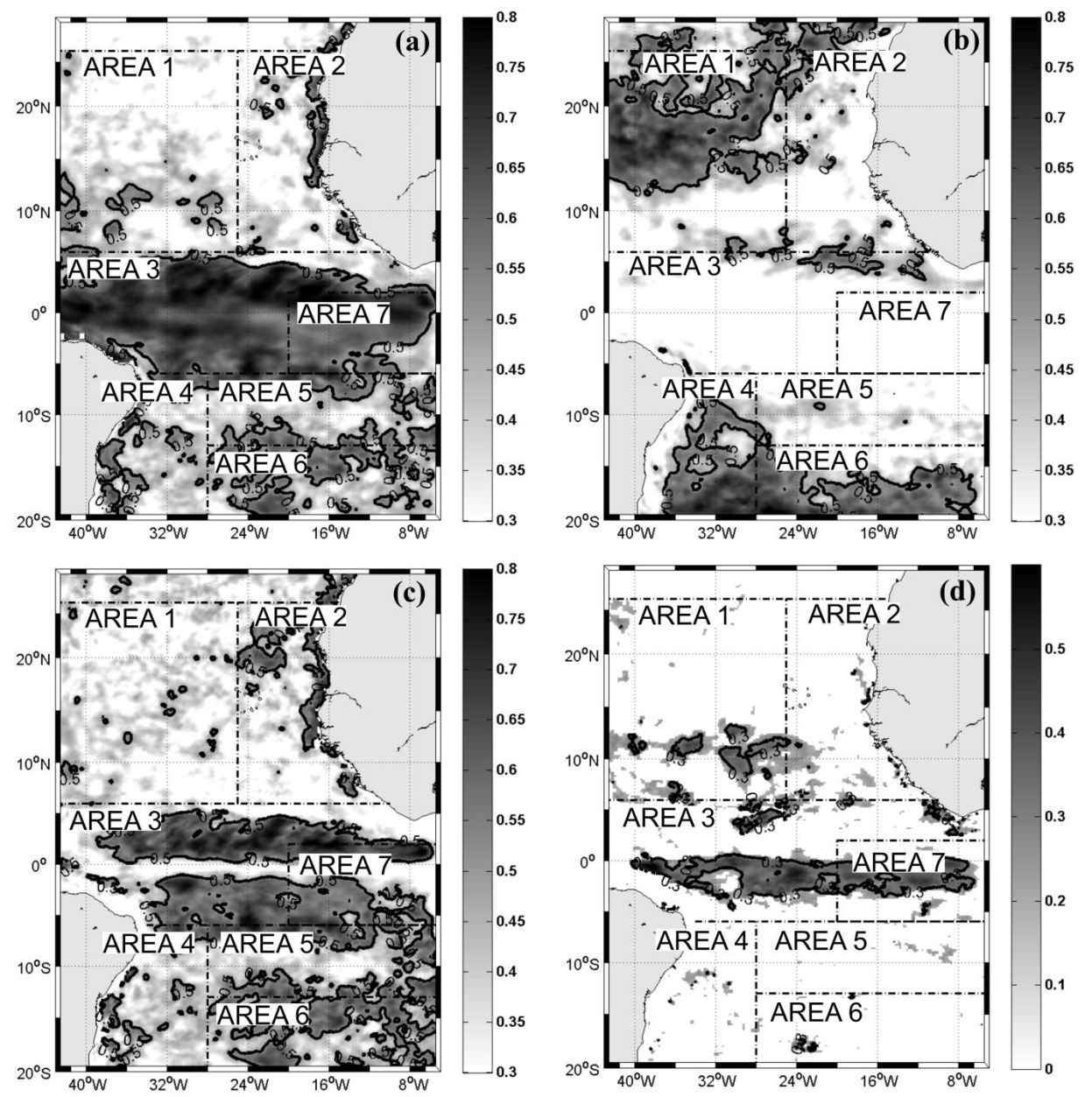

Figure 3. 7 Pearson's correlation maps between interannual anomalies of Temp rate against: (a) Temp ocean (b) Temp forcing (c) Temp hadv and (d) Temp vert. The gray shading consist in results were the correlation was significant ($p < 0.05$) for the 95% of confidence level. The data outside the confidence level were transformed in flawed regions.

Interannual evolutions of the atmospheric and oceanic trend variables entering into the balance of $\partial T/\partial t$, integrated in space for each one of the seven areas previously defined. These areas are described according to a sequential way (Figs. 3.8 to 3.14). Our region 1 (6^o N – 25^o N, 43^o W – 20^o W) covers part of the North Equatorial Current (NEC), the North Equatorial Counter Current (NECC), the northeast trade winds, and are mainly subjected to Ekman pumping. Analyzing the temperature anomalies of the mixed layer at the area 1 (Fig. 3.8 a), we can identify four cold anomalies and five warm anomalies between the years of 2000 to 2010. From the year of 2000 until mid-2009 the anomalies (cold and warm) not exceed the value of $\pm$0.5 °C, although from mid-2009 to 2010 a strong warm anomaly reaches 1.1 °C. The evaluation of the whole oceanic contributions against the atmospheric forcing (Fig. 3.8 b) reveals the predominance of the atmospheric contributions during most of the analyzed period. A balance with the oceanic and atmospheric trends reaching the same order of magnitude can be observed in two periods, from 2000 until late 2001, and from mid-2007 to mid-2008. The analysis by individual term of the oceanic processes (Fig. 3.8 c) shows that this is the vertical diffusion which more contributes to drive the ocean trends. In the periods were the oceanic trends balance the atmospheric forcing, the vertical oceanic terms, mainly driven by vertical diffusion (not shown), are preponderant over the horizontal advection terms. The horizontal advection terms did not exceed 0.1 °C.month^{-1} and in consequence, did not exert much influence. The atmospheric forcing acted in both, to cooling down as heating the temperatures, and reached 0.31 °C.month^{-1} when its dominance over the oceanic terms resulted in the highest verified warm anomaly (year of 2010). The strongest negative value of the atmospheric forcing term was -0.42 °C.month^{-1} in late 2000. This value was in contrast to the vertical diffusion terms (positive and of the same magnitude order), resulting in a weak positive temperature rate of change, which contributed to restore the temperatures from a cold anomaly.

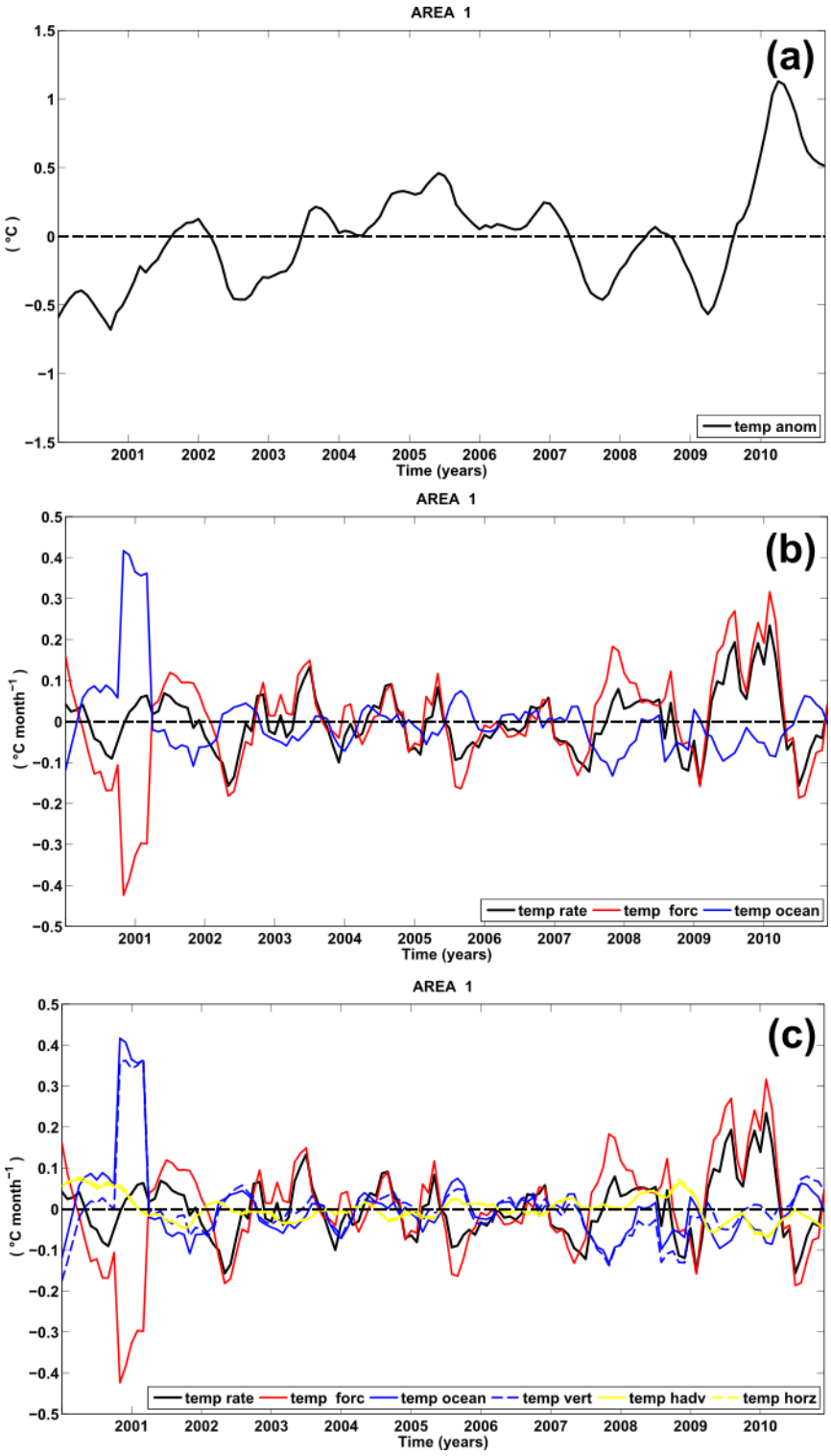

Figure 3. 8 Interannual evolution of the temperature over the mixed layer (°C) and its relative contributions of the temperature terms (°C.month^{-1}) spatially integrated over the area 1 (See Fig. 3.7). (a) Temperature anomalies over the mixed layer. (b) Relative contributions of the total oceanic (blue line) and atmospheric (red line) trends entering into the balance with the temperature rate of change (black line). (c) More detailed oceanic terms presenting the relative contributions of the

horizontal advection (yellow line), horizontal oceanic terms (dashed yellow line) and vertical oceanic terms (dashed blue line); blue, red and black lines are repeated.

In our area 6 (20^o S – 13^o S, 28^o W – 5^o W), a similar pattern to that described above was verified. This region covers a good part of the sSEC branch, is influenced by the southeast trade winds, and is also under the influence of the Ekman pumping. Although the distance between the areas 1 and 6 represents the greatest distance between the analyzed areas, the area 6 also presented the dominance of the surface forcing over the other terms in the determination of the temperature over the mixed layer. These results ratified the trends pointed by the spatial correlations presented at Fig. 3.7 b, however the contributions of the dominant surface forcing at area 6 happen within a smaller range of variation when compared to the area 1. Three periods of temperature cold anomalies (Fig. 3.9 a) were observed from early 2001 to mid-2002, January to June of 2004 and from mid-2005 to late 2007. In contrast three temperature warm anomalies were verified in 2003, mid-2004 to mid-2005 and from 2008 to late 2010. The strong positive anomaly (2003) reaches 0.6 °C followed by the strong negative anomaly (early 2004) that reaches -0.5 °C within a shorter period. Both anomalies were driven by the contributions of the surface forcing (Fig. 3.9 b) which oscillates from the maximum positive (0.2 °C.month^{-1} in December of 2002) to maximum negative value (-0.23 °C. month^{-1} in January of 2004). Analyzing the relative contributions of the more individualized terms (Fig. 3.9 c), we can realize that the oceanic trends are result of the shared actuation of the vertical diffusion and horizontal advection. In a period of exception (end of 2001), the horizontal advection terms were summed to the vertical oceanic to improve the effectiveness of the balance against the surface forcing. During most of the analyzed period, or the oceanic terms did not reach the same order of magnitude of the atmospheric term or they acted one against each other, resulting in an oceanic balance.

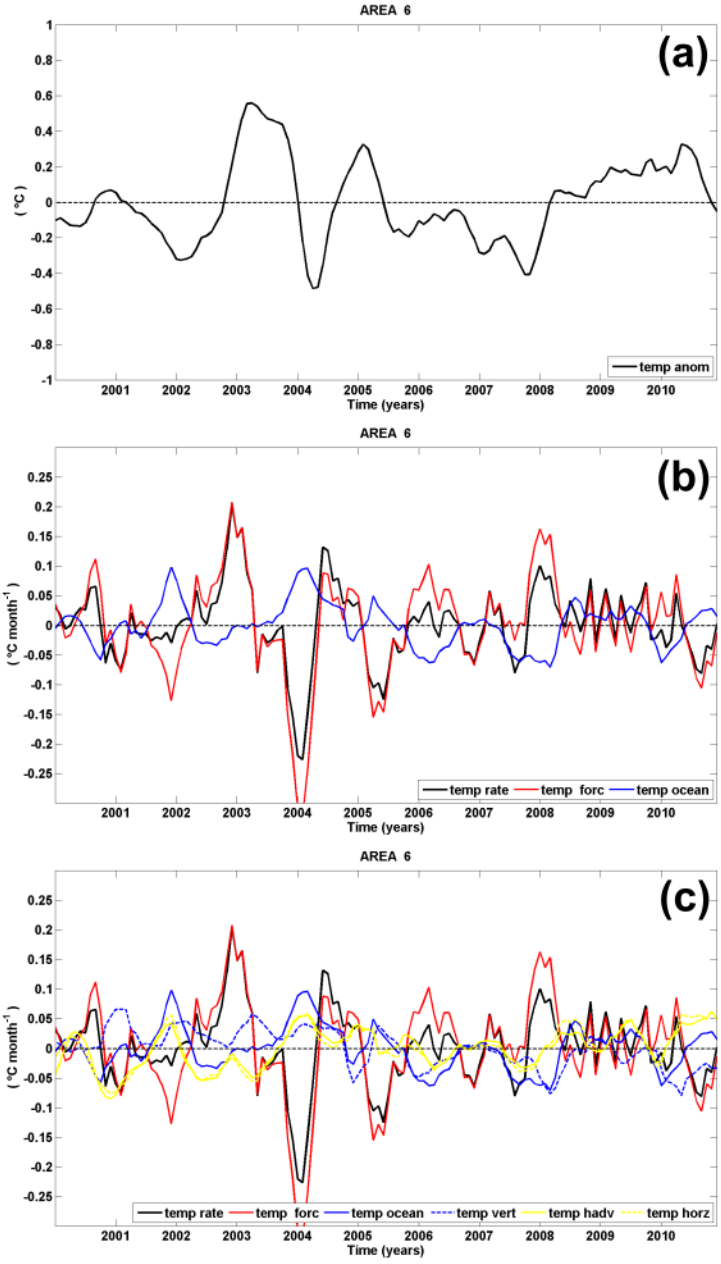

Figure 3. 9 Same as Fig. 3.8, but for area 6.

The region 4, located at broad of the Brazilian coast, is limited at open boundaries by 28°W, 6°S and 20°S. This region includes the termination of the westward sSEC in its eastern region, and the Brazilian Current (BC) which is running southward along the Brazilian coast. The BC is fed by a part of the sSEC divergence flow, and the other part of this flow, moves

northward, giving rise the North Brazilian Current (NBC) in the northern boundary of this region.

Just like the areas analyzed above, our area 4 also presents the same pattern that controls the temperature over the mixed layer. The relative contribution of the atmospheric forcing was determinant during most of the analyzed period (Fig. 3.10 b, c). From year of 2000 to late 2002, a short period at early 2004 and from 2006 to late 2008, we had the presence of cold anomalies over the mixed layer (Fig. 3.10 a). While, in 2003, from mid-2004 to mid-2005 and from 2009 to 2010, were noted the presence of warm anomalies. This last one anomaly it was the strongest over the analyzed period and reached 0.52 °C in late 2009. As already mentioned, when we compare the contributions of the oceanic terms against the surface forcing term (Fig. 3.10 b), the dominance of the atmospheric contributions are visible, although with variations that reaches merely ± 0.15 °C.month^{-1}. Nevertheless, the positive contributions of the surface forcing term, with results in positive local rate of change of temperature during approximately 6 months in 2009, made possible the warm anomaly of more than 0.5 °C verified in this year. Analyzing the more detailed terms (Fig. 3.10 c), we can realize that there is an alternating of dominance between the horizontal advection and vertical terms in the determination of the oceanic temperature trends. This complex pattern, without a marked dominance can be in response to variability of the sSEC and/or of the Brazilian Current inside this area.

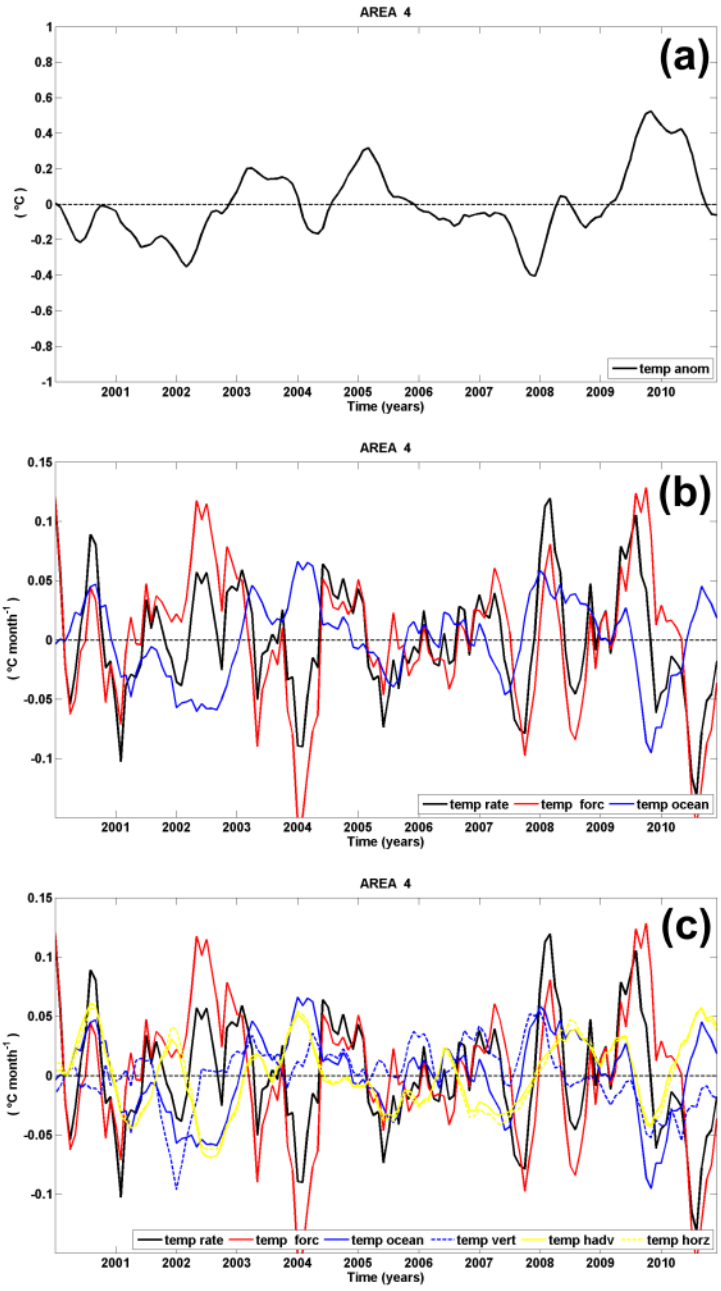

Figure 3. 10 Same as Fig. 3.8, but for area 4.

Our area 2 (6^o N – 25^o N, 20^o W – 5^o W) undergoes the influence of the Canary Current system, which is a system that contains coastal upwelling, filaments, and eddies, being a very complex region dynamically. This region presented strong interannual variations (Fig. 3.6 a, b). Analysing the temperature anomalies inside mixed layer (Fig. 3.11 a), were noted five warm

anomalies and four cold anomalies during the studied period. The stronger negative anomaly reaches -1.1 °C (early 2009) while the highest warm anomaly reaches 0.9 °C just after the cold event (early 2010). With exception of a short period in 2009, where the surface forcing term imposed dominance over other terms, during all studied period, this area showed a balance between the surface forcing term and the oceanic terms (Fig. 3.11 b), reaching magnitudes of the same order. This equilibrium between the oceanic and atmospheric trends was maintained through the contributions to the temperature tendency which range from $\pm$0.2 °C .month^{-1} to $\pm$0.7 °C .month^{-1}. Analyzing the more detailed temperature trends (Fig. 3.11 c), we noted that the contributions of the oceanic temperature trends are most of the time result of summation of the vertical temperature trends and the contributions induced by the horizontal advection. The continuous contribution of the horizontal advection, being important in the determination of the oceanic trends, denotes the strong influence of the Canary current over this area.

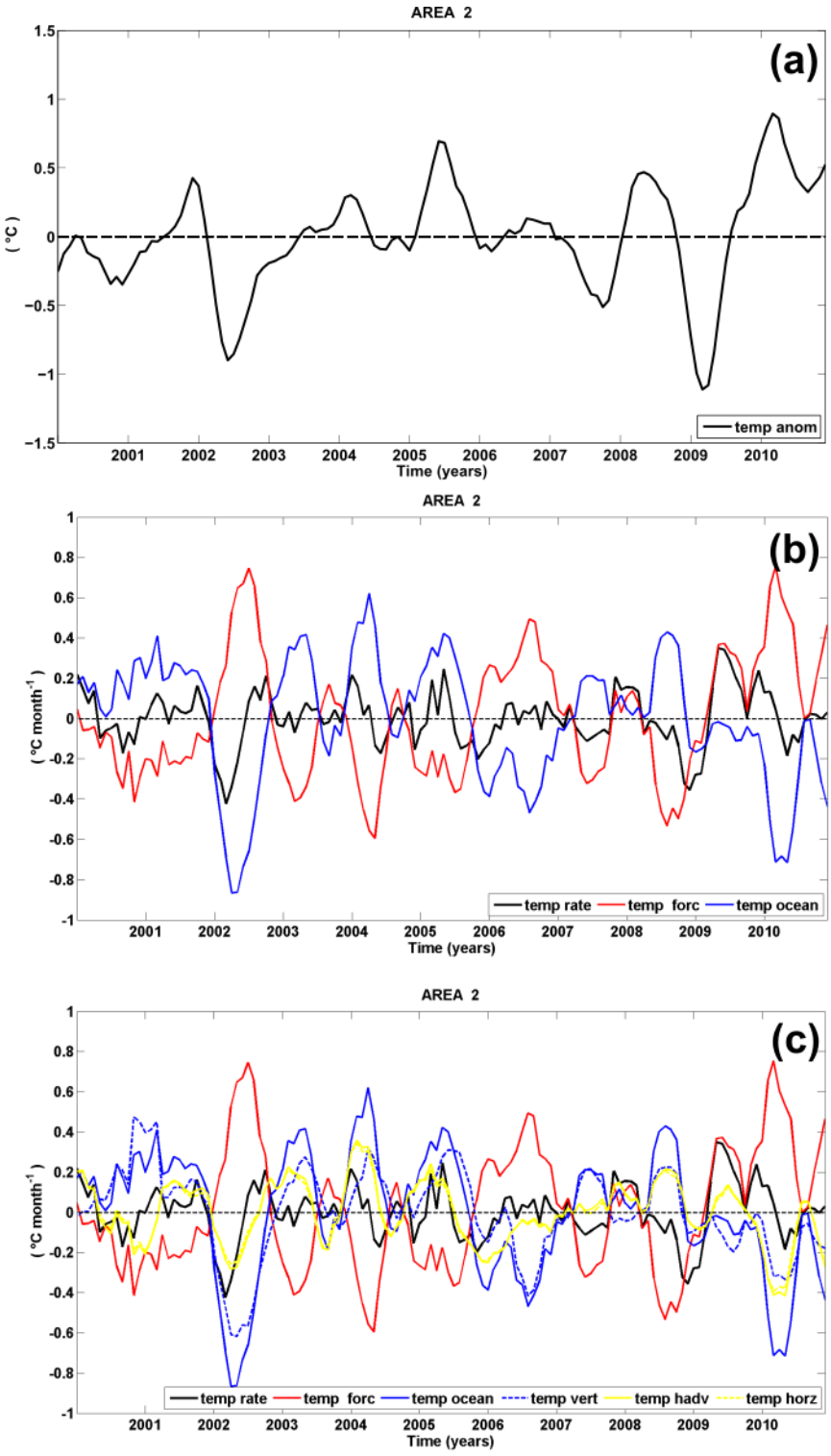

Figure 3. 11 Same as Fig. 3.8, but for area 2.

Our area 3 is the equatorial region (6^o S – 6^o N, 43^o W – 5^o W). The equatorial region is subject to various dynamic processes, like equatorial upwellings, eddies and tropical instability waves. A complex current and counter-currents system dominates the dynamic processes over the mixed layer, which comprehends the westward flows of the cSEC and nSEC branches, in contrast with the eastward flows of the Equatorial Under-current (EUC) and the NECC. The analysis of the temperature trends inside the mixed layer over the equatorial region presented four cold anomalies and four warm anomalies along of the 11 analyzed years (Fig. 3.12 a). The cold anomalies can be observed from the year of 2000 to mid-2003, a short period in early 2004, almost entire year of 2007 and about nine months of 2009. The more pronounced negative anomaly happened during the late 2000 and reached -0.5 °C, nevertheless, the negative anomaly of 2007 also reached the same order of amplitude (-0.4 °C). The warm anomalies occurred in a short period in late 2003, from mid-2004 to the end of 2006, during the entire year of 2008 and from late 2009 to 2010. The maximum positive anomaly occurred in mid-2010 and reached 0.6 °C. In general, the anomalies of the temperature over the equator are the result of the balance between the oceanic and atmospheric temperature trends (Fig. 3.12 b). With exception of a short period in late 2002 when the oceanic and atmospheric trends are summed, the balance reached between these two trends presented values with range from $\pm$0.1 to $\pm$0.7 °C. The evaluation of the detailed terms (Fig. 3.12 c) revealed that the vertical temperature terms exert a preponderant tendency over the oceanic trends during almost all the evaluated period. The relative contributions of the advective terms to the determination of the temperature inside the mixed layer were below expectations for this area. During most of the time, the advection contributions to the temperature trend oscillated inside of $\pm$0.1 °C.month^{-1}. We believe that this trend can be being underestimated in reason of this area be a very complex region dynamically and thermodynamically, where currents and counter-currents can contribute with opposite signals to the temperature tendency over the mixed layer, which makes it inappropriate for an evaluation performed through a regional average.

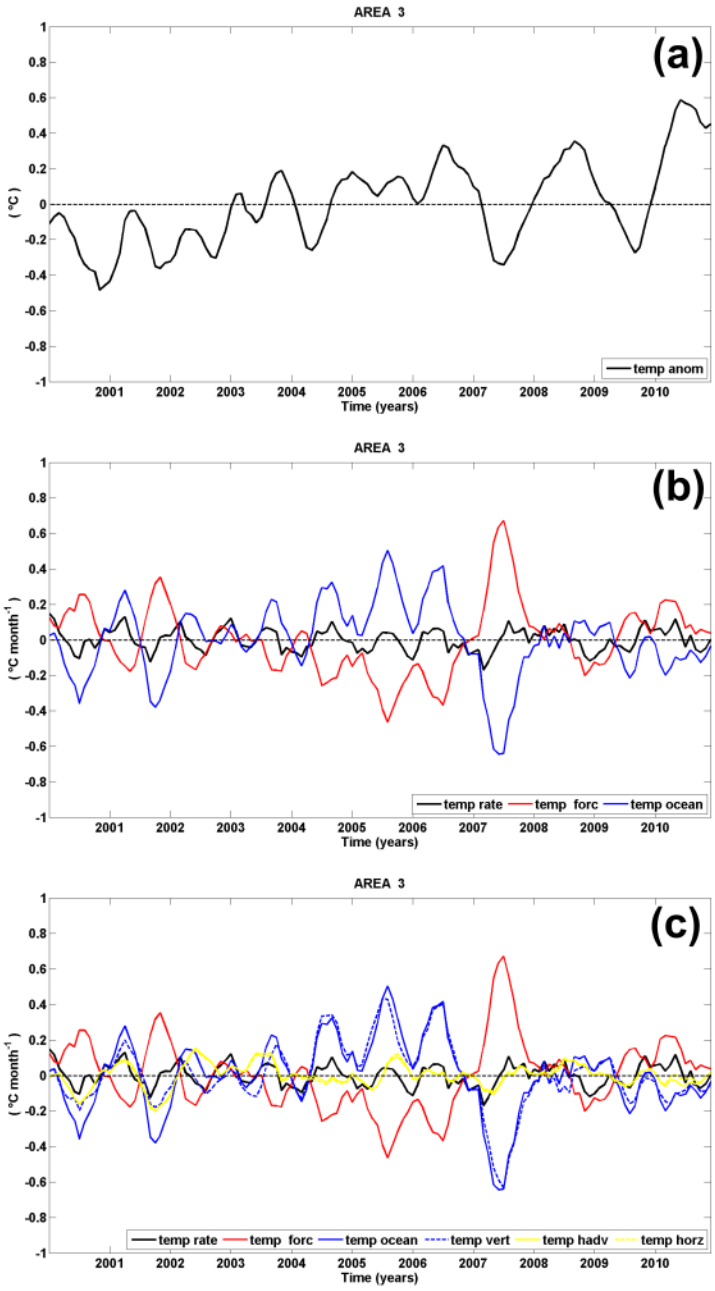

Figure 3. 12 Same as Fig. 3.8, but for area 3.

After perform our equatorial evaluation of the relative contributions of the temperature terms over the mixed layer, we analyzed a sub-region inside the equator (area 7; 6^{o} S – 2^{o} N, 20^{o} W -5^{o} W). This region showed a well-marked pattern of enhanced interannual variability (Fig. 3.6) for both SST and temperature over the mixed layer. As already expected, this regions

presented a high frequency of anomalies (Fig. 3.13 a), being that the three negative anomalies more significant (< -0.4 °C) occurred in late 2000, late 2001 and early 2007. In contrast, if we consider the most significant warm anomalies using the same amplitude of variation, we noted two anomalies, one in 2006 and another in 2008. The warm anomaly of 2008 lasts more than a year reaching the early 2009, and its long duration can result in impacts for the climate over the surrounding continents. When we evaluated the temperature trends (Fig. 3.13 b), the equatorial pattern is repeated, presenting a balance between the oceanic and atmospheric temperature trends. However, this balance pattern is reached with increased amplitudes, which reached about $\pm$1.4 °C.month^{-1} in 2007. The analysis of the more detailed terms (Fig. 3.13 c) revealed that the vertical oceanic terms are the dominant term over this area, ratifying the pattern already observed to entire equator.

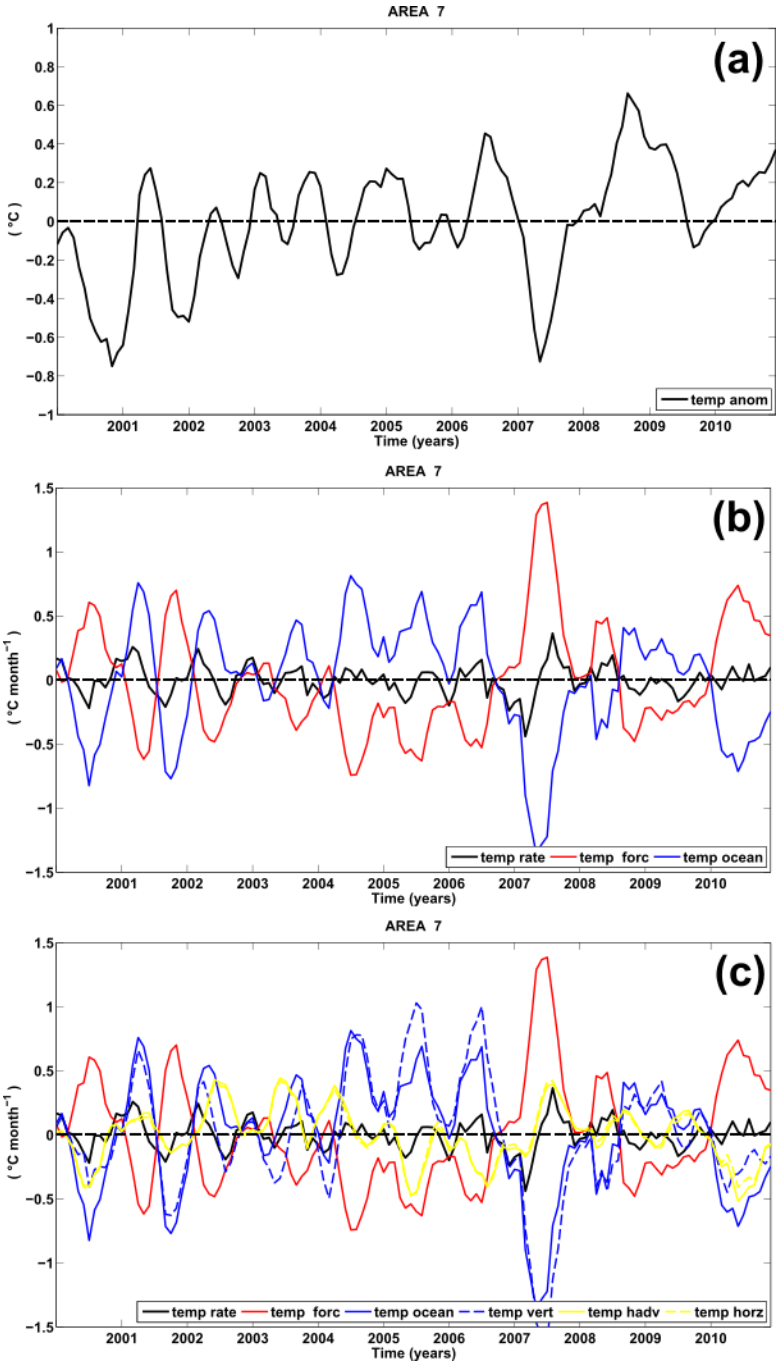

Figure 3. 13 Same as Fig. 3.8, but for area 7.

Finally, our area 5(13^{o} S – 6^{o} S, 28^{o} W – 5^{o} W), which is an oceanic area placed between the equator and the southern oceanic area of the domain. This region could be influenced by two SEC branches, by the southeast trade winds, and can also be under the influence of the Ekman

pumping. Evaluating the interannual anomalies of the temperature over the mixed layer (Fig. 3.14 a) at this area, it was noted that during the first six years of studied period (2000 to 2005) the cold anomalies were predominant, while after that (from yearly 2006 to 2010) the temperature variations were dominated by the warm anomalies. The strongest negative anomaly it was observed in mid-2002 and reached -0.4 °C in contrast with the warm period which the maximum value reached 0.7 °C in mid-2010. The contrast between the oceanic and atmospheric temperature trends showed contributions of similar magnitudes presenting maximum range of about 0.2 °C.month^{-1} (Fig. 3.14 b). When we analyzed the more detailed terms (Fig. 3.14 c), the oceanic trends revealed a very complex temporal distribution, where was difficult to achieve a distinguish pattern between the more individual trends. There were periods when the zonal advection controls the oceanic temperature trends in contrast with other periods, where the vertical oceanic trends (leaded by the vertical diffusion) imposed the dominance over the oceanic trends. This complex variability of the individual terms can be in consequence of this region suffer influence of two SEC branches in its northern and southern borders.

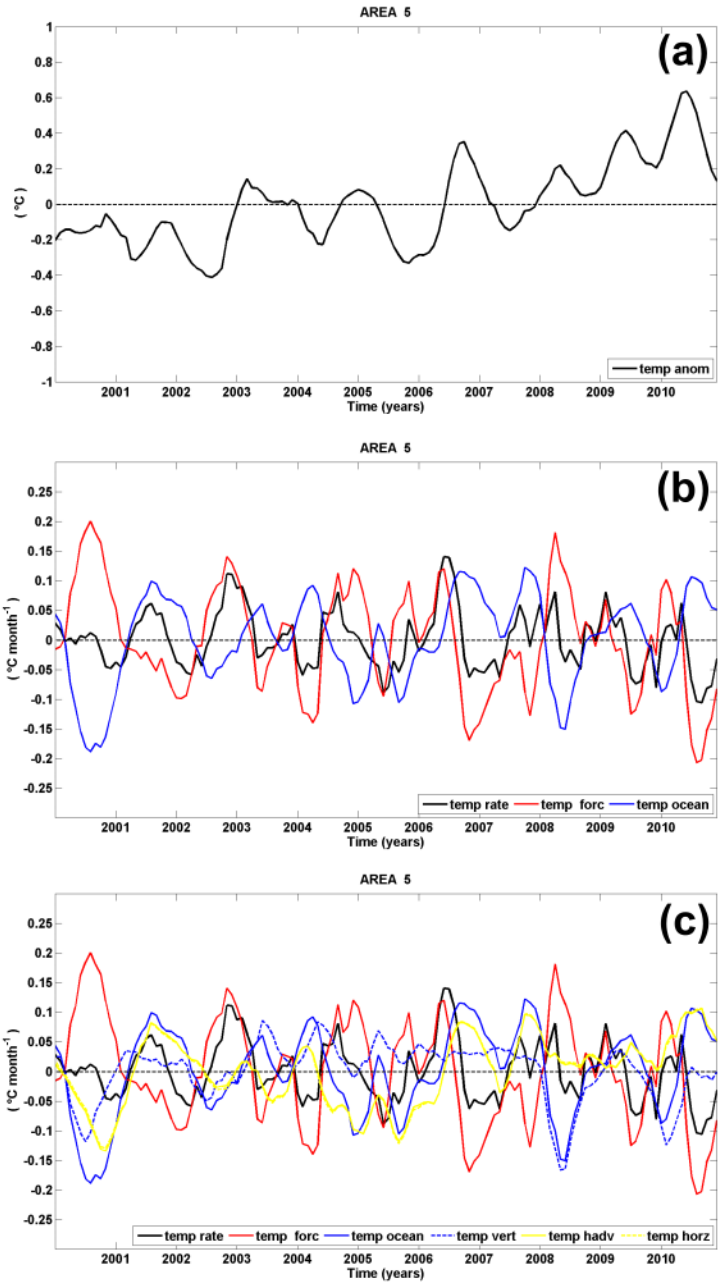

Figure 3. 14 Same as Fig 3.8, but for area 5.

3.7. Summary and discussion

A numerical effort was conducted to allow us perform a diagnosis of the main temperature trends over the tropical Atlantic. The simulation was configured to have an increased number of vertical points at the upper ocean, focusing on better reproduce the

thermodynamics of the mixed layer. The numerical diagnostic outputs of the ROMS model were used to describe the patterns of distribution of the temperature tendency terms in sectored regions inside the tropical Atlantic (TA). The regions presented here to better understand the thermodynamics of the upper TA were used by Servain and Lazar (2010) in a climatological evaluation and allowed us to establish a comparison with the interannual evolutions shown here.

Through an analysis of the relative contributions of temperature tendency terms over the mixed layer, we have shown that the surface forcing (net heat flux) was the dominant term in the temperature determination for our regions 1, 4 and 6, which are the northern oceanic region, the southwest region and the southern oceanic region, respectively. These results are in accordance with the previous work of Foltz and McPhaden (2006), which shown that variations of mixed layer heat storage in the tropical North and South Atlantic ocean are driven primarily by latent heat loss and shortwave radiation. These authors investigated the role of horizontal oceanic heat advection in the tropical Atlantic, and concluded that this nonlinear term acts to damp the surface flux–forced changes in SST.

When we establish a comparison between the interannual predominant terms and the seasonal dominant terms presented in Servain and Lazar (2010) in these regions (1, 4 and 6), we confirm that the main role exerted by the surface forcing in the temperature determination is the same pattern observed seasonally. In the seasonal timescale several authors confirm that the furthest away from the equator more evident is the dominance of the net heat flux over the other terms (Foltz et al. 2003, Peter et al. 2006, Servain and Lazar 2010). However, when we analyzed the oceanic contributions to the temperature tendency over these areas, just our area 1 confirm the same pattern showed in the seasonal evaluation (dominated by the vertical diffusion). Our areas 4 and 6 (Southwestern and South oceanic areas, respectively) presented a combined force between the horizontal advection and vertical oceanic terms in the determination of the total oceanic temperature tendency. Seasonally, these regions had the oceanic trends dominated by the vertical diffusion. We can attribute this discrepancy between the timescales to an increased interannual variability of the sSEC and Brazilian Current over these regions.

The evaluations over the equatorial area (area 3) revealed that the temperature rate of change results of a balance between the oceanic trends and surface forcing. This balance happens when the two trends (oceanic and atmospheric) have the same order of magnitude, and the local

rate of temperature change is resulted of a small unbalance of the absolute fractions. This pattern was repeated by the other areas (2, 5 and 7) with exceptions made just for short periods, which are non-representatives of the evaluated period (years of 2000-2010).

The equatorial pattern of the temperature determination described above also corroborates with the previous studies performed in the seasonal timescale (e.g. Foltz et al. 2003, Peter et al. 2006, Servain and Lazar 2010) showing that the interannual variations over the equatorial Atlantic are also mainly controlled by the balance between the surface atmospheric forcing and the vertical diffusion.

A sub-region inside the equatorial Atlantic (area 7) was chosen to be evaluated apart, considering the high levels of interannual variability (Fig. 3.6). It was verified in 2008 a warm anomaly that reaches its peak phase in austral winter, when the cold tongue is well developed over the equator. According with Wang (2001) the equatorial Atlantic mode seems to be phase-locked with the seasonal cycle. This author performed evaluations of the SST over the ATL3 region (3^o S - 3^o N, 20^o W-0^o) and confirm an interannual oscillation which the more significant events (SST anomaly > 0.7 °C) occurring with a periodicity of about 30 months. Although, the anomalies presented in our study were bellow this amplitude level, these anomalies consists in mixed layer anomalies, therefore differences in amplitude were expected.

The most significant anomalies were identified at region 2 (northeastern Atlantic) exceeding -1°C in cold anomalies and reaching 0.9 °C in the more developed warm anomaly. As also verified in the equator, this region presented a balance between the oceanic and atmospheric temperature terms. However, it was the region where the contributions of the horizontal advection seem to play the same role of the vertical diffusion to balance the atmospheric surface forcing.

The analysis of temperature anomalies over the mixed layer at the region 5 (oceanic region between 13^oS - 6^oS, 28^oW - 5^oW) presented two periods of dominance, a cold period (2000-2006) in contrast with a warm period (2006-2010). Although the temperature rate of change had oscillated between negative and positive values along the studied period, the positive excursions during the cold anomalies phase were not sufficient to produce warm anomalies, being the opposite also true. The more detailed terms analysis revealed that the horizontal

advection developed an important role in the temperature determination over the mixed layer, being during most of the time the preponderant oceanic term over the vertical diffusion. Vianna and de Menezes (2003) showed that the circulation variability between 5° S – 15° S is mostly in the interannual band with a very weak annual cycle. Our results for this area also corroborate the results of Foltz and McPhaden (2006) which showed that this region is the most effective region over the TA where the horizontal advection damps the surface flux terms.

References

Bourlès B, Lumpkin R, McPhaden MJ, et al (2008) The Pirata Program: History, accomplishments, and future directions. Bull Am Meteorol Soc 89:1111–1125. doi: 10.1175/2008BAMS2462.1

Brandt P, Funk A, Hormann V, et al (2011) Interannual atmospheric variability forced by the deep equatorial Atlantic Ocean. Nature 473:497–500. doi: 10.1038/nature10013

Carton J a., Cao X, Giese BS, Da Silva AM (1996) Decadal and Interannual SST Variability in the Tropical Atlantic Ocean. J Phys Oceanogr 26:1165–1175. doi: 10.1175/1520-0485(1996)026<1165:DAISVI>2.0.CO;2

Carton J a., Giese BS (2008) A Reanalysis of Ocean Climate Using Simple Ocean Data Assimilation (SODA). Mon Weather Rev 136:2999–3017. doi: 10.1175/2007MWR1978.1

Carton J a., Huang B (1994) Warm Events in the Tropical Atlantic. J Phys Oceanogr 24:888–903. doi: 10.1175/1520-0485(1994)024<0888:WEITTA>2.0.CO;2

Chang P, Saravanan R, Ji L, Hegerl GC (2000) The Effect of Local Sea Surface Temperatures on Atmospheric Circulation over the Tropical Atlantic Sector. J Clim 13:2195–2216.

Chang P, Yamagata T, Schopf P, et al (2006) Climate Fluctuations of Tropical Coupled Systems—The Role of Ocean Dynamics. J Clim 19:5122–5174. doi: 10.1175/JCLI3903.1

De Boyer Montégut C, Madec G, Fischer AS, et al (2004) Mixed layer depth over the global ocean: An examination of profile data and a profile-based climatology. J Geophys Res C Ocean 109:1–20. doi: 10.1029/2004JC002378

Fairall CW, Bradley EF, Rogers DP, et al (1996) Bulk parameterization of air-sea fluxes for Tropical Ocean-Global Atmosphere Coupled-Ocean Atmosphere Response Experiment. J Geophys Res 101:3747–3764.

Foltz GR (2003) Seasonal mixed layer heat budget of the tropical Atlantic Ocean. J Geophys Res 108:1–13. doi: 10.1029/2002JC001584

Foltz GR, McPhaden MJ (2006) The role of oceanic heat advection in the evolution of tropical North and South Atlantic SST anomalies. J Clim 19:6122–6138. doi: 10.1175/JCLI3961.1

Fratantoni DM, Johns WE, Townsend TL, Hurlburt HE (2000) Low-Latitude Circulation and Mass Transport Pathways in a Model of the Tropical Atlantic Ocean*. J Phys Oceanogr 30:1944–1966. doi: 10.1175/1520-0485(2000)030<1944:LLCAMT>2.0.CO;2

Goni GJ, Baringer MO (2002) Surface currents in the tropical Atlantic across high density XBT line AX08. Geophys Res Lett 29:2000–2003. doi: 10.1029/2002GL015873

Graham NE, Barnett TP (1987) Sea Surface Temperature, Surface Wind Divergence, and Convection over Tropical Oceans. Science (80-) 238:657–659.

Huang B, Shukla J (2005) Ocean – Atmosphere Interactions in the Tropical and Subtropical Atlantic Ocean. J Clim 18:1652–1672.

Kanamitsu M, Ebisuzaki W, Woollen J, et al (2002) NCEP–DOE AMIP-II Reanalysis (R-2). Bull Am Meteorol Soc 83:1631–1643. doi: 10.1175/BAMS-83-11-1631

Kouadio Y, Servain J, Machado L, Lentini C (2012) Heavy rainfall episodes in the eastern northeast brazil linked to large-scale ocean-atmosphere conditions in the tropical atlantic. Adv Meteorol. doi: 10.1155/2012/369567

Large, W, McWilliams, J, Doney, S, (1994) Oceanic vertical mixing: A review and a model with a nonlocal boundary layer parameterization. Rev. Geophys. 32, 363–403.

Lazar A, Murtugudde R, Busalacchi J (2000) A model study of temperature anomaly propagation from the subtropics to tropics within the South Atlantic thermocline. Geophys Res Lett 28:1271–1274. doi: 10.1029/2000GL011418

Lemarié F, Kurian J, Shchepetkin A, et al (2012) Are there inescapable issues prohibiting the use of terrain-following coordinates in climate models? Ocean Model 42:57–79. doi: 10.1016/j.ocemod.2011.11.007

Liu WT, Katsaros KB, Businger JA (1979) Bulk Parameterization of Air-Sea Exchanges of Heat and Water Vapor Including the Molecular Contraints at the Interface. J Atmos Sci 36:1722–1735.

Lumpkin R, Garzoli SL (2005) Near-surface circulation in the Tropical Atlantic Ocean. Deep Res Part I Oceanogr Res Pap 52:495–518. doi: 10.1016/j.dsr.2004.09.001

Marchesiello P, Capet X, Menkes C, Kennan SC (2011) Submesoscale dynamics in tropical instability waves. Ocean Model 39:31–46. doi: 10.1016/j.ocemod.2011.04.011

Maximenko N, Hafner J (2010) SCUD: Surface Currents from Diagnostic model. 17p.

Maximenko N, Niiler P, Rio MH, et al (2009) Mean dynamic topography of the ocean derived from satellite and drifting buoy data using three different techniques. J Atmos Ocean Technol 26:1910–1919. doi: 10.1175/2009JTECHO672.1

Penven P, Marchesiello P, Debreu L, Lefèvre J (2008) Software tools for pre- and post-processing of oceanic regional simulations. Environ Model Softw 23:660–662. doi: 10.1016/j.envsoft.2007.07.004

Servain J (2003) Modes of tropical Atlantic climate variability observed by PIRATA. Geophys Res Lett 30:1–4. doi: 10.1029/2002GL015124

Servain J, Lazar A (2010) Ocean dynamics contribution to seasonal mixed layer heat budget in the tropical Atlantic. Clima do Altântico Trop. e Impactos sobre o Nord. pp 35–75

Servain, J, (1991). Simple climatic indices for the tropical Atlantic Ocean and some applications. J. Geophys. Res. 96, 15137-15146.

Shchepetkin, AF (2005) If-less KPP. ROMS/TOMS Workshop: Adjoint Modeling and Applications, La.Jolla, CA, October 24-28 http://www.myroms.org/Workshops/ROMS2005/Nonlinear/AlexanderShchepetkin.pdf.

Shchepetkin AF, McWilliams JC (2005) The regional oceanic modeling system (ROMS): A split-explicit, free-surface, topography-following-coordinate oceanic model. Ocean Model 9:347–404. doi: 10.1016/j.ocemod.2004.08.002

Shchepetkin AF, McWilliams JC (2008) Computational Kernel Algorithms for Fine-Scale, Multiprocess, Longtime Oceanic Simulations. Handb Numer Anal 14:121–183. doi: 10.1016/S1570-8659(08)01202-0

Smith, WHF, Sandwell, DT, (1997) Global seafloor topography from satellite altimetry and ship depth soundings. Science. 277, 1957-1962.

Stramma L, Rhein M, Brandt P, et al (2005) Upper ocean circulation in the western tropical Atlantic in boreal fall 2000. Deep Res Part I Oceanogr Res Pap 52:221–240. doi: 10.1016/j.dsr.2004.07.021

Stramma L, Schott F (1999) The mean flow field of the tropical Atlantic Ocean. Deep Res II 46:279–303. doi: 10.1016/S0967-0645(98)00109-X

Vianna ML, Menezes VV De (2003) A seasonal and interannual study of the western equatorial Atlantic upper thermocline circulation variability. Interhemispheric Water Exch. Atl. Ocean. Elsevier Ltd, pp 138–173

Wang C (2001) Atlantic Climate Variability and Its Associated Atmospheric Circulation Cells. J Clim 15:1516–1536.

Wang W, McPhaden MJ (2000) The Surface-Layer Heat Balance in the Equatorial Pacific Ocean. Part II: Interannual Variability*. J Phys Oceanogr 30:2989–3008. doi: 10.1175/1520-0485(2001)031<2989:TSLHBI>2.0.CO;2

Wu L, Zhang Q, Liu Z (2004) Toward understanding tropical Atlantic variability using coupled modeling surgery. Earth's Clim. Ocean. Interact. pp 157–170

Xie SP, Carton J a. (2004) Tropical Atlantic variability: Patterns, mechanisms, and impacts. Earth's Clim. Ocean. Interact. pp 121–142

Zebiak S (1993) Air Sea interactions in the equatorial Atlantic. J Clim 6:1567 – 1586.

Zeng X, Beljaars A (2005) A prognostic scheme of sea surface skin temperature for modeling and data assimilation. Geophys Res Lett 32:1–4. doi: 10.1029/2005GL023030

Zhang X, McPhaden MJ (2010) Surface layer heat balance in the eastern equatorial pacific ocean on interannual time scales: Influence of local versus remote wind forcing. J Clim 23:4375–4394. doi: 10.1175/2010JCLI34